Polish Academy of Sciences
Institute of Fundamental Technological Research

Archives of Mechanics

Archiwum Mechaniki Stosowanej

volume 50 issue 5

FIFTY YEARS OF THE ARCHIVES OF MECHANICS

Agencja Reklamowo-Wydawnicza A. Grzegorczyk
Warszawa 1998

ARCHIVES OF MECHANICS IS DEVOTED TO

Theory of elasticity and plasticity • Theory of nonclassical continua • Physics of continuous media • Mechanics of discrete media • Nonlinear mechanics • Rheology • Fluid gas-mechanics • Rarefied gas • Thermodynamics

---

Printed in Poland, Editorial Office: Świętokrzyska 21,
00-049 Warszawa (Poland)

e-mail: publikac@ippt.gov.pl

Arkuszy wydawniczych 11. Arkuszy drukarskich 8.
Papier offset. kl III 70 g. B1.
Oddano do składania 1 września 1998 r.
Druk ukończono w grudniu 1998 r.
Skład i łamanie: G. Wasilewska
Druk i oprawa: Drukarnia OMIKRON, Stare Babice ul. Kutrzeby 15,
tel. (022) 752 94 16

Arch. Mech., 50, 5, pp. 811–827, Warszawa 1998
FIFTY YEARS OF THE ARCHIVES OF MECHANICS

The dependence of dynamic phase transitions on parameters

K. PIECHÓR (WARSZAWA)

We consider phase changes described by a second order ordinary differential equation. The equation depends parametrically on the states of rest and the speed of the wave. We prove that, under some additional conditions, the solution is differentiable with respect to any of these parameters. As an application of the general theory we discuss the case when the data are close to the Maxwell line and obtain results generalising those of the previous authors.

1. Introduction

We treat the phase boundary as a one-dimensional travelling wave connecting two different states of rest. The speed of the wave cannot be arbitrary but it is an unknown, determined totally by the value of just one of the states of rest. In other words, the question of existence of phase boundaries is a sort of nonlinear eigenvalue problem. For a very limited number of cases we know exactly the structure of the phase boundary and its speed [1, 2]. In the general case, it is only proved that once one state of rest is given, there is a unique value of speed and uniquely determined other state of rest such that the travelling wave connecting them exists and moves at this speed [3 – 8].

The aim of this paper is to formulate sufficient conditions ensuring differentiability of the phase boundary structure, the speed of the wave and the other state of rest as functions of one of the two states of rest.

The paper is organised as follows. In the next section we present the equation of the phase boundary deduced from the capillarity equations which we have derived from a model kinetic theory of van der Waals fluids [9]. In Sec. 3 we generalise this problem and prove a theorem on the differentiability of its solution with respect to a group of parameters treated as "independent". In the final Sec. 4, we apply this theory to our model equation of phase boundaries as well as to the case of isothermal phase transitions. We confine our interest to the case when the data are close to the so-called Maxwell line, in order to avoid complicated formulae. In the latter case our results not only agree with the previous authors' results but also generalise them. Moreover, we show that our model theory agrees qualitatively with the isothermal one.

2. The model equations of capillarity and the travelling wave problem

The model equations of capillarity we are going to consider consist of the following system of two partial differential equations [9]:

$$\frac{\partial}{\partial t}w - \frac{\partial}{\partial x}u = 0, \tag{2.1}$$

$$\frac{\partial}{\partial t}u + \frac{\partial}{\partial x}p(w,u) = \varepsilon\frac{\partial}{\partial x}\left(\mu\frac{\partial}{\partial x}u\right) + \alpha\varepsilon^2\frac{\partial}{\partial x}\left[\frac{5}{w^6}\left(\frac{\partial}{\partial x}w\right)^2 - \frac{2}{w^5}\frac{\partial^2}{\partial x^2}w\right]. \tag{2.2}$$

In Eqs. (2.1), (2.2), the variable $t > 0$ is the time, $x \in \mathrm{R}^1$ is the Lagrangian coordinate, u is the velocity, w is the specific volume, p is the pressure, and $\varepsilon\mu$ is the coefficient of viscosity.

The pressure formula reads

$$p = p(w,u) = \frac{1-u^2}{2(w-b)} - \frac{a}{w^2}, \tag{2.3}$$

where a and b are positive constants; a is the ratio of the mean value of the potential of the attractive intermolecular forces to the mean kinetic energy of molecules, and b characterises close packing. In the adopted dimensionless units b is equal to unity.

Next, $\varepsilon > 0$ characterises the order of magnitude of the viscosity effect, and $\mu = \mu(w,u)$ is given by [9]

$$\mu(w,u) = \frac{w^2(1-u^2) + 2b^2\rho^2(w)}{8w^3\rho(w)}, \qquad \rho(w) = \frac{w}{w-b}. \tag{2.4}$$

Finally, $\alpha\varepsilon^2$, with $\alpha = \text{const} > 0$, characterises the intensity of the capillarity effects which are represented by the space derivative of the term in the square brackets [ ].

We consider Eqs. (2.1), (2.2) in the domain $\mathcal{D}$ defined by [10]

$$\mathcal{D} = \left\{(w,u) : w > b, \qquad u^2 < 1 - \frac{a}{2b}, \qquad \frac{a}{2b} < 1\right\}. \tag{2.5}$$

For $(w,u) \in \mathcal{D}$, the mass density $1/w$ does not exceed the close-packing density $1/b$, and the pressure p and the viscosity μ are positive.

A travelling wave solution to (2.1), (2.2) is a solution of the form

$$(w,u)(x,t) = (w,u)(\xi), \qquad \xi = \frac{x-st}{\varepsilon} \in \mathrm{R}^1, \tag{2.6}$$

such that

$$\lim_{\xi\to-\infty}(w,u)(\xi) = (w_l,u_l), \tag{2.7}$$

$$\lim_{\xi\to+\infty}(w,u)(\xi) = (w_r,u_r), \tag{2.8}$$

$$\lim_{\xi\to\pm\infty}(w',u') = (0,0), \tag{2.9}$$

$$\lim_{\xi\to\pm\infty}(w'',u'') = (0,0), \tag{2.10}$$

where $s = \text{const}$ is the wave speed, and $()' = \dfrac{d}{d\xi}()$.

The following procedure is routine. We substitute (2.6) into Eqs. (2.1), (2.2), perform one integration with respect to ξ, and use the limit conditions (2.7)–(2.10). Having done that, we find that the left and right limit states are related by

$$\begin{aligned} sw_r + u_r &= sw_l + u_l, \\ -su_r + p(w_r,u_r) &= -su_l + p(w_l,u_l). \end{aligned} \tag{2.11}$$

These relations are called the Rankine-Hugoniot conditions and were in detail analysed in [10].

Next, we find the velocity u. It is given by

$$u = u_l - s(w - w_l), \tag{2.12}$$

where $w = w(\xi)$ is a solution of the following limit value problem:

$$\alpha\left[\frac{2}{w^5}w'' - \frac{5}{w^6}w'^2\right] + s\mu(w,s,w_l)w' + f(w,s,w_l) = 0, \tag{2.13}$$

where

$$\mu(w,s,w_l) = \mu(w,u_l - s\,(w - w_l)) > 0, \tag{2.14}$$

$$f(w,s,w_l) = p\,(w,u_l - s(w - w_l)) - p(w_l,u_l) + s^2(w - w_l), \tag{2.15}$$

subject to the conditions

$$\lim_{\xi\to-\infty} w(\xi) = w_l, \tag{2.16}$$

$$\lim_{\xi\to+\infty} w(\xi) = w_r, \tag{2.17}$$

$$\lim_{\xi\to\pm\infty} w'(\xi) = 0, \qquad \lim_{\xi\to\pm\infty} w''(\xi) = 0. \tag{2.18}$$

These conditions must be supplemented by Eqs.(2.11) which we write in the form

$$f(w_l, s, w_l) = 0, \qquad f(w_r, s, w_l) = 0. \tag{2.19}$$

In this paper we assume that

$$f'_w(w_l, s, w_l) < 0, \qquad f'_w(w_r, s, w_l) < 0. \tag{2.20}$$

Our problem contains a number of parameters like w_r, s, w_l, u_l, etc. These parameters are not independent, since some of them are related by the Rankine-Hugoniot conditions (2.11). However, our problem, under assumptions (2.19), (2.20), has a solution if and only if the parameters satisfy an additional relation, unknown in advance. The total number of relations, including the implicit one, is less than the total number of parameters. Therefore, we can split them into two groups: dependent and independent ones. Of course, this splitting is not dictated by the limit value problem itself, it is rather a result of our current interest. Also, it is not obligatory to consider the dependence of solutions on all parameters; simply, we can treat some of them as fixed.

Altogether, there is a great variety of specific problems we can be interested in. Therefore, in order to avoid repeating similar arguments, each time we ask a question concerning the character of dependence of the solution on certain parameters we choose, we formulate an "abstract" problem of dependence of the solution on the parameters and prove its solvability. In Sec. 4 we show how to reduce our specific problem to the "abstract" one.

Let us explain that we cannot answer the posed question basing on the well known theorem on continuous dependence of solutions of ordinary differential equations on the parameters, because it is not clear in advance whether the implicit, unknown relation between the parameters is a differentiable function or not.

3. The abstract problem

The problem we consider consists in determining a function and a set of functions $y(\xi, \lambda) : \mathrm{R}^1 \times \Lambda \to Y \subset \mathrm{R}^1$, and a set of functions $\kappa(\lambda) = (\kappa_1(\lambda), \kappa_2(\lambda), ..., \kappa_k(\lambda)) : \Lambda \to K$, where Λ is an open subset of R^l, K is an open subset of R^k , and the range Y of $y(\xi, \lambda)$ contains the closed interval [0,1]. The functions $y(\xi, \lambda)$ and $\kappa(\lambda)$ are such that:

i) $y(\xi, \lambda)$ satisfies the differential equation

$$y'' = g(y, y', \kappa, \lambda), \tag{3.1}$$

and the limit conditions: for any $\lambda \in \Lambda$

$$\lim_{\xi \to -\infty} y(\xi, \lambda) = 0, \qquad \lim_{\xi \to +\infty} y(\xi, \lambda) = 1, \tag{3.2}$$

$$\lim_{\xi \to -\infty} (y'(\xi, \lambda), y''(\xi, \lambda)) = (0, 0), \tag{3.3}$$

$$\lim_{\xi \to +\infty} (y'(\xi, \lambda), y''(\xi, \lambda)) = (0, 0), \tag{3.4}$$

where the dash denotes differentiation with respect to ξ.

ii) The functions $\kappa_i(\lambda)$, $i = 1, 2, ..., k-1$, satisfy a system of $k-1$ algebraic equations of the form

$$G_i(\kappa, \lambda) = 0, \qquad i = 1, 2, ..., k-1. \tag{3.5}$$

We take the following assumptions concerning the functions g and $G(\kappa, \lambda) = (G_1(\kappa, \lambda), G_2(\kappa, \lambda), ..., G_{k-1}(\kappa, \lambda))$:

H1. $g(y, z, \kappa, \lambda) \in C^{m+\tau}(Y \times \mathrm{R} \times K \times \Lambda)$ for some integer $m > 0, \tau > 0$.

H2. For any $(\kappa, \lambda) \in K \times \Lambda$

$$g(0, 0, \kappa, \lambda) = 0, \tag{3.6}$$

$$g(1, 0, \kappa, \lambda) = 0, \tag{3.7}$$

$$g'_y(0, 0, \kappa, \lambda) > 0, \tag{3.8}$$

$$g'_y(1, 0, \kappa, \lambda) > 0. \tag{3.9}$$

H3. $G_i(\kappa, \lambda) \in C^{m+\tau}(K \times \Lambda), \qquad i = 1, 2, ..., k-1.$

COMMENTS

i) Conditions (3.6), (3.7) make Eq. (3.1) and the limit values (3.2)–(3.4) compatible.

ii) Conditions (3.8), (3.9) are crucial for our considerations. They mean that the rest points (0,0) and (1,0) in the (y, y') - plane are saddle points.

Equation (3.1) is autonomous, i.e. if $y(\xi)$ is its solution so is $y(\xi + c)$, for any constant c. To get rid of this ambiguity we impose an additional condition:

$$y(0, \lambda) = \frac{1}{2}[y(-\infty, \lambda) + y(+\infty, \lambda)] = \frac{1}{2}. \tag{3.10}$$

Our aim is to prove that, roughly speaking, if $y_0(\xi), \kappa_0 \in \mathrm{R}^k, \lambda_0 \in \mathrm{R}^l$ is a solution to (3.1)–(3.5) then, under some additional conditions to be specified, the problem has also a solution in a vicinity of λ_0. The Implicit Function Theorem seems to be the proper tool to perform this task, but some difficulty arises from the fact that the number of unknowns is greater than that of the equations. Elimination of this difficulty is possible owing to the fact that we are looking for special solutions, namely those which satisfy (3.2), (3.3) for any λ. It means that we have to be cautious and choose suitable functional spaces.

Since our course of action follows the Implicit Function Theorem we start, for the reader's convenience, from its presentation (cf. [12])

IMPLICIT FUNCTION THEOREM [12]. *Let*

(i) *X, Y, Z be normed affine spaces and $\mathfrak{X}, \mathfrak{Y}, \mathfrak{Z}$ the corresponding vector spaces;*

(ii) *$\mathcal{D}(\mathfrak{Y}, \mathfrak{Z})$ be the set of linear continuous mappings of the space $\mathfrak{Y}$ onto $\mathfrak{Z}$;*

(iii) *W be an open subset of $X \times Y$, and $(x_0, y_0) \in W, x_0 \in X, y_0 \in Y$;*

(iv) *$F : W \to Z$ be a continuous mapping of W onto Z and $F(x_0, y_0) = z_0$, $z_0 \in Z$.*

If

i) *for every fixed $x \in X$ and $(x, y) \in W$, the mapping F has the Fréchet derivative $F_y \in \mathcal{L}(\mathfrak{Y}, \mathfrak{Z})$;*

ii) *$F_y : W \to \mathcal{L}(\mathfrak{Y}, \mathfrak{Z})$ is a linear continuous mapping of W onto $\mathcal{L}(\mathfrak{Y}, \mathfrak{Z})$;*

iii) *the linear mapping $F_y(x_0, y_0) : \mathfrak{Y} \to \mathfrak{Z}$ has continuous inverse linear mapping.*

Then there are subsets $U \subset X$, $V \subset Y$ open in X, Y, respectively, $x_0 \in U$, $y_0 \in V$, such that for every $x \in U$ there is a unique element $y \in V$, denoted by $y = f(x)$, satisfying $f(x) \in V$, $F(x, f(x)) = z_0$, $f(x_0) = y_0$; $f(x)$ is a continuous mapping of U onto V.

If additionally, the Fréchet derivative $F_x(x_0, y_0)$ exists and is a linear continuous mapping of $\mathfrak{X}$ onto $\mathfrak{Z}$, then the mapping f is differentiable at the point x_0 and its Fréchet derivative is given by the formula

$$f'(x_0) = -F_y^{-1}(x_0, y_0) \circ F_x(x_0, y_0),$$

or implicitly

$$F_x(x_0, y_0) + F_y(x_0, y_0) \circ f'(x_0) = 0.$$

■

Now we define the spaces suitable for our problem.

DEFINITION 1. *The space $\mathfrak{X}$ is defined as the Euclidean space R^l with elements denoted by $\lambda \in \Lambda \subset R^l$, the affine space $X = A(R^l)$, where $A(R^n)$ denotes the affine space associated with R^n.* ■

The definitions of the other spaces are more complicated.

DEFINITION 2. *The set of functions $y(\xi) \in C^i(R^1)$, for $i = 0, 1, 2$, vanishing exponentially together with their first i derivatives as $|\xi| \to \infty$ we denote by $\mathcal{B}_i$; the norms are taken in the form*

$$\|y\|_i = \sup_{\xi \in R^1} \left(|y(\xi)| + \ldots + |y^{(i)}(\xi)| \right).$$

The subspace of $\mathcal{B}_i$ consisting of functions such that

$$y(0) = \frac{1}{2} [y(-\infty) + y(+\infty)] = 0$$

is denoted by $\mathcal{B}_i^0$. ■

Of course, $\mathcal{B}_i$ and $\mathcal{B}_i^0$ are Banach spaces.

DEFINITION 3. *The affine space B_2^0 associated with the normed vector space $\mathcal{B}_2^0$ is defined as the set of functions $y(\xi) \in C^2(R^1)$ satisfying exponentially* (3.2) *and such that $\lim_{|\xi|\to\infty} y^{(i)}(\xi) = 0$, $i = 1, 2$, also exponentially.* ■

DEFINITION 4. *The normed vector space $\mathcal{Y}$ is defined by the equality $\mathcal{Y} = \mathcal{B}_2^0 \times R^k$ with the usual product norm; the affine space Y associated with $\mathcal{Y}$ is defined by $Y = B_2^0 \times A(R^k)$.* ■

DEFINITION 5. *The normed vector space $\mathcal{Z}$ is defined by the equality $\mathcal{Z} = \mathcal{B}_0 \times R^{k-1}$ with the usual product norm; the affine space Z associated with $\mathcal{Z}$ is defined by $Z = B_0 \times A(R^{k-1})$.* ■

As to the mapping F mentioned in the Implicit Function Theorem, we take the pair $F = (A(y, \kappa, \lambda), G(\kappa, \lambda)) : X \times Y \to Z$, where $A(y)$ is defined by

$$A(y, \kappa, \lambda) = y'' - g(y, y', \kappa, \lambda).$$

Let $(y_0(\xi), \kappa_0, \lambda_0)$ be a solution to (3.1)–(3.5) with $y_0(\xi) \in \mathcal{B}_2^0$. The Fréchet derivative of F with respect to (y, κ) evaluated at this solution is equal to

$$D_{(y,\kappa)}F(y_0, \kappa_0, \lambda_0)(h, \Delta\kappa) = (L[y_0, \kappa_0, \lambda_0](h, \Delta\kappa), \nabla_k G(\kappa_0, \lambda_0) \cdot \Delta\kappa),$$

where $h \in \mathcal{B}_2^0$, $\Delta\kappa \in \mathrm{R}^k$, and the operator $L[y_0, \kappa_0, \lambda_0]$ is the Fréchet derivative of $A(y, \kappa, \lambda)$. Explicitly,

$$L[y_0, \kappa_0, \lambda_0](h, \Delta\kappa) = h'' - g'_z(y_0, y'_0, \kappa_0, \lambda_0)h'$$
$$-g'_y(y_0, y'_0, \kappa_0, \lambda_0)h - \nabla_\kappa g(y_0, y'_0, \kappa_0, \lambda_0) \cdot \Delta\kappa : \mathcal{Y} \to \mathcal{Z}.$$

Let $L_{\mathrm{hom}}[y_0, \kappa_0, \lambda_0]h$ denote the "homogeneous part" of $L[y_0, \kappa_0, \lambda_0]$, i.e.

$$L_{\mathrm{hom}}[y_0, \kappa_0, \lambda_0]h = h'' - g'_z(y_0, y'_0, \kappa_0, \lambda_0)h' \tag{3.11}$$
$$-g'_y(y_0, y'_0, \kappa_0, \lambda_0)h : \mathcal{B}_2^0 \to \mathcal{B}_0.$$

The adjoint operator $L^*_{\mathrm{hom}}[y_0, \kappa_0, \lambda_0] : \mathcal{B}_2^0 \to \mathcal{B}_0$ is defined by:

$$\int_{-\infty}^{+\infty} g(\xi)(L_{\mathrm{hom}}[y_0, \kappa_0, \lambda_0]h)(\xi)d\xi = \int_{-\infty}^{+\infty} (L^*_{\mathrm{hom}}[y_0, \kappa_0, \lambda_0]g)(\xi)h(\xi)d\xi$$

for any two functions g and h from $\mathcal{B}_2^0$ or, explicitly,

$$L^*_{\mathrm{hom}}[y_0, \kappa_0, \lambda_0]h = h'' + g'_z(y_0, y'_0, \kappa_0, \lambda_0)h' \tag{3.12}$$
$$-\left[g'_y(y_0, y'_0, \kappa_0, \lambda_0) - \frac{d}{d\xi}g'_z(y_0, y'_0, \kappa_0, \lambda_0)\right]h.$$

We have

PROPOSITION 1. [11] The equation

$$L_{\text{hom}}[y_0, \kappa_0, \lambda_0]h = 0 \tag{3.13}$$

has two linearly independent solutions of the class C^2:

$$h_1(\xi) = y_0'(\xi) \in \mathcal{B}_2^0 \qquad \text{and} \qquad h_2(\xi) = \vartheta(\xi), \tag{3.14}$$

where

$$\vartheta(\xi) = y_0'(\xi) \int_0^\xi \frac{d\zeta}{y_0'^2(\zeta)q(\zeta)}, \tag{3.15}$$

with

$$q(\xi) = q(\xi, \kappa, \lambda) = \exp\left[-\int_0^\xi g_z'(y_0(\zeta), y_0'(\zeta), \kappa, \lambda)d(\zeta)\right]. \tag{3.16}$$

PROPOSITION 2. In the class C^2, the equation $L_{\text{hom}}^*[y_0]h = 0$ has two linearly independent solutions which are

$$h_i^*(\xi) = h_i(\xi)q(\xi), \qquad i = 1, 2, \tag{3.17}$$

where $h_i(\xi)$ are given by (3.14), with $h_l^* \in \mathcal{B}_0^0$.

P r o o f. This result can be verified by a direct check.

PROPOSITION 3. The range of $L_{\text{hom}}[y_0, \kappa_0, \lambda_0]$ as an operator from $\mathcal{B}_2^0$ into $\mathcal{B}_0$ is

$$\mathcal{B}_0^\perp = \left\{h \in \mathcal{B}_0 : \int_{-\infty}^{+\infty} y_0'(\zeta)q(\zeta)h(\zeta)d\zeta = 0\right\}.$$

P r o o f. The result follows immediately from the definition of the adjoint operator $L_{\text{hom}}^*[y_0, \kappa_0, \lambda_0]$ and Proposition 2. The proof is complete.

PROPOSITION 4. The equation

$$L_{\text{hom}}[y_0, \kappa_0, \lambda_0]h = f \tag{3.18}$$

has a solution in $\mathcal{B}_2^0$ if and only if $f \in \mathcal{B}_0^\perp$. The solution is unique and given by

$$h(\xi) = \int_{-\infty}^{+\infty} K(\xi, \zeta)f(\zeta)d\zeta, \tag{3.19}$$

where

$$K(\xi, \zeta) = q(\zeta)\Big\{[H(-\zeta) - H(\xi - \zeta)]\vartheta(\zeta)y_0'(\xi) + \frac{1}{2}[H(\xi - \zeta) - H(\zeta - \xi)]\vartheta(\xi)y_0'(\zeta)\Big\},$$

$H(x)$ is the Heaviside step function

$$H(x) = \begin{cases} 1 & \text{for} \quad x > 0, \\ 0 & \text{for} \quad x < 0. \end{cases}$$

P r o o f. The first part of the statement follows from Proposition 3, whereas the second one is the result of the theory of linear differential equations [11].

THEOREM 1. *Let the functions* $g(y, z, \kappa, \lambda)$ *and* $G(\kappa, \lambda)$ *satisfy Hypotheses* H1–H3, *and let* $y_0(\xi) \in \mathcal{B}_2, \kappa_0 \in \mathrm{R}^k, \lambda_0 \in \mathrm{R}^l$ *be a solution to* (3.1)–(3.5). *If the determinant of the matrix*

$$D_\kappa(\kappa, \lambda) = \begin{pmatrix} \nabla_\kappa G_1(\kappa, \lambda) \\ \nabla_\kappa G_2(\kappa, \lambda) \\ \cdot \\ \cdot \\ \cdot \\ \nabla_\kappa G_{k-1}(\kappa, \lambda) \\ Q_\kappa(\kappa, , \lambda) \end{pmatrix}, \tag{3.20}$$

where

$$Q_\kappa(\kappa, \lambda) = \int_{-\infty}^{+\infty} y'(\zeta, \lambda) q(\zeta, \kappa, \lambda) \nabla_\kappa g(y(\zeta, \lambda), y'(\zeta, \lambda), \kappa, \lambda) d\zeta,$$

evaluated at $y(\xi, \lambda) = y_0(\xi), \kappa = \kappa_0, \lambda = \lambda_0$, *is different from zero, then*

1. *Problem* (3.1)–(3.5) *has a unique solution* $y = y(\xi, \lambda), \kappa = \kappa(\lambda)$ *for* $\xi \in \mathrm{R}^l$ *and* λ *contained in a vicinity of* λ_0, *such that for any fixed value of* λ $y(\xi, \lambda) \in \mathcal{B}_2^0$.

2. *These functions satisfy the equalities*

$$y(\xi, \lambda_0) = y_0(\xi), \qquad \kappa(\lambda_0) = \kappa_0.$$

3. *These functions are continuously differentiable* m *times with respect to* λ, *and the gradients* $\nabla_\lambda y(\xi, \lambda), \nabla_\lambda \kappa(\lambda)$ *are given by* (3.22) *and* (3.23), (3.24), *respectively.*

O u t l i n e o f t h e p r o o f

According to the Inverse Function Theorem it is sufficient to prove that the Fréchet derivative $D_{(y,\kappa)} F(y_0, \kappa_0, \lambda_0)$ has an inverse. Indeed, let us take $(f, \varphi) \in \mathcal{B}_0 \times \mathrm{R}^{k-1}$. We are looking for $(h, \Delta\kappa) \in \mathcal{B}_2^0 \times \mathrm{R}^k$ such that $D_{(y,\kappa)} F(y_0, \kappa_0, \lambda_0)(h, \Delta\kappa) = (f, \varphi)$. Explicitly, this equation is equivalent to the following system of linear equations:

$$\begin{aligned} L[y_0, \kappa_0, \lambda_0](h, \Delta\kappa) &= f, \\ \nabla_\kappa G(\kappa_0, \lambda_0) \cdot \Delta\kappa &= \varphi. \end{aligned} \tag{3.21}$$

The first equation is equivalent to

$$L_{\text{hom}}[y_0, \kappa_0, \lambda_0]h = \nabla_\kappa g(y_0, \kappa_0, \lambda_0) \cdot \Delta\kappa + f.$$

According to Proposition 4, this equation has a unique solution in $\mathcal{B}_2^0$ if and only if

$$\int_{-\infty}^{\infty} y_0'(\zeta) q(\zeta, \kappa_0, \lambda_0) \nabla_\kappa g(y_0(\zeta), y_0'(\zeta), \kappa_0, \lambda_0) d\zeta \cdot \Delta\kappa$$

$$= -\int_{-\infty}^{\infty} y_0'(\zeta) q(\zeta, \kappa_0, \lambda_0) f(\zeta) d\zeta.$$

This equation together with $(3.21)_2$ constitute a system of k linear algebraic equations for k unknowns $\Delta\kappa$. It has a unique solution if and only if the determinant of the matrix (3.20) is different from zero.

From the Implicit Function Theorem we obtain the following expressions for the derivatives $\nabla_\lambda y(\xi, \lambda)$ and $\nabla_\lambda \kappa(\lambda)$:

$$\nabla_\lambda y(\xi, \lambda) = \int_{-\infty}^{+\infty} K(\xi, \zeta) \nabla_\kappa g(y(\zeta, \lambda), y'(\zeta, \lambda), \kappa(\lambda), \lambda) d\zeta \cdot \nabla_\lambda \kappa(\lambda) \tag{3.22}$$

$$+ \int_{-\infty}^{+\infty} K(\xi, \zeta) \nabla_\lambda g(y(\zeta, \lambda), y'(\zeta, \lambda), \kappa(\lambda), \lambda) d\zeta,$$

and

$$\nabla_\kappa G(\kappa(\lambda), \lambda) \cdot \nabla_\lambda \kappa(\lambda) = -\nabla_\lambda G(\kappa(\lambda), \lambda), \tag{3.23}$$

$$Q_\kappa(\kappa(\lambda), \lambda) \cdot \nabla_\lambda \kappa(\lambda) = -Q_\lambda(\kappa(\lambda), \lambda). \tag{3.24}$$

The proof is complete. ■

4. Applications to phase change problems

We consider the following limit value problem:
find a function $w = w(\xi), \xi \in \mathrm{R}^1$, *satisfying the differential equation*

$$A(w)w'' + \frac{1}{2}A_w'(w)w'^2 + s\mu(w, s, w_l)w' + f(w, s, w_l) = 0 \tag{4.1}$$

and the conditions (2.16)–(2.18).

Here, $A(w)$ is assumed to be a strictly positive and continuously differentiable function defined for all $w > b$, and $\mu(w, s, w_l)$, $f(w, s, w_l)$ are defined by (2.14), (2.15), respectively. Also s, w_r, w_l, etc. are the same as in Sec. 2.

We introduce the transformation

$$w \to y(w, w_r, w_l) = \frac{\int_{w_l}^{w} \sqrt{A(\zeta)}d\zeta}{\int_{w_l}^{w_r} \sqrt{A(\zeta)}d\zeta}. \tag{4.2}$$

Since $A(\zeta) > 0$, then $y'_w(w, w_r, w_l) > 0$ for $w_l \leq w \leq w_r$, or $y'_w(w, w_r, w_l) < 0$ for $w_r \leq w \leq w_l$. Hence, this transformation has the inverse $y \to W(y, w_r, w_l)$ such that

$$W(0, w_r, w_l) = w_l, \qquad W(l, w_r, w_l) = w_r. \tag{4.3}$$

By applying transformation (4.2) to Eq. (4.1) we obtain for y an equation of the type (3.1) with

$$g(y, y', s, w_r, w_l) = -\frac{s\mu(W(y, w_r, w_l), s, w_l)}{A(W((y, w_r, w_l))}y' - \frac{f(W(y, w_r, w_l), w, w_l)}{\sqrt{A(W(y, w_r, w_l))}\int_{w_l}^{w_r} \sqrt{A(\zeta)}d\zeta}. \tag{4.4}$$

We check easily that $g(y, y', s, w_r, w_l)$ as defined by (4.4) satisfies Hypotheses H1, H2 formulated in the previous section. Let us also notice that (4.2) transforms the limit conditions (2.16)–(2.18) into (3.2)–(3.4), and (3.10) is a counterpart of

$$w(\xi = 0) = \frac{1}{2}(w_r + w_l). \tag{4.5}$$

We take w_l as the independent parameter λ of Sec. 3, and as the dependent parameters κ we take (s, w_r); the function $G(\kappa, \lambda)$ is assumed in the form:

$$G(s, w_r, w_l) = p(w_r, u_l - s(w_r - w_l)) - p(w_l, u_l) + s^2(w_r - w_l). \tag{4.6}$$

Then the equation $G(s, w_r, w_l) = 0$ expresses the Rankine-Hugoniot condition (2.19). The other parameters such as u_l, a, b are assumed to be fixed.

We can apply now the theory developed in the previous section to the present case of g given by (4.4), G defined by (4.6), and $k = 2$, $l = 1$, assuming of course that we know a solution $w_0(\xi)$, s_0, w_r^0, w_l^0 of (4.1) and (2.16)–(2.19), or equivalently, $y_0(\xi)$, s_0, w_r^0, w_l^0 of (3.1)–(3.5). Having done that we have to retransform the condition $D_\kappa \neq 0$ back to $w = W(y, w_r, w_l)$. However, we resign of doing that because we would obtain very complicated formulae. That is why we limit ourselves to the simpler but physically the most important case when the parameters s, w_r, w_l are near the Maxwell line. This is a particular phase

The first equation is equivalent to

$$L_{\text{hom}}[y_0, \kappa_0, \lambda_0]h = \nabla_\kappa g(y_0, \kappa_0, \lambda_0) \cdot \Delta\kappa + f.$$

According to Proposition 4, this equation has a unique solution in $\mathcal{B}_2^0$ if and only if

$$\int_{-\infty}^{\infty} y_0'(\zeta) q(\zeta, \kappa_0, \lambda_0) \nabla_\kappa g(y_0(\zeta), y_0'(\zeta), \kappa_0, \lambda_0) d\zeta \cdot \Delta\kappa$$

$$= -\int_{-\infty}^{\infty} y_0'(\zeta) q(\zeta, \kappa_0, \lambda_0) f(\zeta) d\zeta.$$

This equation together with $(3.21)_2$ constitute a system of k linear algebraic equations for k unknowns $\Delta\kappa$. It has a unique solution if and only if the determinant of the matrix (3.20) is different from zero.

From the Implicit Function Theorem we obtain the following expressions for the derivatives $\nabla_\lambda y(\xi, \lambda)$ and $\nabla_\lambda \kappa(\lambda)$:

$$\nabla_\lambda y(\xi, \lambda) = \int_{-\infty}^{+\infty} K(\xi, \zeta) \nabla_\kappa g(y(\zeta, \lambda), y'(\zeta, \lambda), \kappa(\lambda), \lambda) d\zeta \cdot \nabla_\lambda \kappa(\lambda) \tag{3.22}$$

$$+ \int_{-\infty}^{+\infty} K(\xi, \zeta) \nabla_\lambda g(y(\zeta, \lambda), y'(\zeta, \lambda), \kappa(\lambda), \lambda) d\zeta,$$

and

$$\nabla_\kappa G(\kappa(\lambda), \lambda) \cdot \nabla_\lambda \kappa(\lambda) = -\nabla_\lambda G(\kappa(\lambda), \lambda), \tag{3.23}$$

$$Q_\kappa(\kappa(\lambda), \lambda) \cdot \nabla_\lambda \kappa(\lambda) = -Q_\lambda(\kappa(\lambda), \lambda). \tag{3.24}$$

The proof is complete. ■

4. Applications to phase change problems

We consider the following limit value problem:
find a function $w = w(\xi), \xi \in \mathrm{R}^1$, *satisfying the differential equation*

$$A(w)w'' + \frac{1}{2}A_w'(w)w'^2 + s\mu(w, s, w_l)w' + f(w, s, w_l) = 0 \tag{4.1}$$

and the conditions (2.16)–(2.18).

Here, $A(w)$ is assumed to be a strictly positive and continuously differentiable function defined for all $w > b$, and $\mu(w, s, w_l)$, $f(w, s, w_l)$ are defined by (2.14), (2.15), respectively. Also s, w_r, w_l, etc. are the same as in Sec. 2.

We introduce the transformation

$$w \to y(w, w_r, w_l) = \frac{\int_{w_l}^{w} \sqrt{A(\zeta)}d\zeta}{\int_{w_l}^{w_r} \sqrt{A(\zeta)}d\zeta}. \tag{4.2}$$

Since $A(\zeta) > 0$, then $y'_w(w, w_r, w_l) > 0$ for $w_l \leq w \leq w_r$, or $y'_w(w, w_r, w_l) < 0$ for $w_r \leq w \leq w_l$. Hence, this transformation has the inverse $y \to W(y, w_r, w_l)$ such that

$$W(0, w_r, w_l) = w_l, \qquad W(l, w_r, w_l) = w_r. \tag{4.3}$$

By applying transformation (4.2) to Eq. (4.1) we obtain for y an equation of the type (3.1) with

$$g(y, y', s, w_r, w_l) = -\frac{s\mu(W(y, w_r, w_l), s, w_l)}{A(W((y, w_r, w_l))}y' - \frac{f(W(y, w_r, w_l), w, w_l)}{\sqrt{A(W(y, w_r, w_l))}\int_{w_l}^{w_r} \sqrt{A(\zeta)}d\zeta}. \tag{4.4}$$

We check easily that $g(y, y', s, w_r, w_l)$ as defined by (4.4) satisfies Hypotheses H1, H2 formulated in the previous section. Let us also notice that (4.2) transforms the limit conditions (2.16)–(2.18) into (3.2)–(3.4), and (3.10) is a counterpart of

$$w(\xi = 0) = \frac{1}{2}(w_r + w_l). \tag{4.5}$$

We take w_l as the independent parameter λ of Sec. 3, and as the dependent parameters κ we take (s, w_r); the function $G(\kappa, \lambda)$ is assumed in the form:

$$G(s, w_r, w_l) = p(w_r, u_l - s(w_r - w_l)) - p(w_l, u_l) + s^2(w_r - w_l). \tag{4.6}$$

Then the equation $G(s, w_r, w_l) = 0$ expresses the Rankine-Hugoniot condition (2.19). The other parameters such as u_l, a, b are assumed to be fixed.

We can apply now the theory developed in the previous section to the present case of g given by (4.4), G defined by (4.6), and $k = 2$, $l = 1$, assuming of course that we know a solution $w_0(\xi)$, s_0, w_r^0, w_l^0 of (4.1) and (2.16)–(2.19), or equivalently, $y_0(\xi)$, s_0, w_r^0, w_l^0 of (3.1)–(3.5). Having done that we have to retransform the condition $D_\kappa \neq 0$ back to $w = W(y, w_r, w_l)$. However, we resign of doing that because we would obtain very complicated formulae. That is why we limit ourselves to the simpler but physically the most important case when the parameters s, w_r, w_l are near the Maxwell line. This is a particular phase

It is reasonable due to the physical reasons to introduce the characteristic speeds $c_{\pm}(w,u)$ being an extension of the notion of the sound speed to general hyperbolic systems. In our case they are defined as the real solutions (if they do exist) of the quadratic equation [10]

$$c^2 - cp'_u(w,u) + p'_w(w,u) = 0.$$

We have

$$p'_w(w,u) = c_-(w,u)c_+(w,u). \tag{4.20}$$

Using (4.17) and (4.20) in (4.15), (4.16) we obtain

i) if $w_l = w_m$:

$$\left[\int_{w_m}^{w_M} \mu(\zeta,u_l)\sqrt{-\frac{2}{A(\zeta)}\int_{w_m}^{\zeta} f(\xi,0,w_m)d\xi d\zeta}\right. \tag{4.21}_1$$

$$\left. - \int_{w_m}^{w_M} (\zeta - w_m)p'_u(\zeta,u_l)d\zeta\right] \frac{ds}{dw_l}\bigg|_{w_l=w_m}$$

$$= (w_M - w_m)c_-(w_m,u_l)c_+(w_m,u_l),$$

$$\frac{dw_r}{dw_l}\bigg|_{w_l=w_m} = \frac{c_-(w_m,u_l)c_+(w_m,u_l)}{c_-(w_M,u_l)c_+(w_M,u_l)}; \tag{4.22}_1$$

and

ii) if $w_l = w_M$,

$$\left[\int_{w_m}^{w_M} \mu(\zeta,u_l)\sqrt{-\frac{2}{A(\zeta)}\int_{w_m}^{\zeta} f(\xi,0,w_m)d\xi d\zeta}\right. \tag{4.21}_2$$

$$\left. - \int_{w_m}^{w_M} (w_M - \zeta)p'_u(\zeta,u_l)d\zeta\right] \frac{ds}{dw_l}\bigg|_{w_l=w_M}$$

$$= -(w_M - w_m)c_-(w_M,u_l)c_+(w_M,u_l),$$

$$\frac{dw_r}{dw_l}\bigg|_{w_l=w_M} = \frac{c_-(w_M,u_l)c_+(w_M,u_l)}{c_-(w_m,u_l)c_+(w_m,u_l)} + \left(\frac{1}{c_-(w_M,u_l)} + \frac{1}{c_+(w_M,u_l)}\right) \tag{4.22}_2$$

$$(w_M - w_m)\frac{ds}{dw_l}\bigg|_{w_l=w_m}.$$

Let us notice that, in general, the coefficient of ds/dw_l in (4.21) can vanish for some value u_l^* of u_l. Unfortunately it is difficult to determine all such critical values of this parameter due to the complexity of the equation resulting from equating this coefficient to zero. That is why we limit ourselves to two particular, but important, cases for which we can explain this problem.

EXAMPLE 1. In many papers ([1 – 4, 6]), so-called *isothermal phase transitions* were discussed. In this case

$$p'_u(w,u) \equiv 0. \tag{4.23}$$

Due to that the problem of the critical values of u_l does not exist and we obtain from (4.21)

$$\left.\frac{ds}{dw_l}\right|_{w_l=w_m} = -\frac{(w_M - w_m)c^2(w_m)}{\int\limits_{w_m}^{w_M} \mu(\zeta,u_l)\sqrt{-\dfrac{2}{A(\zeta)}\int\limits_{w_m}^{\zeta} f(\xi,0,w_m)d\xi d\zeta}}, \tag{4.24}_1$$

$$\left.\frac{dw_r}{dw_l}\right|_{w_l=w_m} = \frac{c^2(w_m)}{c^2(w_M)}, \tag{4.25}_1$$

or

$$\left.\frac{ds}{dw_l}\right|_{w_l=w_M} = \frac{(w_M - w_m)c^2(w_M)}{\int\limits_{w_m}^{w_M} \mu(\zeta,u_l)\sqrt{-\dfrac{2}{A(\zeta)}\int\limits_{w_M}^{\zeta} f(\xi,0,w_m)d\xi d\xi}}, \tag{4.24}_2$$

$$\left.\frac{dw_r}{dw_l}\right|_{w_l=w_M} = \frac{c^2(w_M)}{c^2(w_m)}. \tag{4.25}_2$$

Here, we made use of the fact that in the isothermal case

$$c_+(w,u) = c(w) = -c_-(w,u),$$

where

$$c(w) = \sqrt{-p'_w(w)}.$$

Formulae (4.24), (4.25) generalise the corresponding expressions obtained by TRUSKINOVSKY [2], who assumed additionally that $A(w) = \text{const}$ and $\mu(w,u) = \text{const}$.

EXAMPLE 2. *The model equations of hydrodynamics* [10, 11]. In this case $p(w,u)$ is given by Eq. (2.3). We have

$$-\int_{w_m}^{w_M}(\zeta-w_m)p'_u(\zeta,u_l)d\zeta = u_l\int_{w_m}^{w_M}\frac{\zeta-w_m}{\zeta-b}d\zeta,$$

$$-\int_{w_m}^{w_M}(w_M-\zeta)p'_u(\zeta,u_l)d\zeta = u_l\int_{w_m}^{w_M}\frac{w_M-\zeta}{\zeta-b}d\zeta.$$

We see that in both cases the coefficient of ds/dw_l is positive for $u_l \geq 0$. Hence, it remains positive for negative (but sufficiently close to zero) values of this parameter. Unfortunately, we are unable to say whether the discussed coefficient can vanish for some negative u_l. Consequently, we can claim only that, *at least for small values of* $|u_l|$ *and for* w_l *close to* $w_m = w_m(u_l)$ *or* $w_M(u_l)$ (we remind that the solutions of (4.7), (4.8) depend on u_l), *the solution to the problem* (2.13)–(2.19) *exists, is unique and is differentiable with respect to* w_l.

Of course, we can take the right state of equilibrium w_r or the speed s as the independent parameter and (s,w_l) or, respectively, (w_l,w_r) as the dependent ones and obtain a similar theorem. But from our theory we can deduce more. Namely, we have $\left.\frac{ds}{dw_l}\right|_{w_l=w_m} > 0$ and $\left.\frac{ds}{dw_l}\right|_{w_l=w_M} < 0$, at least in the considered examples. Also we can use the Taylor formula, as we have proved the existence of all the necessary derivatives, to obtain

$$s(w_l) = \begin{cases} (w_l-w_m)\left.\frac{ds}{dw_l}\right|_{w_l=w_m} + O\left((w_l-w_m)^2\right), \\ (w_l-w_M)\left.\frac{ds}{dw_l}\right|_{w_l=w_M} + O\left((w_l-w_M)^2\right). \end{cases} \tag{4.26}$$

This is the so-called "normal growth" approximation [2] introduced intuitively on physical grounds.

In this way we obtain the following conclusions:

The speed of the phase boundary is positive if either $w_l < w_m$ *and* w_l *is close to* w_m *(condensation), or* $w_l > w_M$ *and* w_l *is close to* w_M *(evaporation).*

The speed of the phase boundary is negative if either $w_l > w_m$ *and* w_l *is close to* w_m *(evaporation), or* $w_l < w_M$ *and* w_l *is close to* w_M *(condensation).*

The above results constitute an extension of a theorem proved by SHEARER [6].

References

1. R. ABEYARATNE and J. K. KNOWLES, *Implications of viscosity and strain-gradient effects for the kinetics of propagating phase boundaries in solids*, SIAM J. Appl. Math., **51**, 5, 1205–1211, 1991.

2. L. TRUSKINOVSKY, *About the "normal growth" approximation in the dynamical theory of phase transitions*, Continuum Mech. Thermodyn., **6**, 185–208, 1994.

3. M. SLEMROD, *Admissibility criteria for propagating boundaries in a van der Waals fluid*, Arch. Rational Mech. and Anal., **81**, 301–315, 1983.

4. R. HAGAN and M. SLEMROD, *The viscosity-capillarity admissibility criterion for shocks and phase transitions*, Arch. Rational Mech. and Anal., **83**, 333–361, 1983.

5. M. SLEMROD, *Dynamic phase transitions in a van der Waals fluid*, J. Differential Equations, **52**, 1–23, 1984.

6. M. SHEARER, *Dynamic phase transitions in a van der Waals gas*, Quarterly of Appl. Math., **46**, 4, 631–636, 1987.

7. M. GRINFELD, *Nonisothermal dynamic phase transitions*, Quarterly of Appl. Math., **47**, 1, 71–84, 1989.

8. K. MISCHAIKOV, *Dynamic phase transitions: a connection matrix approach*, [in:] Nonlinear Evolution Equations that Change Type, B. L. KEYFITZ, M. SHEARER [Eds.], 164–180, Springer-Verlag, Berlin 1990.

9. K. PIECHÓR, *A four-velocity model for van der Waals fluids*, Arch. Mech. **47**, 5, 1089–1111, 1995.

10. K. PIECHÓR, *Travelling wave solutions to model equations of van der Waals fluids*, Arch. Mech., **48**, 675–709, 1996.

11. PH. HARTMAN, *Ordinary differential equations*, J. Wiley and Sons Inc., New York 1964.

12. L. SCHWARTZ, *Analyse Mathématique*, vol. I, Hermann, Paris 1967.

POLISH ACADEMY OF SCIENCES
INSTITUTE OF FUNDAMENTAL TECHNOLOGICAL RESEARCH
e-mail: kpiechor@ippt.gov.pl

Received August 18, 1997.

Arch. Mech., 50, 5, pp. 829–847, Warszawa 1998
FIFTY YEARS OF THE ARCHIVES OF MECHANICS

On efficiency of identification of a stochastic crack propagation model based on Virkler experimental data

Z. A. KOTULSKI (WARSZAWA)

In the paper we concentrate on one aspect of the experimental design: how the information coming from an experiment can be utilised for identification of a specific mathematical model. To express the consistency of the data and the model we need some quality measure, allowing to transform our intuition to numbers. As the mathematical tool we propose a version of the statistical procedure of cross-validation of the data. Then we verify the efficiency of the suggested method on the example of the Virkler experimental data of stochastic crack growth and the mathematical model of Paris-Erdogan of the fatigue crack growth.

1. Introduction

Experimental data constitute a basis of the mathematical modelling of physical phenomena. Trying to identify the model's parameters we always ask the question if the data are sufficiently reliable for the applied mathematical procedure. Development of mathematical statistics achieved in recent years made it possible to perform methodologically consistent reasoning to decide whether the obtained experimental results are useful for the proposed model and inversely – whether the model is adequate for the experimental data.

The purpose of the paper is to propose a method of verification of the quality of experimental data coming from some physical phenomenon for identification of a certain mathematical model of this phenomenon. (The same purpose can be written in an inverse way: what is the quality of a certain mathematical model for description of a physical phenomenon generating the observed set of numerical data). After general remarks on collecting the empirical data, we concentrate on a particular model of stochastic crack growth. We make an attempt to verify if the Virkler experimental curves of crack growth can be used for identification of the Paris-Erdogan model of the stochastic crack propagation [10]. The method applied for this purpose is the cross-validation method of verification of predictability of the measured data, widely applied in mathematical statistics (see [1, 5, 11, 12]). At the beginning we present the general (non-linear) formulation of the cross-validation technique. Next we formulate the problem in a linear case and present the formulae for estimation of the linear model parameters when some measurements are missing. Finally we apply the proposed procedure to verification of the Virkler data being the source of knowledge for the simplified Paris-Erdogan model of the stochastic crack growth.

2. Experiment's design and reliability of experimental data

Researchers using experimental data for verification of the mathematical models of physical phenomena have always a dilemma: to make their own experiment or to apply experimental data available in the literature. In both cases they encounter several methodological and technical problems.

Constructing our own experiment, we can do this according to all the rules known as the design of experiment in a way optimal for the specific mathematical model considered [6]. To plan the experiment, one should:

- select the model variables that must be identified;
- select the set of treatments (different factors whose effects are being compared) effecting on the measured quantities;
- specify the experimental material to which the treatments are to be applied;
- construct or select the rules according to which the measured data are connected with the model parameters;
- manipulate the treatments (increase the number of samples, modify the range of controlled experiment parameters, etc.) in such a way that finally, the identified model is possibly complete.

We realise that, in spite of the fact that there is a temptation to manipulate the results of the experiment to improve the quality of identification and validation of the mathematical model (interesting remarks on possible tricks and methods of detecting such manipulations can be found in [9]), one can also really modify the experiment to improve its results. However, sometimes the objective reasons (high cost of experiment, difficulties in keeping constant experiment's conditions, unexpected noises during measurements, etc.) make that the collected data are not satisfactory and one feels to be obliged to verify their validity.

Applying in the modelling procedure the experimental data taken from literature, researchers meet quite different problems. First of all, they never know all the conditions of the experiment. However, even if the description of the experiment itself and of the presented data is sufficient for the modelling purpose, they reach a fundamental barrier: the number of data samples is fixed and cannot be increased by continuation of the experiment. Then they should always answer questions like: Is the set of the experimental data sufficiently large? What would be the effect of estimation if we had more data from the experiment? In other words, one must answer the question if the available experimental data set is sufficiently representative for identification of the proposed mathematical model.

The heuristic idea of verification of experimental data as the basis of identification of the selected mathematical model (the estimation of its parameters) can be formulated in a mathematical way. An example of such a procedure is presented in the following sections.

3. Cross-validation method and estimation

The cross-validation is a method of verifying the consistency of experimental data. In this method we choose two different subsamples from the data sample. One subsample is applied for estimation of the system parameters, the other is used as a reference set to control the quality of estimation. This procedure lets us to test two facts: the integrity of the experimental data (the data sample is in some sense homogeneous if both subsamples of it give similar estimation results), and correctness of the estimation procedure (the algorithm gives similar results for two different subsamples of data taken from the same population).

The standard cross-validation procedure can be modified for any particular problem and any expected purpose of it. Now we present a version of this method useful for verification of the measurements obtained from an experiment.

Consider the following two-dimensional time series:

$$(y_i, x_i), \qquad i = 1, 2, ..., n, \tag{3.1}$$

where the elements of the sequence represent, respectively: x_i – the observed data points, y_i – the values of the process being estimated.

Assume that we know some number of the data pairs $(y_i, x_i), i = 1, 2, ..., n$; we call them the observation history S. Assume also that for the given observation history we can construct the estimator $\hat{y}(x, \boldsymbol{\alpha}, S)$ of the random variable y based on the observation x (the value of the process corresponding to the observation x). In this estimator, the parameter $\boldsymbol{\alpha} \in \mathbf{A}$ ($\boldsymbol{\alpha}$ is some scalar, vector or matrix parameter taking its values from a certain set of parameters $\mathbf{A}$) describes the dependence of the values of the process y_i on the data points x_i, for $i = 1, 2, ..., n$, and it depends on the history S. Parameter $\boldsymbol{\alpha}$ should be also estimated during (or before) the estimation of y. Using the constructed estimator we make an attempt to verify the quality of experimental data using the following cross-validation type procedure.

Consider n observation data points. Assume that a subsample of $n - 1$ data points is used for the estimation of the parameter $\boldsymbol{\alpha}$. We estimate this parameter n times, every time omitting another point. We are interested, how much the omitted data points influence the quality of estimation of $\boldsymbol{\alpha}$ and, consequently, of the process y. To answer this question we define the following scheme of reasoning.

The cross-validation algorithm

I. Estimate the parameter using n-1 samples, minimising the following functional:

$$L(\boldsymbol{\alpha}) = \frac{1}{n-1} \sum_{j=1,2,...i-1,i+1,...,n} L\left[y_j, \hat{y}(x_j, \boldsymbol{\alpha}, S_{/i})\right], \tag{3.2}$$

where $L[\ ,\ ]$ is some loss function and $S_{/i}$ is the observation history of $n-1$ pairs, where the pair (y_i, x_i) is omitted.

II. Apply the procedure of point **I** n times for $i = 1, 2, ..., n$. For each step, fix the estimated value of the parameter α as:

$$\tilde{\alpha} = \tilde{\alpha}(S_{/i}), \quad i = 1, 2, ..., n. \tag{3.3}$$

III. Estimate the states of the observed process y according to the assumed estimation formula, where the parameter is taken as $\tilde{\alpha} = \tilde{\alpha}(S_{/i})$, that is calculate the values $\hat{y}(x_i, \tilde{\alpha}(S_{/i}), S_{/i}), i = 1, 2, ..., n$, minimising the expression:

$$C(S) = \frac{1}{n} \sum_{i=1}^{n} L\left[y_i, \hat{y}(x_i, \tilde{\alpha}(S_{/i}), S_{/i})\right]. \tag{3.4}$$

The value of $C(S)$ calculated in (3.4) for the obtained values of the estimators gives us the quality measure of the estimation procedure.

IV. Estimate the reference values of the process using all the history S. We obtain them by minimising the following functional:

$$C_{\mathrm{ref}}(S) = \frac{1}{n} \sum_{i=1}^{n} L\Big[y_i, \hat{y}(x_i, \alpha(S), S)\Big]. \tag{3.5}$$

Let us remark that in some cases the procedure (3.5) using the complete history S, can give the exact estimated values of the process y, that is $\hat{y}(x_i, \alpha(S), S) = y_i$ and, consequently, $C_{\mathrm{ref}}(S) = 0$. However, for some specific estimators this can not be satisfied, and then we should compare the measures (3.4) and (3.5).

The cross-validation procedure enables us to verify the integrity of the experimental data. It detects, how much information about a single measurement is contained in the rest of the measurements of the observation history. If in the data population there are some outstanding results, they will contribute a significant income to the quality measure (3.4). When the observation history contains a lot of such data points, the value of $C(S)$ becomes much greater than $C_{\mathrm{ref}}(S)$ and we can expect that any increase of the number of data points in the identification procedure can effect in a significant change of the model parameters being estimated.

Let us remark that the procedure of cross-validation is performed for a finite number of data points n. The number n growing to infinity in the validation procedure does not guarantee the convergence of the quality measure $C(S)$.

In the above procedure we have assumed as a reference set, the one-point subsamples. In general one can do this by estimating the model parameter $\alpha \in \mathbf{A}$

and omitting several data points, and then in the verification step using the entire experiment history S. In Sec. 8 we apply such a method at a practical example.

4. Linear estimation for non-complete set of experimental data

In this section we consider the known linear estimation procedure. It proves to be very useful for the cross-validation technique in the case when the process is linearly dependent on the model parameters.

Assume that we have the following set of observations:

$$x_i, \qquad i = 1, 2, ..., n. \tag{4.1}$$

The process to estimate is denoted by:

$$y_i(\boldsymbol{\alpha}), \qquad i = 1, 2, ..., n, \tag{4.2}$$

where $\boldsymbol{\alpha}$ is the (vector) parameter to be fixed during the estimation procedure.

Since the model is assumed to be linear, the process y can be represented as:

$$y_i = \sum_{j=1}^{p} A_{ij}, \alpha_j, \qquad i = 1, 2, ..., n. \tag{4.3}$$

The values of the observations x and the process y are connected by the following observation equation:

$$x_i = y_i + e_i, \qquad i = 1, 2, ..., n, \tag{4.4}$$

or

$$x_i = \sum_{j=1}^{p} A_{ij}\alpha_j + e_i, \qquad i = 1, 2, ..., n, \tag{4.5}$$

where $A_{ij}, i = 1, 2, ..., n, j = 1, ..., p$ are the elements of the system matrix, and $e_i, i = 1, 2, ..., n$ are the elements of the random disturbance (noise) vector.

The formulation of the estimation problem

We assume that our observation process (set of n observations) can be written down in the following matrix form [6]:

$$\mathbf{x} = \mathbf{A}\boldsymbol{\alpha} + \mathbf{e}, \tag{4.6}$$

where

$$\mathbf{x} = (x_1, x_2, ..., x_n)^T \tag{4.7}$$

is the observation vector,

$$\mathbf{A} = \begin{bmatrix} A_{11} & \dots & A_{1p} \\ . & . & . \\ . & . & . \\ . & . & . \\ A_{n1} & \dots & A_{np} \end{bmatrix} \tag{4.8}$$

is the system matrix,

$$\boldsymbol{\alpha} = (\alpha_1, \dots, \alpha_p)^T \tag{4.9}$$

is the vector of parameters to estimate,

$$\mathbf{e} = (e_1, \dots, e_n) \tag{4.10}$$

is the noise (random disturbance or error) vector.

For the efficiency of the model it is assumed that

- A_{ij}, the elements of the system matrix, are some known constants
- x_i, the elements of the observation vector, are normally distributed;
- x_i are independent;
- all the variables x_i have identical variance σ^2.

From the above conditions we can deduce that the elements e_i of the noise vector are Gaussian, independent random variables (we assume: with a zero mean) and with identical variance σ^2.

To complete the vector formulation of the problem we rewrite equation (4.3) in the form

$$\mathbf{y} = \mathbf{A}\boldsymbol{\alpha}. \tag{4.11}$$

Then the estimated value the process is

$$\hat{\mathbf{y}} = \mathbf{A}\hat{\boldsymbol{\alpha}}, \tag{4.12}$$

where $\hat{\boldsymbol{\alpha}}$ is the estimated value of the control parameter $\boldsymbol{\alpha}$.

If the rank of the coefficient (system) matrix $\mathbf{A}$ is p, then the matrix $\mathbf{A}^T\mathbf{A}$ is non-singular and the mean-square linear estimator $\hat{\boldsymbol{\alpha}}$ can be expressed as:

$$\hat{\boldsymbol{\alpha}} = (\mathbf{A}^T\mathbf{A})^{-1}\mathbf{A}^T\mathbf{x}. \tag{4.13}$$

Having introduced the basic definitions and facts, we are ready to present the linear version of the scheme of cross-validation analogous to the one presented in the previous section. However, in the linear case we assume the reference subsample as a certain k-element subset of the observation history.

Consider the observations $x_1, x_2, \dots, x_n$. Assume that the observations x_1, $x_2, \dots, x_{n-k}$ are used for the estimation of the model parameter $\boldsymbol{\alpha}$, and that

$x_{n-k+1}, ..., x_n$ are omitted in this procedure. Then the matrices and vectors in the state equation (4.6) can be reduced to the following form:

$$\mathbf{x} = \begin{bmatrix} \mathbf{x}_1 \\ \mathbf{x}_2 \end{bmatrix}, \qquad \mathbf{A} = \begin{bmatrix} \mathbf{A}_1 \\ \mathbf{A}_2 \end{bmatrix}, \qquad \mathbf{e} = \begin{bmatrix} \mathbf{e}_1 \\ \mathbf{e}_2 \end{bmatrix}, \tag{4.14}$$

where

$$\mathbf{x}_1 = (x_1, ..., x_{n-k})^T, \tag{4.15}$$

$$\mathbf{x}_2 = (x_{n-k+1}, ..., x_n)^T. \tag{4.16}$$

The other matrices and vectors are uniquely defined by this division of the observation vector.

By assumption (last k observations are missing) we find the mean-square estimator of the parameter from the following state equation:

$$\mathbf{x}_1 = \mathrm{A}_1 \boldsymbol{\alpha} + \mathbf{e}_1, \tag{4.17}$$

that is $\boldsymbol{\alpha}$ is the solution of the following normal equation:

$$\mathbf{A}_1^T \mathbf{A}_1 \hat{\boldsymbol{\alpha}} = \mathbf{A}_1^T \mathbf{x}_1. \tag{4.18}$$

If $\hat{\boldsymbol{\alpha}}$ is the calculated value of the estimator, then we assume

$$\mathbf{x}_2 = \mathbf{A}_2 \tilde{\boldsymbol{\alpha}}, \tag{4.19}$$

as a substitute for the missing observations. Since the normal equation for the complete system is

$$\mathbf{A}_1^T \mathbf{A}_1 \boldsymbol{\alpha} + \mathbf{A}_2^T \mathbf{A}_2 \boldsymbol{\alpha} = \mathbf{A}_1^T \mathbf{x}_1 + \mathbf{A}_2^T \mathbf{x}_2, \tag{4.20}$$

we assume the observed process in the form

$$\begin{bmatrix} \mathbf{y}_1 \\ \mathbf{y}_2 = \mathbf{A}_2 \tilde{\boldsymbol{\alpha}} \end{bmatrix}, \tag{4.21}$$

and now $\tilde{\boldsymbol{\alpha}}$ is also the solution of the normal equation.

Let us remark that the quality measure used in calculation of $\tilde{\boldsymbol{\alpha}}$ is:

$$C(S) = \frac{1}{n-k} \sum_{i=1}^{n-k} (x_i - A_{i1}\alpha_1 - ... - A_{ip}\alpha_p)^2. \tag{4.22}$$

It is seen that the above formulae (after the appropriate permutation of the variables) can be used for calculations in the cross-validation method presented in Sec. 3 in the linear case.

Let us remark that the procedure of linear estimation of parameters is (under quite general assumptions) asymptotically convergent, that is, if in (4.13) we take into account a sufficiently great number of observations, we obtain as a result the almost exact value of the expectation of the parameter α. However, in our considerations we deal with a finite number of observations and, moreover, apply this estimator at the algorithm of cross-validation which is not convergent itself (see previous Sec. 3). Therefore the cross-validation procedure gives us only qualitative information about the experimental data.

5. Mathematical model of crack growth

In the literature, various models of stochastic crack growth are used [10]. For the purpose of presentation of the cross-validation method we adopt one of the classical models. Consider the following randomised Paris-Erdogan equation for the fatigue crack growth under homogeneous cyclic stressing [2, 3]:

$$\Delta a = XC(\Delta K)^m, \tag{5.1}$$

with

$$\Delta K = \Delta\sigma F\left(\frac{a}{b}\right)\sqrt{\pi a}, \tag{5.2}$$

$$F\left(\frac{a}{b}\right) = \frac{1}{\sqrt{\cos\pi\dfrac{a}{b}}}, \qquad \text{for } \frac{a}{b} < 0.7, \tag{5.3}$$

where: a is the crack length, b is the specimen width, Δa is the increment of crack length caused by a single stress cycle, ΔK is the range of the stress intensity at the crack tip, C, m are constants depending on the specimen material, $\Delta\sigma$ is the stress range, X is a random variable changing independently from one crack increment to another, and satisfying the following conditions:

$$E\{X\} = 1, \qquad E\left\{(X-1)^2\right\} = \delta. \tag{5.4}$$

The process of the stochastic crack growth modelled by the discrete randomised Paris-Erdogan equation (5.1)–(5.3) can be equivalently described by the following continuous stochastic differential equation [2, 3]:

$$\frac{da}{\left(F\left(\dfrac{a}{b}\right)\sqrt{\pi a}\right)^m} = C(\Delta\sigma)^m(1+\xi(t))dt. \tag{5.5}$$

Equation (5.5) has been obtained from (5.1) under the following essential assumption on the random variable X:

$$X = 1 + \xi(t), \tag{5.6}$$

where $\xi(t)$ is a white noise with a zero mean and the intensity δ. The time parameter t is considered to be the number of cycles of the external excitation of the material sample.

Equation (5.5) can be integrated at time intervals $[N_i, N_{i+1}]$ and the corresponding crack length intervals $[a_i, a_{i+1}]$ for the whole specimen life-time $(i = 1, 2..., n)$:

$$\int_{a_{N_i}}^{a_{N_{i+1}}} \left[F\left(\frac{x}{b}\right)\sqrt{\pi x}\right]^{-m} dx = C(\Delta\sigma)^m \int_{N_i}^{N_{i+1}} [1 + \xi(t)]dt. \tag{5.7}$$

Then we can write down the above equation in the following form:

$$[\Phi(a_{N_{i+1}} + a_{N_i})]^{-m} (a_{N_{i+1}} - a_{N_i}) = C(\Delta\sigma)^m (N_{i+1} - N_i)\eta_{i,i+1}, \tag{5.8}$$

where $\eta_{i,i+1}$ is a Gaussian random variable with

$$E\{\eta_{i,i+1}\} = 1, \qquad \mathrm{Var}\{\eta_{i,i+1}\} = \frac{\delta}{N_{i+1} - N_i}, \tag{5.9}$$

and

$$\Phi(a_{N_{i+1}} + a_{N_i}) = F\left(\frac{a_{N_{i+1}} + a_{N_i}}{2b}\right)\sqrt{\pi\frac{a_{N_{i+1}} + a_{N_i}}{2}}. \tag{5.10}$$

Calculating the natural logarithm (logarithm to base e) of the integrated crack growth equation (5.8), we obtain the following:

$$\ln(a_{N_{i+1}} - a_{N_i}) - \ln(N_{i+1} - N_i) = \ln\left[\Phi(a_{N_{i+1}} + a_{N_i})\Delta\sigma\right] m + \ln C + \zeta_{i,i+1}. \tag{5.11}$$

Now, using the experimental measurements $(a_{N_i}, N_i), i = 1, 2, ..., n$, we want to estimate the model parameters m and $\ln C$. Since the model is linear with respect to these parameters, we must adopt the method of linear estimation presented in Sec. 4 for equation (5.11). We identify the terms in equation (5.11) as:

$$x_i = \ln(a_{N_{i+1}} - a_{N_i}) - \ln(N_{i+1} - N_i), \tag{5.12}$$

$$A_{i1} = \ln\left[\Phi(a_{N_{i+1}} + a_{N_i})\Delta\sigma\right], \tag{5.13}$$

$$A_{i2} = 1, \tag{5.14}$$

$$\alpha_1 = m, \tag{5.15}$$

$$\alpha_2 = \ln C. \tag{5.16}$$

In the above we have assumed that random fluctuations of the crack length increments are small in comparison with the crack length, and the coefficients A_{ik} can be considered as deterministic constants. Moreover, for simplicity, we assume that the random variables representing the growth disturbance (noise)

$$c_i = \zeta_{i,i+1}, \tag{5.17}$$

are Gaussian with a zero mean and with equal variances σ^2. In the formulation of the model, in formula (5.9), we have assumed that the variances of the noises are of the form:

$$\operatorname{Var}\{\eta_{i,i+1}\} \approx \frac{\delta}{N_{i+1} - N_i}. \tag{5.18}$$

We know that, under realistic values of the numbers of cycles N_i, these variances are small and the denominators $N_{i+1} - N_i$, in (5.18) do not differ too much for all i. Therefore we can assume that the variances of random variables $\zeta_{i,i+1} = \ln \eta_{i,i+1}$ are for all i (approximately) equal:

$$\operatorname{Var}\{\zeta_{i,i+1}\} \approx \sigma^2 \tag{5.19}$$

and, moreover, the distribution of $\zeta_{i,i+1}$ can be approximately considered to be Gaussian.

6. Experimental data and estimation of the model parameters

As it is seen from the previous section, the parameters to be estimated in our simplified stochastic crack propagation model are m and $\ln C$. Now we must construct the numerical procedure of the parameter identification. We know that m and $\ln C$ are random variables and the algorithm must take this fact into account. Therefore we apply the statistical method of conditioning [7] for this model. This means that our procedure of identification of the statistical distribution of the pair $(m, \ln C)$ will be performed in the following two steps.

STEP 1. We consider the trajectory of the stochastic crack growth for the fixed elementary event $\omega' \in \Omega$. We assume, that this trajectory is governed by the Paris-Erdogan randomised equation (5.1) with the parameters $(m(\omega'), \ln C(\omega'))$. Using the crack growth model defined in Sec. 5 and the parameters estimation schedule from Sec. 4, we calculate the numerical values of the parameters $(m(\omega'), \ln C(\omega'))$.

STEP 2. We repeat the procedure of Step 1 for all the trajectories collected at the experiment (observed elementary events $\omega_i \in \Omega$)) obtaining the set of pairs $(m(\omega_i), \ln C(\omega_i))$, for $\omega_i \in \Omega$. Using the estimated values of the parameters $(m(\omega_i), \ln C(\omega_i))$, we identify the probabilistic distribution of the two-dimensional random variable $(m, \ln C)$.

REMARK. Let us remark that if the above procedure is applied for estimation of the value of the parameter $C(\omega)$ (or its mean value), then the proposed algorithm introduces some additional error of estimation. It is connected with this fact that

$$E(\ln C(\omega)|\text{measurements}) \neq \ln E(C(\omega)|\text{measurements}), \tag{5.20}$$

what means that the distributions (and, what it follows, the moments) of two random variables: the estimated value of $\ln C(\omega)$ and the random variable being the logarithm of the estimated value of $C(\omega)$ – are not equal. The difference of the above distributions is quite small if the variance of the estimated parameter $C(\omega)$ of the model is small. Finally let us remark that in our method of validation of the experimental data we use only one of the parameters ($\ln C(\omega)$, not $C(\omega)$), so we avoid a danger of inaccuracy caused by non-linear transformation of distributions.

7. Modelling stochastic crack growth using experimental data

The experiment of measurement of the stochastic crack growth is very complicated. It requires rigorous preparation of the material samples, exact repetition of excitations, environmental conditions, etc. Therefore in the literature one can find only a few papers where such data is presented. The examples of such results can be found in [4] and [13].

In our paper, as a material for the practical illustration of the above theoretical considerations, we use the Virkler experimental data of stochastic crack growth under periodic loading [13]. The results of this experiment are shown in Fig. 1. The authors performed the experiment for 68 samples of material, obtaining the trajectories of crack growth, each containing 164 measurement points. The experiment has been performed for the 2024-T3 aluminium alloy. The dimensions of all the samples were: length $a_{\text{tot}} = 558.8$ (mm), width $b = 152.4$ (mm) and thickness $d = 2.54$ (mm). The length of the fatigue crack was observed in the interval $9.00 \leq a \leq 49.8$ (mm); the stress intensity during the experiment was $\Delta\sigma = 48.28$, and the sinusoidal excitation frequency was 20 Hz.

The experimental trajectories are the fundamental basis for identification of the model parameters. To perform the procedure, we apply the algorithm proposed in Sec. 6, performed in two steps. In the first step we identify parameters $(m, \ln C)$ for each of the 68 trajectories of the stochastic crack growth. The estimated values of the parameter pairs are presented in Fig. 2.

It is seen that the parameters m_i and $\ln C_i$ are, with high accuracy, linearly dependent on each other. This means that in the second step of identification of the model, it is sufficient to consider only one parameter of the pair. Following the literature [3], we assume the normal distribution of the random variables $m(\omega)$ and $\ln C(\omega)$. This means that, in order to know the distributions, it is

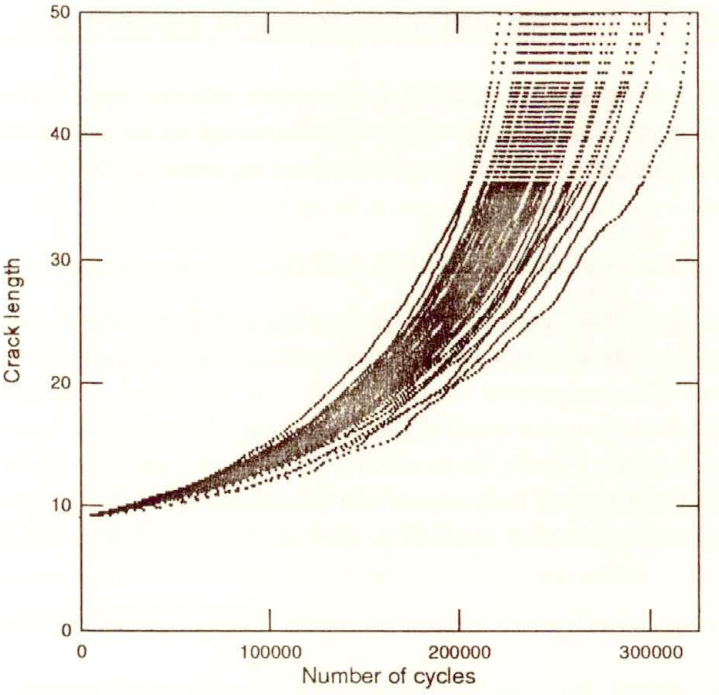

FIG. 1. Trajectories of the stochastic crack growth (results of the Virkler experiment).

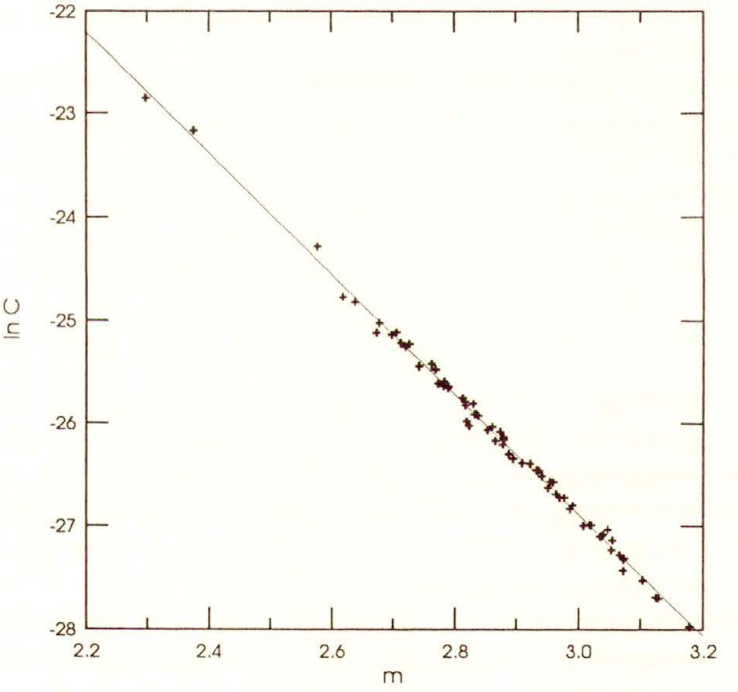

FIG. 2. Parameters $(m_i, \ln C_i)$ identified from the Virkler data.

enough to calculate their mean values and variances. In the second step of the conditioning procedure we estimate the moments of the parameter m according to the maximum likelihood estimators:

$$E\{m\} = \frac{1}{N}\sum_{i=1}^{N} m(\omega_i), \tag{7.1}$$

$$\mathrm{Var}\{m\} = \frac{1}{N}\sum_{i=1}^{N}(m(\omega_i) - E\{m\})^2. \tag{7.2}$$

Since we have observed the linear dependence of the parameters m and $\ln C$:

$$\ln C = Am + B, \tag{7.3}$$

to complete the identification of the model we should calculate the coefficients A, B, using the formula (4.13) for the linear estimator, and the experimental data presented in Fig. 2. The obtained moments of the random variables $m(\omega)$ and $\ln C(\omega)$ and the values of the parameters A and B are:

$$E\{m\} = 2.874, \tag{7.4}$$

$$\mathrm{Var}\{m\} = 0.02736, \tag{7.5}$$

$$A = -5.847, \tag{7.6}$$

$$B = -9.35, \tag{7.7}$$

$$E\{\ln C\} = AE\{m\} + B = -26.155, \tag{7.8}$$

$$\mathrm{Var}\{\ln C\} = A^2\mathrm{Var}\{m\} = 0.939. \tag{7.9}$$

8. Reliability of the experimental data and cross-validation

The procedure used for the identification of the model parameters needs the experimental data to obtain concrete numerical results. In our procedure we applied the data in two steps. In every step we performed the identification under an implicit assumption that the collected data are appropriate for our purpose. However, there is always a danger that this assumption cannot be justified. The general ideas concerning this fact have been presented in Sec. 1. Now we will show how the concrete example of estimation of the Paris-Erdogan model parameters on the basis of Virkler data, demonstrates the general idea of the cross-validation.

Let us discuss the results obtained in two steps of our conditioning procedure.

STEP 1. In this step we identify the sample parameters $(m_i, \ln C_i)$ for all 68 trajectories obtained in the experiment. For every trajectory we obtain a certain value of the parameters $(m, \ln C)$. To verify the validity of the estimated values,

we try to reconstruct the Paris-Erdogan (deterministic or averaged) trajectories. The result of the calculation is presented in Fig. 3. During reconstruction of the trajectories we failed at 9 cases of 68 (9 times the sample paths with the identified parameters exploded before reaching the considered number of cycles). To explain this fact let us remark that (as it is visible in Fig. 1) some experimental trajectories of stochastic cracks are of the shape which is non-similar to the exponential Paris-Erdogan curve. Moreover, the length in time (number of cycles) is different for each experimental curve. Therefore the life-time of the modelled crack growing in the sample cannot be precisely determined. The discussion of analogous problems can be found in [8].

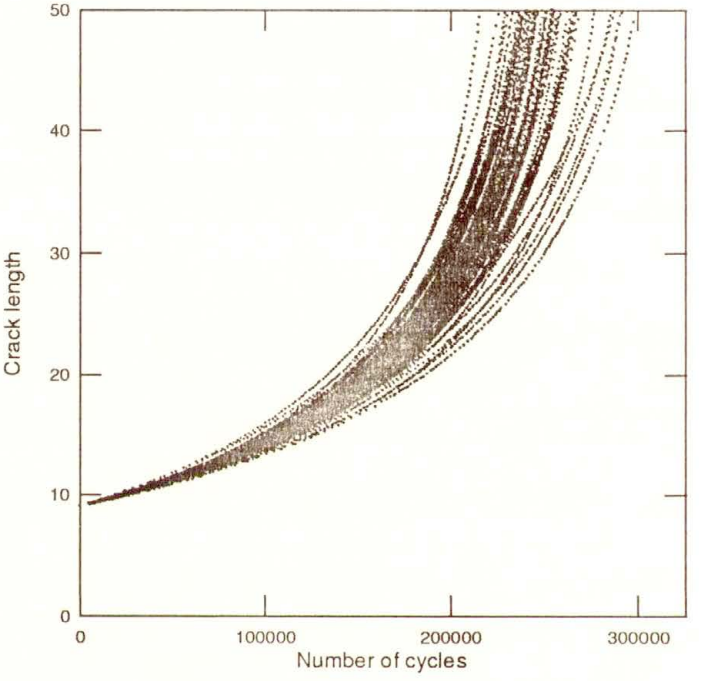

FIG. 3. Deterministic trajectories with parameters $(m_i, \ln C_i)$ estimated from the Virkler experimental data.

To study the effect of the trajectory length on the success of the procedure of the model parameters identification, we make the following calculations. We omit some number of the measurement points at the end of every curve in the procedure of Step 1. The results of such numerical experiment (the number of the identified pairs of the parameters for which the reconstruction of the Paris-Erdogan trajectory was impossible) are presented in the following table (the length of the trajectory is 164).

STEP 2. We estimate the model parameters (identify their distributions) basing on the data partially identified in Step 1. Now we try to verify the validity

of the data for the complete identification procedure. We examine the reliability of the experimental data using the linear interdependence of two parameters in the Paris-Erdogan model of the stochastic crack growth. To do this, we compare the results of model identification obtained by two different methods.

Number of omitted data points on trajectory	Number of unsuccessful identifications
0	9
10	10
20	12
30	16
40	20
50	25
60	37
70	43
80	51

Assume that the value of the parameter m_i for fixed i is known (it is identified in the procedure of Step 1). Now we can calculate the values of the parameters A and B in the linear dependence (7.3).

METHOD 1. In this method the coefficients A and B are identified according to the formulae of Sec. 4 with the use of all the pairs of the estimated values $(m_i, \ln C_i)$.

METHOD 2. In this method the coefficients A and B are identified with the use of all the pairs of $(m_j, \ln C_j)$ except for the i-th pair.

Now, having the values of A and B estimated, we are able to calculate (according to (7.3)) the approximate value of the model parameter $\ln C_i$ for every m_i.

The first performed test shows, what is the influence of the i-th measured trajectory on the approximation quality of $\ln C_i$. Figure 4 shows the result of classical (one-point) cross-validation of the experimental data. The points on the plot marked with crosses represent the value of mean-square error of the approximation of the value of $\ln C_i$ estimated from the trajectory by $\ln C_i = Am_i + B$, where the parameters A and B were calculated by the Method 1. Points marked with circles represent the analogous error but for parameters A and B calculated according to the Method 2. It is seen that the differences in the approximation errors are significant for 9 measurements. This means that 9 measurements are not appropriate for the identification of the parameters of the Paris-Erdogan model. They contain a lot of information specific for themselves but useless for approximation of the general properties of the model.

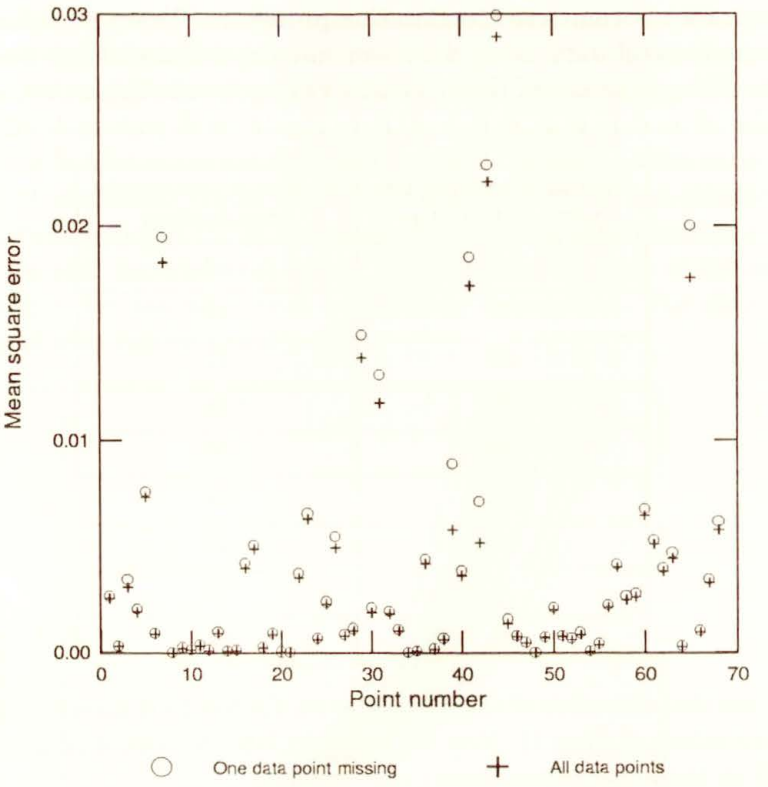

FIG. 4. The mean square error for approximation of the parameter $\ln C_i$.

The following identification method treats the cross-validation problem more generally.

METHOD 3. In this method, the coefficients A and B are identified with the use of all the pairs of the estimated values $(m_j, \ln C_j)$ except the k randomly selected pairs.

The results of the Method 3 are presented in Fig. 5. There are 3 lines in the plot. The dashed line shows the value of the mean square error of the approximation of the parameter $\ln C_i$, with the value m_i and formula (7.3), where the constants A and B were calculated according to the Method 2 (this is the sum of the errors for all 68 experimental trajectories). The solid lines show the analogous error but when the coefficients A and B are calculated according to the Method 3. The functions depend on k, the number of the omitted points (for two different random selections).

It is seen that, in general, omission in the approximation procedure of $\ln C_i$, at a given point just the measurement made at this point, gives the effect comparable to neglecting more than 30 randomly selected points (that is about 50% of the points considered in the estimation procedure). This means that each curve of

the Virkler data is strongly informative for the estimation of the value of the parameters calculated for this curve.

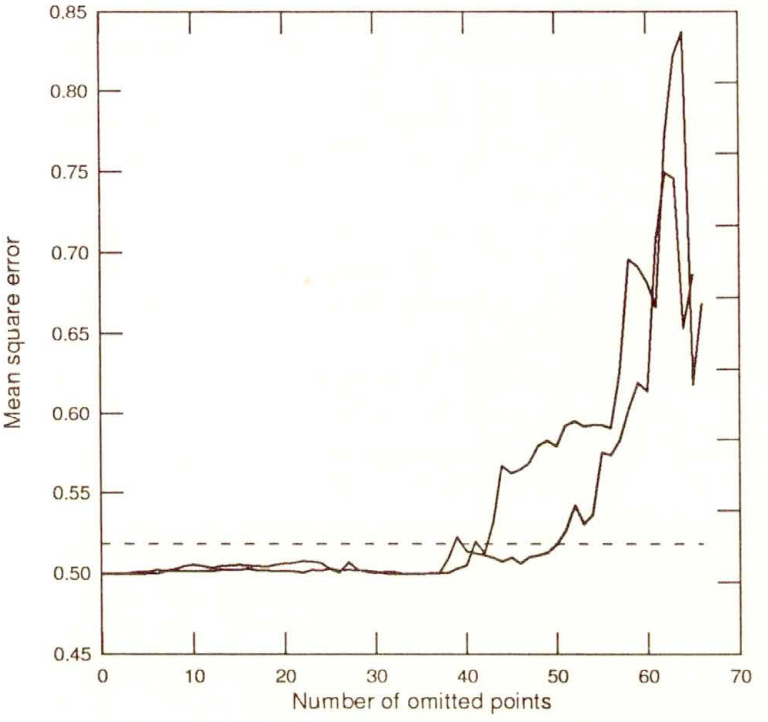

FIG. 5. The averaged mean square error of estimation of the parameter $\ln C_i$.

9. Closing remarks

One of the most important tasks of the experiment's design is the verification of the consistency of the measured experimental data. To analyse the data, we have applied the method analogous to the statistical procedure of cross-validation. Since the results of measurement had to be applied for identification of the parameters of a certain mathematical model, we applied this model (or, more precisely its parameters) as the quality measure of the set of experimental data. Such a methodology is very intuitive: the collected data can be more appropriate for one model, less appropriate or useless for another. The reasons for this fact can be very different. It can happen that some model is not adequate for description of the observed physical phenomenon and this fact must be always taken into account in the identification process. However, this is not the only reason of failure of the procedure. Sometimes the algorithms of the model parameters estimation require a specific structure of data. Therefore one must carefully design the experiment planning its duration, sampling in time, location of sensors over the sample, etc.,

taking into account the final destination of the obtained data. Summing up, validation of the experimental data must be always connected with the model where the data are utilised.

In this paper we have considered the following practical problem: for a given set of experimental data (Virkler data on the fatigue-crack length) and the mathematical model of a physical phenomenon (Paris-Erdogan randomised model of fatigue-crack growth), verify the validation of the data for identification of the model parameters. The conclusions regarding possibility of application of the Virkler data in the Paris-Erdogan model are the following:

- Virkler data applied in identification of the Paris-Erdogan randomised model are sensitive to the length in time (duration) of the sample trajectories. They are also very sensitive to omitting the results of certain sample measurements in the identification procedure.
- After the cross-validation procedure applied to the Paris-Erdogan equation, we must say that while the model gives a good qualitative description of the stochastic crack growth, there is a small possibility of prediction of the behaviour of the crack in a certain sample of a material. To estimate the parameters of certain trajectory with good accuracy, we should include into our calculations the experimental results obtained just for this trajectory.
- In the experiments of a kind analogous to the Virkler one, the number of the measured samples and the length of the observed trajectory is essential for the quality of identification of any mathematical model of the tested phenomenon.

To conclude our considerations we must say that while every experiment, before it is made, must be carefully designed, then the following cross-validation procedure can strongly confirm the applicability of the obtained data for mathematical modelling. This procedure indicates in particular the coherence of the obtained experimental data and the applied theoretical model of the phenomenon.

Acknowledgements

I wish to thank Professor KAZIMIERZ SOBCZYK for pointing the problem and a support during preparation of this paper.

References

1. P. CHAUDHURI, A. DEWANJI, *On a likelihood-based approach in nonparametric smoothing and cross-validation*, Statistics & Probability Letters, **22**, 7–15, 1995.
2. O. DITLEVSEN, *Random fatigue crack growth – a first passage problem*, DCAM, Rep.No. **298**, 1985.
3. O. DITLEVSEN, R. OLESEN, *Statistical analysis of the Virkler data on fatigue crack growth*, Engn. Fracture Mechanics, **25**, 2, 177–195, 1986.

4. H. GHONEM, S. DORE, *Experimental study of the constant-probability crack growth curves under constant amplitude loading*, Engn. Fracture Mechanics, **27**, 1, 1–25, 1987.

5. D. K. HILDEBRAND, J. D. LAING, H. ROSENTHAL, *Prediction analysis of cross classifications*, J.Wiley & Sons, New York 1977.

6. D. D. JOSHI, *Linear estimation and design of experiments*, John Wiley and Sons, New York, New Delhi 1987.

7. Z. KOTULSKI, K. SOBCZYK, *Effects of parameter uncertainty on the response of vibratory systems to random excitation*, J. Sound and Vibration, **119**, 1, 159–171, 1987.

8. C. J. LU, W. Q. MEEKER, *Using degradation measures to estimate a time-to-failure distribution*, Technometrics, **35**, 2, 161–174, 1993.

9. C. RADHAKRISHNA RAO, *Statistics and truth*, Council of Scientific and Industrial Research, New Delhi 1989.

10. K. SOBCZYK, B. F. SENCER, Jr., *Random fatigue: From data to theory*, Academic Press, 1992.

11. M. STONE, *Cross-validatory choice and assessment of statistical predictions*, Proc. Royal Statist. Soc. of London B, **36**, 2, 111–147, 1974.

12. M. STONE, *Cross-Validation: A Review*, Math.Operat.-Forschung Statist., Ser. Statistic, **9**, 127–139, 1978.

13. D. A. VIRKLER, B. M. HILLBERRY, P. K. GOEL, *The statistical nature of fatigue crack propagation*, Transactions of the ASME – Journal of Engineering Materials and Technology, **101**, 148–153, 1979.

POLISH ACADEMY OF SCIENCES
INSTITUTE OF FUNDAMENTAL TECHNOLOGICAL RESEARCH
e-mail: zkotulsk@ippt.gov.pl

Received December 8, 1997.

Arch. Mech., 50, 5, pp. 849–863, Warszawa 1998
FIFTY YEARS OF THE ARCHIVES OF MECHANICS

On elastic energy of structures under proportional loading

A. GAWĘCKI (POZNAŃ)

THE PAPER CONCERNS the proportional loading of structures made of time-independent materials. It has been shown that the elastic energy can be a decreasing function of the load multiplier if unilateral constraints are introduced into an elastic-plastic structure. Results obtained in the work seem to be of importance for the theory of structures and may have some theoretical implications. An exhaustive example illustrates the theory.

1. Introduction

THE PRESENT PAPER CONCERNS the problems of energy in structural systems. The energy, being a scalar quantity, is a diagnostic measure of the current mechanical state of the system and is of importance for theoretical considerations.

The elastic energy of structures made of the elastic-perfectly plastic materials will be evaluated. The load is assumed to be proportional and the problem is to establish whether the elastic energy is a monotone function of the load multiplier or not. It seems that the answer is "yes", but there is no theorem concerning this question known to the author. However, the problem is not trivial in general cases of time-independent systems. A case will be shown when the elastic energy can decrease while the proportional load increases.

The distortion approach has been applied in our considerations. The essence of this approach consists in the observation that all deformations due to nonlinearity of the material and/or boundary conditions are caused by the presence of distortions imposed on the linear elastic structure. Distortions are defined as enforced deformations which are not kinematically admissible, in general. The concept of distortions was introduced in the last years of the 19th century and, among others, was used in the papers of V. VOLTERRA [1] and G. COLONNETTI [2]. The distortion approach allowed us to obtain many valuable results, particularly in the thermoelasticity and shakedown theory of elastic-plastic structures. Some information concerning this topic can be found in the monographs of W. NOWACKI [3] and J. A. KÖNIG [4].

All considerations presented herein are carried out in the framework of the kinematically linear theory. The FEM-oriented matrix description, worked out by G. MAIER [5] and his co-workers, is used.

The elastic energy will be estimated for elastic (E), elastic-perfectly plastic (EpP), slackened-elastic (SE) and slackened-elastic-perfectly plastic ($SEpP$)

structures. "Slackening" is a structural property, consisting in the presence of gaps (clearances) at structural joints. Thus, on the macro scale, the slackened structure behaviour exhibits the locking effects. Deformations of slackened systems are due to elastic ε_E, plastic ε_P and also concentrated clearance strains ε_L (i.e. relative displacements of members and connection elements). The plastic and clearance strains can be treated as distortions imposed on the linear elastic structure. It should be pointed out however that clearance strains are "load-dependent" distortions, because they can vary during the deformation processes. More details concerning the slackened systems can be found in [7, 8].

2. Mathematical description of elastic systems with distortions

Consider an linear elastic system subjected to external loads $\mathbf{p}$ and distortions ε_R. The elasticity coefficients are assumed to be constant and independent of distortions. A current mechanical state, independently of the deformation history, can then be described by the following system of matrix relations:

$$\begin{aligned} \mathbf{C}\mathbf{u} &= \boldsymbol{\varepsilon} = \boldsymbol{\varepsilon}_E + \boldsymbol{\varepsilon}_R, \\ \mathbf{C}^T\boldsymbol{\sigma} &= \mathbf{p}, \\ \boldsymbol{\sigma} &= \mathbf{E}\boldsymbol{\varepsilon}_E. \end{aligned} \tag{2.1}$$

In Eqs. (2.1) $\mathbf{p}$, $\mathbf{u}$, $\boldsymbol{\sigma}$ and $\boldsymbol{\varepsilon}$ denote the vectors of loads (or generalized loads), displacements (or generalized displacements), stresses (or generalized stresses) and strains (or generalized strains), respectively. All these state variables are consistent in the sense of the virtual work equation:

$$\mathbf{p}^T\mathbf{u} = \boldsymbol{\sigma}^T\boldsymbol{\varepsilon}, \tag{2.2}$$

where T denotes the transpose. $\mathbf{C}$ is the geometric compatibility matrix, which depends only on the geometry and boundary conditions of the system. $\mathbf{E}$ denotes the strictly positive definite, square and symmetric matrix of elasticity. Since the kinematically linear approach is used, the strain vector $\boldsymbol{\varepsilon}$ can be split into elastic $\boldsymbol{\varepsilon}_E$ and distortion $\boldsymbol{\varepsilon}_R$ parts.

From (2.1) the following matrix relations can be derived, [8]:

$$\begin{aligned} &\mathbf{p} = \mathbf{K}\mathbf{u} - \mathbf{C}^T\mathbf{E}\boldsymbol{\varepsilon}_R, && \mathbf{u}_e = \mathbf{K}^{-1}\mathbf{p}, && \mathbf{u}_r = \mathbf{K}^{-1}\mathbf{C}^T\mathbf{E}\boldsymbol{\varepsilon}_R, \\ &\mathbf{u} = \mathbf{u}_e + \mathbf{u}_r, && \boldsymbol{\sigma}_e = \mathbf{E}\mathbf{C}\mathbf{K}^{-1}\mathbf{p}, && \boldsymbol{\sigma}_r = \mathbf{Z}\boldsymbol{\varepsilon}_R, \\ &\boldsymbol{\sigma} = \boldsymbol{\sigma}_e + \boldsymbol{\sigma}_r, && \mathbf{K} = \mathbf{C}^T\mathbf{E}\mathbf{C}, && \mathbf{Z} = \mathbf{E}\mathbf{C}\mathbf{K}^{-1}\mathbf{C}^T\mathbf{E} - \mathbf{E}. \end{aligned} \tag{2.3}$$

where $\mathbf{K}$ is the square, symmetric and strictly positive definite stiffness matrix. In Eqs. (2.3) subscript e relates to the linear elastic structure without distortions, subjected to load $\mathbf{p}$, and subscript r indicates all the quantities due to the presence of distortions.

The distortion influence matrix $\mathbf{Z}$ is square and symmetric. It is well-known that the same stress state can be induced by various distortions, but any difference between these distortions is kinematically admissible. Thus, the matrix $\mathbf{Z}$ has to be singular. It is easy to show that

$$\mathbf{ZC} \equiv \mathbf{0} \quad \text{and} \quad \mathbf{C}^T\mathbf{Z} \equiv \mathbf{0}. \tag{2.4}$$

From (2.4) we can formulate the following properties of distortions, namely:

• any kinematically admissible distortion field (i.e. $\boldsymbol{\varepsilon}_R = \mathbf{Cu}_r$) does not induce self-stresses $\boldsymbol{\sigma}_r$:

$$\boldsymbol{\sigma}_r = \mathbf{Z}\boldsymbol{\varepsilon}_R = \mathbf{ZCu}_r \equiv \mathbf{0}; \tag{2.5}$$

• the self-stresses due to the presence of distortions ($\boldsymbol{\sigma}_r = \mathbf{Z}\boldsymbol{\varepsilon}_R$) are in equilibrium with zero-valued external loads:

$$\mathbf{p}_r = \mathbf{C}^T\boldsymbol{\sigma}_r = \mathbf{C}^T\mathbf{Z}\boldsymbol{\varepsilon}_R \equiv \mathbf{0}. \tag{2.6}$$

Compute now the total elastic energy W_E of a load-free ($\mathbf{p} = \mathbf{0}$) elastic structure subjected to steady distortions $\boldsymbol{\varepsilon}_R$:

$$W_E = \frac{1}{2}\boldsymbol{\sigma}^T\boldsymbol{\varepsilon}_E = \frac{1}{2}\boldsymbol{\sigma}^T(\mathbf{Cu} - \boldsymbol{\varepsilon}_R) = \frac{1}{2}\mathbf{p}^T\mathbf{u} - \frac{1}{2}\boldsymbol{\sigma}^T\boldsymbol{\varepsilon}_R = -\frac{1}{2}\boldsymbol{\sigma}^T\boldsymbol{\varepsilon}_R. \tag{2.7}$$

The elastic energy is positive definite unless the distortions $\boldsymbol{\varepsilon}_R$ are kinematically admissible. Hence

$$\boldsymbol{\sigma}^T\boldsymbol{\varepsilon}_R = \boldsymbol{\varepsilon}_R^T\mathbf{Z}\boldsymbol{\varepsilon}_R \leq 0. \tag{2.7}'$$

From (2.7)′ it is clearly seen that matrix $\mathbf{Z}$ is negative semi-definite.

In order to avoid a possible confusion, it should be mentioned that the distortion description used herein corresponds to the standard approach which is slightly different from the Colonnetti's one where the total strain vector is divided into three parts (for details see [9]), namely

$$\boldsymbol{\varepsilon} = \boldsymbol{\varepsilon}_e^{(p)} + (\boldsymbol{\varepsilon}_e^{(R)} + \boldsymbol{\varepsilon}_R). \tag{2.8}$$

In Eq. (2.8) $\boldsymbol{\varepsilon}_e^{(p)}$ denotes the compatible strain vector due to the load vector $\mathbf{p}$ in bvarepe pure elastic structure, while $\boldsymbol{\varepsilon}_e^{(R)}$ is the elastic strain vector induced by the distortions $\boldsymbol{\varepsilon}_R$ in the absence of the load $\mathbf{p}$. Thus, the sum $\boldsymbol{\varepsilon}_e^{(p)} + \boldsymbol{\varepsilon}_R$ is kinematically admissible. Consequently, the relations between the standard and Colonnetti's descriptions take the form:

$$\begin{aligned} \boldsymbol{\varepsilon}_E &= \boldsymbol{\varepsilon}_e^{(p)} + \boldsymbol{\varepsilon}_e^{(R)}, \\ \boldsymbol{\sigma}_e &= \mathbf{E}\boldsymbol{\varepsilon}_e^{(p)} = \mathbf{ECu}_e = \mathbf{E}\boldsymbol{\varepsilon}_E - \boldsymbol{\sigma}_r, \\ \boldsymbol{\sigma}_r &= \mathbf{E}\boldsymbol{\varepsilon}_e^{(R)} = \mathbf{E}(\mathbf{Cu}_r - \boldsymbol{\varepsilon}_R) = \mathbf{E}\boldsymbol{\varepsilon}_E - \boldsymbol{\sigma}_e = \mathbf{Z}\boldsymbol{\varepsilon}_R. \end{aligned} \tag{2.9}$$

3. Bounds on the elastic energy

Assume that an elastic structure is subjected to two load and distortion systems $\mathbf{p}_1$, $\boldsymbol{\varepsilon}_{R1}$ and $\mathbf{p}_2$, $\boldsymbol{\varepsilon}_{R2}$, respectively. The difference of the elastic energies of both the systems can be expressed as

$$\Delta W_E = W_{E2} - W_{E1} = \frac{1}{2}\boldsymbol{\sigma}_2^T\boldsymbol{\varepsilon}_{E2} - \frac{1}{2}\boldsymbol{\sigma}_1^T\boldsymbol{\varepsilon}_{E1}. \tag{3.1}$$

Turning now to the general case of deformable systems we use the positive definiteness of the elasticity matrix $\mathbf{E}$ in order to formulate the following inequality:

$$(\boldsymbol{\varepsilon}_{E2} - \boldsymbol{\varepsilon}_{E1})^T\mathbf{E}(\boldsymbol{\varepsilon}_{E2} - \boldsymbol{\varepsilon}_{E1}) = (\boldsymbol{\sigma}_2 - \boldsymbol{\sigma}_1)^T(\boldsymbol{\varepsilon}_{E2} - \boldsymbol{\varepsilon}_{E1}) \geq 0, \tag{3.2}$$

where the equality sign occurs if both the elastic strain vectors are equal to each other. Inequality (3.2), using Eqs. (2.1), can be rewritten in the form

$$(\mathbf{p}_2 - \mathbf{p}_1)^T(\mathbf{u}_2 - \mathbf{u}_1) - (\boldsymbol{\sigma}_2 - \boldsymbol{\sigma}_1)^T(\boldsymbol{\varepsilon}_{R2} - \boldsymbol{\varepsilon}_{R1}) \geq 0. \tag{3.2$'$}$$

On the other hand, inequality (3.2) leads to

$$(\boldsymbol{\sigma}_2 - \boldsymbol{\sigma}_1)^T\boldsymbol{\varepsilon}_{E1} \leq (\boldsymbol{\sigma}_2 - \boldsymbol{\sigma}_1)^T\boldsymbol{\varepsilon}_{E2}. \tag{3.2$''$}$$

It can be easily shown that if $a \leq b$ then $a \leq (a+b)/2 \leq b$. Using this result in inequality (3.2)$''$ we obtain

$$(\boldsymbol{\sigma}_2 - \boldsymbol{\sigma}_1)^T\boldsymbol{\varepsilon}_{E1} \leq \frac{1}{2}(\boldsymbol{\sigma}_2 - \boldsymbol{\sigma}_1)^T(\boldsymbol{\varepsilon}_{E2} + \boldsymbol{\varepsilon}_{E1}) \leq (\boldsymbol{\sigma}_2 - \boldsymbol{\sigma}_1)^T\boldsymbol{\varepsilon}_{E2}. \tag{3.3}$$

Since $\boldsymbol{\sigma}_1^T\boldsymbol{\varepsilon}_{E2} = \boldsymbol{\sigma}_2^T\boldsymbol{\varepsilon}_{E1}$, we can conclude that the intermediate term of (3.3) represents the difference between the elastic energies of two systems of loads and distortions, namely:

$$\begin{aligned}\frac{1}{2}(\boldsymbol{\sigma}_2 - \boldsymbol{\sigma}_1)^T(\boldsymbol{\varepsilon}_{E1} + \boldsymbol{\varepsilon}_{E2}) &= \frac{1}{2}\boldsymbol{\sigma}_2^T\boldsymbol{\varepsilon}_{E2} - \frac{1}{2}\boldsymbol{\sigma}_1^T\boldsymbol{\varepsilon}_{E1} \\ &= W_{E2} - W_{E1} = \Delta W_E.\end{aligned} \tag{3.4}$$

Thus, Ineq. (3.3) takes the form

$$(\boldsymbol{\sigma}_2 - \boldsymbol{\sigma}_1)^T\boldsymbol{\varepsilon}_{E1} \leq \Delta W_E \leq (\boldsymbol{\sigma}_2 - \boldsymbol{\sigma}_1)^T\boldsymbol{\varepsilon}_{E2}. \tag{3.4$'$}$$

The left-hand side of (3.4)$'$ can be modified as follows:

$$(\boldsymbol{\sigma}_2 - \boldsymbol{\sigma}_1)^T\boldsymbol{\varepsilon}_{E1} = (\boldsymbol{\sigma}_2 - \boldsymbol{\sigma}_1)^T(\mathbf{C}\mathbf{u}_1 - \boldsymbol{\varepsilon}_{R1}) = (\mathbf{p}_2 - \mathbf{p}_1)^T\mathbf{u}_1 + (\boldsymbol{\sigma}_1 - \boldsymbol{\sigma}_2)^T\boldsymbol{\varepsilon}_{R1},$$

or, using the reciprocal principle (cf. [8])

$$(\boldsymbol{\sigma}_2 - \boldsymbol{\sigma}_1)^T\boldsymbol{\varepsilon}_{E1} = (\mathbf{u}_2 - \mathbf{u}_1)^T\mathbf{p}_1 + \boldsymbol{\sigma}_1^T(\boldsymbol{\varepsilon}_{R1} - \boldsymbol{\varepsilon}_{R2}).$$

Similar transformations of the right-hand side of (3.4)′ allow us to construct the following inequalities, [8]:

$$
\begin{aligned}
L_1 &\leq \Delta W_E \leq R_1, \\
L_2 &\leq \Delta W_E \leq R_2,
\end{aligned}
\tag{3.5}
$$

where

$$
\begin{aligned}
L_1 &= (\mathbf{p}_2 - \mathbf{p}_1)^T \mathbf{u}_1 + (\sigma_1 - \sigma_2)^T \boldsymbol{\varepsilon}_{R1}, \\
R_1 &= (\mathbf{p}_2 - \mathbf{p}_1)^T \mathbf{u}_2 + (\sigma_1 - \sigma_2)^T \boldsymbol{\varepsilon}_{R2}, \\
L_2 &= (\mathbf{u}_2 - \mathbf{u}_1)^T \mathbf{p}_1 + (\boldsymbol{\varepsilon}_{R1} - \boldsymbol{\varepsilon}_{R2})^T \boldsymbol{\sigma}_1, \\
R_2 &= (\mathbf{u}_2 - \mathbf{u}_1)^T \mathbf{p}_2 + (\boldsymbol{\varepsilon}_{R1} - \boldsymbol{\varepsilon}_{R2})^T \boldsymbol{\sigma}_2.
\end{aligned}
\tag{3.6}
$$

$$\Delta W_E = (L_1 + R_1)/2; \quad \Delta W_E = (L_2 + R_2)/2; \quad L_1 = L_2 \text{ and } R_1 = R_2.$$

The equality signs relate to the particular cases of kinematically admissible distortions which do not induce any additional stresses.

It should be pointed out that inequalities (3.5) hold true for any unspecified loading paths. These inequalities will be used to evaluate the elastic energy for various types of structures under proportional loads.

4. Elastic energy changes during proportional loading

4.1. Definitions and assumptions

The proportional loading can be defined as follows:

$$\mathbf{p} = \mu_0 \mathbf{p}_0, \tag{4.1}$$

where μ_0 is a positive definite scalar multiplier, and $\mathbf{p}_0$ denotes a reference load vector. Consider two levels of proportional loads $\mathbf{p}_1$ and $\mathbf{p}_2$, which are associated with two load multipliers μ_1 and μ_2, respectively. If $\mathbf{p}_1 = \mu_1 \mathbf{p}_0$ and $\mathbf{p}_2 = \mu_2 \mathbf{p}_0$ then for $\mu_2 > \mu_1 > 0$ we obtain:

$$\mathbf{p}_2 = \mu \mathbf{p}_1, \tag{4.2}$$

where $\mu = \mu_2/\mu_1 > 1$.

Since the problem is considered in the frame of kinematically linear theory, the total strain in general cases of $SEpP$ structures is a sum of individual partial strains. In particular, the distortion vector consists of clearance and plastic strains:

$$\boldsymbol{\varepsilon}_R = \boldsymbol{\varepsilon}_L + \boldsymbol{\varepsilon}_P. \tag{4.3}$$

Usually, during proportional loading of structures no local plastic unloading occurs. Such a behaviour corresponds to the path-independent (holonomic) model. Further considerations are restricted to this model.

If a $SEpP$ structure is subjected to proportional load $\mathbf{p}$, which induces clearance and plastic distortions, then the following inequality holds:

$$\mathbf{p}^T\mathbf{u} = \boldsymbol{\sigma}^T\boldsymbol{\varepsilon} = \boldsymbol{\sigma}^T(\boldsymbol{\varepsilon}_L + \boldsymbol{\varepsilon}_E + \boldsymbol{\varepsilon}_P) = \boldsymbol{\sigma}^T\boldsymbol{\varepsilon}_L + \boldsymbol{\sigma}^T\boldsymbol{\varepsilon}_E + \boldsymbol{\sigma}^T\boldsymbol{\varepsilon}_P > 0. \tag{4.4}$$

The inequality sign results from the following. The product of stress and elastic strains $\boldsymbol{\sigma}^T\boldsymbol{\varepsilon}_E$ is positive due to the definition of elasticity matrix. The clearance work $\boldsymbol{\sigma}^T\boldsymbol{\varepsilon}_L$ in slackened structures is always positive semi-definite (cf. [6]). The product of stresses and plastic strains $\boldsymbol{\sigma}^T\boldsymbol{\varepsilon}_P$ represents the positive semi-definite plastic dissipation in EpP sysytems. Relation (4.4) is also valid for the remaining kinds of structures (i.e. E, SE, EpP) because they are particular cases of the $SEpP$ structure.

The yield condition and contact condition are assumed to be convex. For the holonomic model, these assumptions can be expressed in the following mathematical form:

$$\begin{aligned} (\boldsymbol{\sigma}_1 - \boldsymbol{\sigma}_2)^T\boldsymbol{\varepsilon}_{P1} &\geq 0, \\ (\boldsymbol{\varepsilon}_{L1} - \boldsymbol{\varepsilon}_{L2})^T\boldsymbol{\sigma}_1 &\geq 0. \end{aligned} \tag{4.5}$$

In (4.5) $\boldsymbol{\sigma}_1$, $\boldsymbol{\varepsilon}_{P1}$ and $\boldsymbol{\varepsilon}_{L1}$ denote true vectors of stress and strains, whereas $\boldsymbol{\sigma}_2$ and $\boldsymbol{\varepsilon}_{L2}$ are arbitrary statically admissible stress and kinematically admissible clearance strain vectors, respectively. Moreover, using inequalities (4.5) and assuming that $\boldsymbol{\sigma}_2$, $\boldsymbol{\varepsilon}_{P2}$ and $\boldsymbol{\varepsilon}_{L2}$ represent true associated stress and distortion states, we obtain

$$\begin{aligned} (\boldsymbol{\sigma}_1 - \boldsymbol{\sigma}_2)^T(\boldsymbol{\varepsilon}_{P1} - \boldsymbol{\varepsilon}_{P2}) &\geq 0, \\ (\boldsymbol{\sigma}_1 - \boldsymbol{\sigma}_2)^T(\boldsymbol{\varepsilon}_{L1} - \boldsymbol{\varepsilon}_{L2}) &\geq 0, \end{aligned} \tag{4.6}$$

hence

$$(\boldsymbol{\sigma}_1 - \boldsymbol{\sigma}_2)^T[(\boldsymbol{\varepsilon}_{L1} + \boldsymbol{\varepsilon}_{P1} + \boldsymbol{\varepsilon}_D) - (\boldsymbol{\varepsilon}_{L2} + \boldsymbol{\varepsilon}_{P2} + \boldsymbol{\varepsilon}_D)] \geq 0, \tag{4.7}$$

where $\boldsymbol{\varepsilon}_D$ denotes a steady distortion vector. All the possible distortions which can occur in the class of time-independent structural systems considered herein can be presented as

$$\boldsymbol{\varepsilon}_{Li} + \boldsymbol{\varepsilon}_{Pi} + \boldsymbol{\varepsilon}_D = \boldsymbol{\varepsilon}_{Ri}; \qquad i = 1, 2. \tag{4.8}$$

Substituting (4.7) to inequality (3.2)$'$ yields

$$(\mathbf{p}_2 - \mathbf{p}_1)^T(\mathbf{u}_2 - \mathbf{u}_1) \geq 0. \tag{4.9}$$

Using (4.2) in Ineq. (4.9) we obtain

$$(\mu - 1)\mathbf{p}_1^T(\mathbf{u}_2 - \mathbf{u}_1) \geq 0,$$
$$(1 - \mu^{-1})\mathbf{p}_2^T(\mathbf{u}_2 - \mathbf{u}_1) \geq 0.$$

For proportional loading $(\mu - 1) > 0$ and $(1 - \mu^{-1}) > 0$. Thus, we can state that

$$\begin{aligned} \mathbf{p}_1^T(\mathbf{u}_2 - \mathbf{u}_1) &> 0, \\ \mathbf{p}_2^T(\mathbf{u}_2 - \mathbf{u}_1) &> 0. \end{aligned} \tag{4.10}$$

Relations (4.10) will be used in further considerations.

4.2. Linear elastic systems

In elastic structures $\boldsymbol{\varepsilon}_i = \boldsymbol{\varepsilon}_{Ei}$ and $\boldsymbol{\varepsilon}_{Ri} \equiv \mathbf{0}$ $(i = 1, 2)$. From $(3.5)_2$ we have

$$\mathbf{p}_1^T(\mathbf{u}_2 - \mathbf{u}_1) \leq \Delta W_E \leq \mathbf{p}_2^T(\mathbf{u}_2 - \mathbf{u}_1) \quad \text{for} \quad \mu > 1.$$

According to $(4.10)_1$ $\mathbf{p}_1^T(\mathbf{u}_2 - \mathbf{u}_1) > 0$, hence $\Delta W_E = W_{E2} - W_{E1} > 0$. It corresponds to the obvious conclusion that the elastic energy in linear elastic systems is an increasing function of the load multiplier.

It will be shown that the same conclusion is also valid for elastic systems with any initial, load-independent distortions. Consider an elastic structure that exhibits steady distortions $\boldsymbol{\varepsilon}_D$. Denote by subscripts 1 and 2 the elastic energies of the self-stresses and load $\mathbf{p}$, acting on the structure without distortions, respectively. Then

$$1: \ \mathbf{p}_1 = \mathbf{0}, \quad \boldsymbol{\varepsilon}_{R1} = \boldsymbol{\varepsilon}_D, \quad \mathbf{C}\boldsymbol{\sigma}_1 = \boldsymbol{\varepsilon}_{E1} + \boldsymbol{\varepsilon}_D, \quad \boldsymbol{\sigma}_1 = \mathbf{E}\boldsymbol{\varepsilon}_{E1} = \mathbf{Z}\boldsymbol{\varepsilon}_D;$$
$$2: \ \mathbf{p}_2 = \mathbf{p}, \quad \boldsymbol{\varepsilon}_{R2} = \mathbf{0}, \quad \mathbf{C}\boldsymbol{\sigma}_2 = \boldsymbol{\varepsilon}_{E2}, \quad \boldsymbol{\sigma}_2 = \mathbf{E}\boldsymbol{\varepsilon}_{E2}.$$

The total elastic energy W_E including the distortion and load effects reads

$$W_E = \frac{1}{2}(\boldsymbol{\sigma}_1 + \boldsymbol{\sigma}_2)^T(\boldsymbol{\varepsilon}_{E1} + \boldsymbol{\varepsilon}_{E2}) = \frac{1}{2}\boldsymbol{\sigma}_1^T\boldsymbol{\varepsilon}_{E1} + \frac{1}{2}\boldsymbol{\sigma}_1^T\boldsymbol{\varepsilon}_{E2}$$
$$+ \frac{1}{2}\boldsymbol{\sigma}_1^T\boldsymbol{\varepsilon}_{E2} + \frac{1}{2}\boldsymbol{\sigma}_2^T\boldsymbol{\varepsilon}_{E1} = W_{E1} + W_{E2} + \boldsymbol{\sigma}_1^T\boldsymbol{\varepsilon}_{E2}.$$

The last term in the above expression vanishes due to the virtual work principle $(\mathbf{p}_1 = \mathbf{0})$:

$$\boldsymbol{\sigma}_1^T\boldsymbol{\varepsilon}_{E2} = \boldsymbol{\sigma}_1^T\mathbf{C}\boldsymbol{\sigma}_2 = \mathbf{C}^T\boldsymbol{\sigma}_1\mathbf{u}_2 = \mathbf{p}_1^T\mathbf{u}_2 = 0.$$

So, the elastic energy can be decomposed into the energy of steady distortions and the energy of external loads; the mutual, load-distortion energy is equal

to zero. The same result has been obtained in [10]. However, this interesting observation is valid only for linear elastic systems. Since the external load energy is distortion-independent, the elastic energy is an increasing function of the load multiplier.

Finally, let us determine the explicit form of expression for the elastic energy of self-stresss:

$$W_{E1} = \frac{1}{2}\boldsymbol{\sigma}_1^T\boldsymbol{\varepsilon}_{E1} = \frac{1}{2}\boldsymbol{\varepsilon}_D^T\mathbf{Z}\boldsymbol{\varepsilon}_{E1} = \frac{1}{2}\boldsymbol{\varepsilon}_D^T\mathbf{Z}(\mathbf{C}\mathbf{u}_1 - \boldsymbol{\varepsilon}_D) = -\frac{1}{2}\boldsymbol{\varepsilon}_D^T\mathbf{Z}\boldsymbol{\varepsilon}_D$$

$$= -\frac{1}{2}\boldsymbol{\varepsilon}_D^T\mathbf{Z}(\mathbf{C}\mathbf{u}_1 - \boldsymbol{\varepsilon}_{E1}) = \frac{1}{2}\boldsymbol{\varepsilon}_D^T\mathbf{Z}\mathbf{E}^{-1}\boldsymbol{\sigma}_1 = \frac{1}{2}\boldsymbol{\varepsilon}_D^T(\mathbf{Z}\mathbf{E}^{-1}\mathbf{Z})\boldsymbol{\varepsilon}_D. \tag{4.11}$$

From (4.11) we conclude that $\mathbf{Z}\mathbf{E}^{-1}\mathbf{Z} = -\mathbf{Z}$. Indeed, using the definition of matrix $\mathbf{Z}$ and taking into account that $\mathbf{Z}\mathbf{C} \equiv \mathbf{0}$, we find

$$\mathbf{Z}\mathbf{E}^{-1}\mathbf{Z} = \mathbf{Z}\mathbf{E}^{-1}(\mathbf{E}\mathbf{C}\mathbf{K}^{-1}\mathbf{C}^T\mathbf{E} - \mathbf{E}) = \mathbf{Z}(\mathbf{C}\mathbf{K}^{-1}\mathbf{C}^T\mathbf{E} - \mathbf{I}) = -\mathbf{Z}. \tag{4.12}$$

4.3. Elastic-perfectly plastic systems

For both levels of loads $\mathbf{p}_1$ and $\mathbf{p}_2$, the total strains consist of elastic and plastic (distortion) parts:

$$\boldsymbol{\varepsilon}_i = \boldsymbol{\varepsilon}_{Ei} + \boldsymbol{\varepsilon}_{Ri}; \qquad \boldsymbol{\varepsilon}_{Ri} = \boldsymbol{\varepsilon}_{Pi}; \qquad i = 1, 2, \tag{a}$$

so, from $(3.5)_1$ and (a) we obtain

$$\Delta W_E \geq L_1 = (\mathbf{p}_2 - \mathbf{p}_1)^T\mathbf{u}_1 + (\boldsymbol{\sigma}_1 - \boldsymbol{\sigma}_2)^T\boldsymbol{\varepsilon}_{R1} = (\mu - 1)\mathbf{p}_1^T\mathbf{u}_1 + (\boldsymbol{\sigma}_1 - \boldsymbol{\sigma}_2)^T\boldsymbol{\varepsilon}_{P1}.$$

Since $(\mu - 1) > 0$, and according to (4.4), $\mathbf{p}_1^T\mathbf{u}_1 > 0$, the first right-hand side term is positive. If the yield condition is convex, the second right-hand side term is non-negative (cf. (4.5)). Thus, $\Delta W_E > 0$ and the elastic energy is an increasing monotone function of load multiplier μ.

4.4. Slackened-elastic systems

In slackened systems the strain vector can be divided into elastic and clearance parts

$$\boldsymbol{\varepsilon}_i = \boldsymbol{\varepsilon}_{Ei} + \boldsymbol{\varepsilon}_{Ri}; \qquad \boldsymbol{\varepsilon}_{Ri} = \boldsymbol{\varepsilon}_{Li}; \qquad i = 1, 2. \tag{a}$$

The elastic energy is an increasing function of the load multiplier if L_2 is positive definite. Using inequality $(3.5)_2$ we obtain:

$$L_2 = \mathbf{p}_1^T(\mathbf{u}_2 - \mathbf{u}_1) + \boldsymbol{\sigma}_1^T(\boldsymbol{\varepsilon}_{R1} - \boldsymbol{\varepsilon}_{R2}) = \mathbf{p}_1^T(\mathbf{u}_2 - \mathbf{u}_1) + \boldsymbol{\sigma}_1^T(\boldsymbol{\varepsilon}_{L1} - \boldsymbol{\varepsilon}_{L2}) > 0. \tag{b}$$

The positive definiteness of L_2 results from $(4.10)_2$ and from the convexity of the contact condition (cf. $(4.5)_2$). In view of (b) we can state that this conclusion holds also true in the case where steady distortions ε_D are additionally imposed on the slackened-elastic structure.

4.5. Slackened-elastic-perfectly plastic systems

Similarly to the previous case, the strain vector is the sum of elastic and distortion parts. However, distortion strains in slackened-elastic-plastic systems consist of clearance and plastic strains:

$$\text{(a)} \qquad \varepsilon_i = \varepsilon_{Ei} + \varepsilon_{Ri}; \quad \varepsilon_{Ri} = \varepsilon_{Li} + \varepsilon_{Pi}; \quad i = 1, 2.$$

Such systems demonstrate a lot of interesting effects and their behaviour is very complicated, particularly when plastic and clearance strains are simultaneously present. A complexity of this problem comes from the fact that clearance distortions, contrary to plastic ones, are always load-dependent. Therefore the signs of L_1, L_2, R_1 and R_2 in Ineqs. (3.5) cannot be evaluated. It is interesting to notice that even positive definiteness of right-hand sides of (3.5) does not have to be always guaranteed.

Let us consider, for example, the expression for R_2:

$$\text{(b)} \qquad R_2 = (\mathbf{u}_2 - \mathbf{u}_1)^T \mathbf{p}_2 + (\varepsilon_{L1} - \varepsilon_{L2})^T \sigma_2 + (\varepsilon_{P1} - \varepsilon_{P2})^T \sigma_2.$$

According to $(4.10)_2$, the first term in (b) is positive. On the other hand, the remaining terms consists of the non-positive definite part $(\varepsilon_{L1} - \varepsilon_{L2})^T \sigma_2$ (cf. $(4.5)_2$) and the part due to plastic strains $(\varepsilon_{P1} - \varepsilon_{P2})^T \sigma_2$, its sign being undeterminate, in general; however, for proportional loading the negative sign can be expected. Similar results can be obtained for L_1, L_2 and R_1. A numerical example of Sec. 5 will explain this problem.

5. Numerical Example

Consider a simple beam shown in Fig. 1.

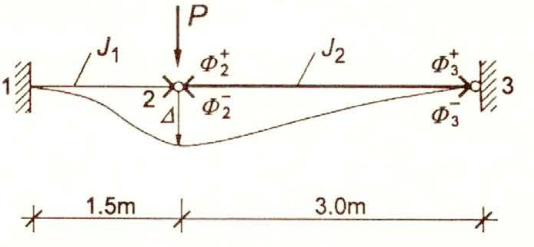

FIG. 1. Slackened beam with clearance hinges.

The beam is composed of two elements of ideal I-cross-sections. The moments of inertia and depths for both the elements are equal to $J_1 = 4500$ cm^4, $J_2 = 10000$ cm^4 and $h_1 = 30$ cm, $h_2 = 40$ cm, respectively. Two kinds of the material of the beam are assumed: the linear elastic of infinite strength, and the linear elastic-perfectly plastic with the yield stress $\sigma_Y = 300$ MPa. The corresponding full plastic bending moments of the cross-section for the beam-elements are $M_{Y1} = 90$ kNm and $M_{Y2} = 150$ kNm. The Young's modulus for both the materials is assumed to be the same: $E = 200$ GPa. In addition, at points 2 and 3 the so-called clearance hinges are introduced. In other words, the angle of free relative rotations of adjacent beam-elements $\phi_i (i = 2, 3)$ at these points can vary between the limits: $-\phi_i^- \leq \phi_i \leq \phi_i^+$. Angles ϕ_i play here the role of clearance strains. The cases where clearance hinges are introduced correspond to the systems which are slackened. If the clearance moduli (i.e. limit free rotations at clearance hinges) are equal to zero $\phi_i^- = \phi_i^+ = 0$, the beam becomes a common structure with bilateral constraints. Then the beam is fully fixed at both the supports (point 1 and point 3). So, we can consider the following four kinds of the system:

- elastic (E) $(\sigma_Y \to \infty, \phi_i^- = \phi_i^+ = 0)$,
- elastic-perfectly plastic (EpP) $(\sigma_Y = 300 \text{ MPa}, \phi_i^- = 0, \phi_i^+ = 0)$,
- slackened-elastic (SE) $(\sigma_Y \to \infty, \phi_i^- \neq \phi, \phi_i^+ \neq 0)$,
- slackened-elastic-perfectly plastic ($SEpP$) $(\sigma_Y = 300 \text{ MPa}, \phi_i^- \neq \phi, \phi_i^+ \neq 0)$.

Further considerations will be carried out for identical and symmetrically distributed rotation gaps, i.e. $\phi_2^- = \phi_2^+ = \phi_3^- = \phi_3^+ = \phi_0$. Variations of these gaps within the limits $< 0, 0.009$ rad $>$ allow us to analyse the elastic energy as a function of slackening intensity, including also the beam with bilateral constraints.

The beam is subjected to concentrated load P acting at point 2. The load increases proportionally up to $P_Y = 200$ kN (i.e. to the limit load for the elastic-perfectly plastic beam) and then the beam is proportionally unloaded.

Particular cases of the types specified above of the structure can be examined with respect to the elastic energy at given levels of the proportional loading. Additionally, the energy variations during unloading will be also presented.

The beam with rotation clearances belongs to a particular class of skeletal $SEpP$ structures where distortions are concentrated at the clearance, plastic or clearance-plastic hinges. The loading and unloading of the structure induce opening or closing of these hinges. As a consequence, the boundary conditions of elements (i.e. structure types) are changeable.

The current elastic energy W_E for particular kinds of the beam is calculated as a function of "deflection length" S_Δ or "load length" S_P. The current deflection of the beam Δ, deflection length S_Δ and load length S_P are defined as follows:

$$\Delta = \sum_{j=1}^{m} \Delta^{(j)}; \qquad S_\Delta = \sum_{j=1}^{m} \left|\Delta^{(j)}\right|; \qquad S_P = \sum_{j=1}^{m} \left|P^{(j)}\right|,$$

where $\Delta^{(j)}$ and $P^{(j)}$ denote the deflection rate of point 2 and the external load rate in the j-th step of the calculations, respectively. Symbol m denotes a current calculation step.

$P - \Delta$ diagrams for E, EpP, SE and $SEpP$ beams for $\phi_0 = 0.009$ rad are presented in Fig. 2a, while in Fig. 2b the elastic energy W_E versus the deflection

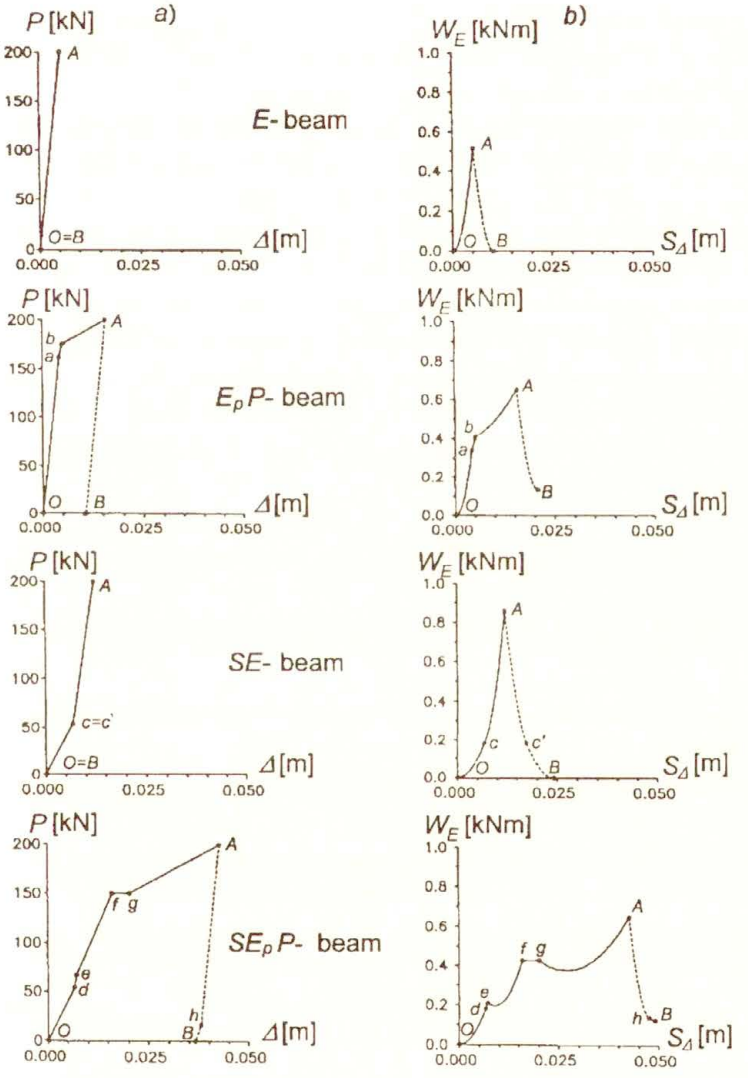

FIG. 2. Elastic energy for proportional loading of the beam; a) $P - \Delta$ diagrams, b) Elastic energy W_E versus deflection length S_Δ.

length S_Δ is plotted. Segments OA and segments AB correspond to proportional loading (solid lines) and unloading (dashed lines) of the beam, respectively. All the intermediate points indicate the structure type changes.

$P-\Delta$ relations for the E-beam and EpP-beam take a well-known form of concave functions. On the other hand, the presence of clearances induces locking effects which lead to convexity of $P(\Delta)$ functions. It is clearly seen for the SE-beam. The behaviour of $SEpP$-beam is much more complex; both the convexity (e.g. segment $O-d-e$) and concavity of $P(\Delta)$ function are noted. The $P(\Delta)$ convexity concerns also the unloading curve (segment $A-h-B$). Moreover, there exists the horizontal segment which corresponds to a "clearance-plastic mechanism" (cf. segment $f-g$). Obviously, the rates of elastic energy on this segment are equal to zero.

In the range of proportional loading, the elastic energy appears to be a monotone increasing function with respect to the beam deflection, except the case of the $SEpP$-beam (cf. Fig. 2b). It confirms the theoretical results of Sec. 4. Indeed, we can state that the elastic energy in the $SEpP$-beam can be a partially decreasing function of the load multiplier. Note that the energy of residual stresses does not have to coincide with that of the EpP-beam.

From Fig. 2 it follows that the elastic energy variations during the deformation processes must depend on the values of clearance moduli. In order to examine this problem we calculate W_E as a function of S_P during proportional loading for increasing values of rotation gaps, ϕ_0. Figure 3 shows $W_E(S_P)$ diagrams for particular kinds of the beam.

According to the results of Sec. 4, the elastic energy in the E-beam and SE-beam is an increasing function of the load multiplier (see Fig. 3a). From Fig. 3b it follows that for a sufficiently large values of ϕ_0, the elastic energy in the $SEpP$-beam can decrease while the load multiplier increases.

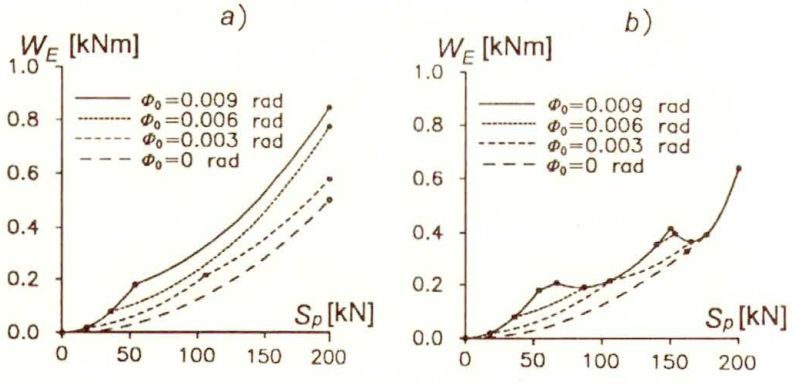

FIG. 3. Elastic energy variations for increasing gaps; a) Slackened-elastic beam, b) Slackened-elastic-perfectly plastic beam.

Now, the question arises: what is the physical and structural interpretation of the decreasing energy function?

Analysing the problem from the physical point of view we conclude that a part of the elastic energy can be converted into the plastic dissipation. Then the decrease in current elastic energy is observed. Obviously, such a phenomenon can occur only for structures whose material exhibits both the elastic and plastic deformations. To make the problem more clear, the current elastic energy W_E and the current total dissipation D in the $SEpP$–beam ($\phi_0 = 0.009$ rad) versus deflection length S_Δ are plotted in Fig. 4. It is seen that the elastic energy starts to drop down just as the plastic dissipation begins (cf. points e and g in Fig. 4).

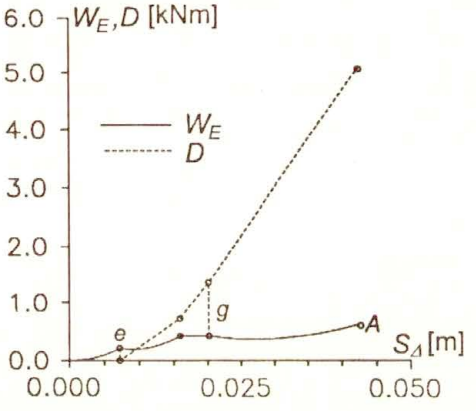

FIG. 4. Elastic energy W_E and total plastic dissipation D in $SEpP$–beam during proportional loading.

Next additional question is: "why can it occur only for the $SEpP$–beam?" An explanation of this problem can be found in Fig. 5 where changes of the structure type and the corresponding generalized stress (bending moment) distributions are presented. Figure 5a relates to $P = P_e = 65$ kN (point e in Fig. 4) and $P_{e\Delta} = P_e + \Delta P = 65 + 5 = 70$ kN. For $P = P_e$ the beam is fully fixed at the left-hand support and pin-ended at the right-hand support. The load increasing up to $P_{e\Delta}$ induces the structure type change; the beam becomes pin-ended at both the supports. Similar situation arises for $P = P_g = 150$ kN (point g in Fig. 4) and $P_{g\Delta} = P_g + \Delta P = 150 + 5 = 155$ kN. For $P = P_g$ at point 2 the new plastic hinge forms whereas at point 3 the clearance hinge closes and the beam becomes statically determinate. The structure-type changes give modifications of bending moment distributions. It can be easily checked that the elastic energy rates starting from $P = 65$ kN and $P = 150$ kN are negative. So, we can conclude that the elastic energy decrease is induced by deformation-dependent boundary condition changes. Such untypical changes can appear only for slackened-elastic-plastic structures where clearance and plastic strains simultaneously appear.

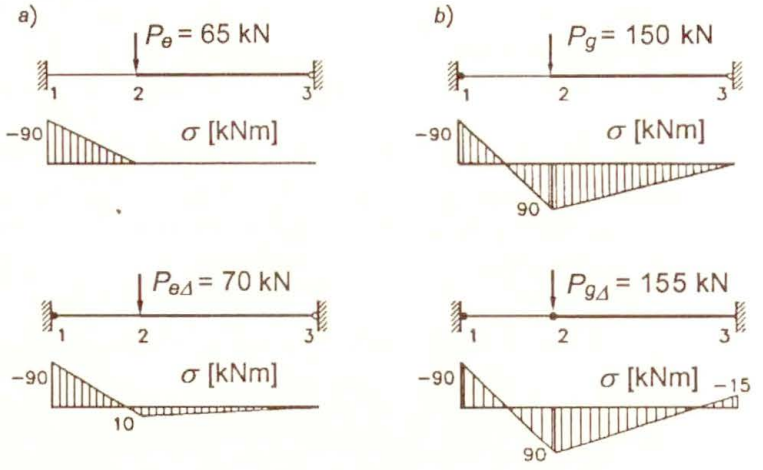

FIG. 5. Structure type and bending moment changes during proportional loading of $SEpP$–beam; a) load level e ($P = 65$ kN), b) load level g ($P = 150$ kN).

6. Final remarks

The present paper concerns the proportional loading of structures made of time-independent materials. It appears that this particular and simplest case of loading is not yet sufficiently recognized. It has been shown that the elastic energy can be a decreasing function of the load multiplier if unilateral constraints (i.e. gaps at structural connections) are introduced into an elastic-plastic structure. The results obtained in the paper seem to be of importance for the theory of structures and may have many theoretical implications. We have in mind, for instance, the damage mechanics where the elastic energy is usually assumed as an increasing function of the load multiplier. The problem appears to be much more significant due to the fact that damaged bodies contain internal gaps and therefore, this assumption seems to be not quite justified.

In spite the fact that the present work concerns discretized systems, the author believes that the results obtained herein can be generalized to continuous bodies made of time-independent materials.

Acknowledgements

This work was supported by the Polish Scientific Research Committee [KBN] under Grant No. 8T11F 017 10. This support is gratefully acknowledged.

References

1. V. VOLTERRA, *Sulle distorsioni dei solidi elastici piú volte connessi*, Rend. Lincei 5-e série, 1-er sem., **14**, 1905.

2. G. COLONNETTI, *Sul principio di reciprocita*, Rend. Lincei, 5-e série, 1-er sem., **21**, 393–398, 1912.

3. W. NOWACKI, *Thermoelasticity*, Pergamon Press-PWN, Oxford-Warszawa 1962.

4. J. A. KÖNIG, *Shakedown of elastic-plastic structures*, PWN-Elsevier, Warszawa 1987.

5. G. MAIER, *Mathematical programming methods in analysis of elastic-plastic structures* [in Polish], Arch. Inż. Ląd., **31**, 2, 387–411, 1975.

6. A. GAWĘCKI, *Elasto-plasticity of slackened systems*, Arch. Mech., **44**, 363–390, 1992.

7. A. GAWĘCKI, *Mechanics of slackened systems*, CAMES, **1**, 3–25, 1994.

8. A. GAWĘCKI, *Bounds on energy in discrete deformable systems*, Arch. Mech., **45**, 4, 439–455, 1993.

9. F. GENNA, *A nonlinear inequality, finite element approach to the direct computation of shakedown load safety factors*, Int. Mech. Sci., **30**, 10, 769–789, 1988.

10. A. GARSTECKI and Z. MRÓZ, *Optimal design of supports of elastic structures subjected to loads and initial distortions*, Mech. Struct. & Mach., **15**, 1, 47–68, 1987.

POZNAŃ UNIVERSITY OF TECHNOLOGY
INSTITUTE OF STRUCTURAL ENGINEERING

Received February 6, 1998.

Arch. Mech., 50, 5, pp. 865–875, Warszawa
FIFTY YEARS OF THE ARCHIVES OF MECHANICS

On two motions of a particle driven by equivalent ergodic and chaotic reflection laws

J. SZCZEPAŃSKI, Z. A. KOTULSKI (WARSZAWA)

IN THE PAPER we analyse dynamical systems describing the motion of a free particle in a domain on a plane (a square). We show that topologically equivalent reflection laws (each of them ergodic and chaotic) governing particle's motion at the moment of reflection can lead to two dynamical systems with entirely different qualitative properties. We also indicate a general problem of transferring such properties like chaos and ergodicity from a subsystem to the extended one.

1. Introduction

THE MOTION OF A FREE PARTICLE in a bounded domain is inherently determined by the shape of the boundary and the reflection law at this boundary. The reflection law is responsible for the global behaviour of the velocity of the particle during its contact with the boundary of the domain. In such dynamical systems (in the idealised theoretical model), the fundamental physical laws like the conservation of linear momentum and the conservation of energy are assumed to be satisfied what leads to extensively studied classical billiards. This means that the incidence angle is equal to the reflection one. In general, analysing the transformation of the angles of the moving particle at the moment of reflection one can observe that the reflection law itself is a dynamical system. This has created a temptation to consider the reflection law as an independent dynamical system.

The theory of the non-classical reflection laws found its place in the literature [1–5]. Up to now there are only hypotheses on what happens when the particle reaches the boundary, more or less confirmed by experiment. Reflection law models are an intermediate case between the deterministic systems first considered by SCHNUTE and SHINBROT [2] and systems with random reflection laws [6]. Namely, we admit a system with a strictly deterministic reflection laws that are not one-to-one maps. Thus, in this case it can happen that two different initial configurations in the phase space lead to the same final configuration what is impossible in the Schnute and Shinbrot model. There is a number of maps playing the role of the reflection law. The authors investigate the properties of the reflection laws finding that they can lead to such phenomena like: non-slip reflection on the boundary, non-increasing entropy, chaos, ergodicity (mixing property) of systems describing behaviour of the particle.

The reflection laws describe the global behaviour of the velocity of a freely moving particle during its contact with the boundary of the domain. From this

point of view, non-classical reflection laws do not satisfy such a fundamental physical law as the conservation of linear momentum. However, one can find some situations where such laws can describe realistic physical phenomena. Consider for example the container, the wall of which has some microstructure (Fig. 1). We assume that the mass of the reflected particle is negligible in comparison to the mass of the container. Then the reflection process, observed as non-classical, can in fact be the effect of few classical elastic reflections where, for every micro-reflection, the conservation of linear momentum is satisfied. In this model, due to the small scale of the microreflection, we identify the outgoing positions with the incoming point.

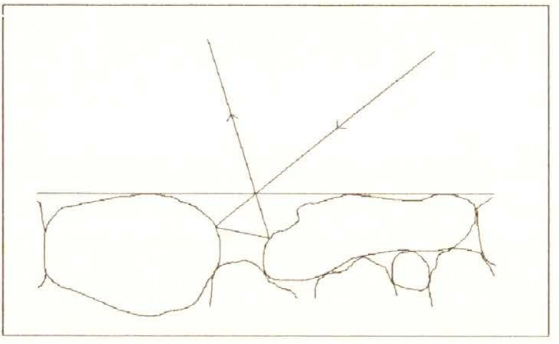

FIG. 1. Effect of the boundary microstructure on the reflection law.

After the reflection law was extracted from the extended dynamical system describing the motion of freely moving particle and then independently considered, one can ask the following questions: What are the properties of the extended system if we use non-classical reflection law? What is the effect of the specific properties of the reflection law (like chaos or ergodicity) on the behaviour of the particle? Is the particle motion chaotic or ergodic? Let us remark that this is a different problem than the chaotic or ergodic motion of the particle observed in classical billiard systems (connected with a specific shape of the domain's boundary). In this paper we just try to answer the question of transferring the specific properties from a non-classical reflection law to the dynamical system of a moving particle. We perform our considerations in two dimensions, where qualitative results we are interested in can be observed. Extensions of the results to more-dimensional spaces lead to some technical problems, what can be also observed in the case of the widely studied classical billiards theory. However, the results in two dimensions can give some suggestions concerning the behaviour of more-dimensional systems.

Problems of transferring of imposed properties from a dynamical system to its extension appear in various situations [4, 5, 7, 8] and seem to be interesting

both from the theoretical and practical point of view. They naturally arise from the problems of physics, engineering dynamics, mathematical economy and many others. In general, by an extended dynamical system we understand a system with state space of dimension greater than the original one and functionally dependent on it. Such a system can be a simple extension of the given dynamical system obtained by adding more co-ordinates without changing the form of the primary ones, or it can be some higher-dimensional dynamical system driven by the lower-dimensional one. In this paper we consider the transfer problems in the case of a free particle motion inside a bounded plane domain. We assume the reflection law as a primary dynamical system and the motion of the reflecting particle as an extended system.

To establish a reflection law model one must select a domain with a certain shape of the boundary and define the reflection law. Usually, the boundary is assumed to be a closed, sufficiently smooth curve. The reflection law can be quite general; in our considerations we assume that the particle moves with a constant velocity, changing the direction at the moment of reflection. In the particular case of the reflection law conserving the angle of incidence (the angle of incidence is equal to the angle of reflection), one obtains the class of dynamical systems called billiards. This conservative reflection law (as a map) is neither ergodic nor chaotic (see formula (*) in the next Section). However, it is well known that in appropriate domains it can lead to ergodic or chaotic motion of a particle. Thus, to obtain ergodic [9] and chaotic properties [8, 10–11] of a reflection law, one must assume another map relating the incident and outcoming angles. Such models have been studied in [1–5].

Applying various reflection laws, we face some natural questions when describing the motion of particles:

- Fix a reflection law. Do the ergodic and chaotic properties of the law transfer to the same properties of particles' motion for some typically used shapes of the domain?
- Fix a shape of the domain. Do topologically conjugate ergodic and chaotic reflection laws generate equivalent motion of the particle?

Some insight into the first problem was given in [5]. It was shown that for two simple domains, the ergodic and chaotic properties of the same reflection law can transfer in a quite different manner. In this paper we deal with the second question.

2. Formulation

Now we specify the model. We assume that the domain of a moving particle is a square. In the domain, the particle moves along straight lines with a constant velocity; when it encounters a wall it "reflects", that is, its velocity instantaneously

changes (according to some reflection law) to another "reflected" value to make the particle remain inside the domain. The motion of the particle is described by two co-ordinates (Fig. 2):

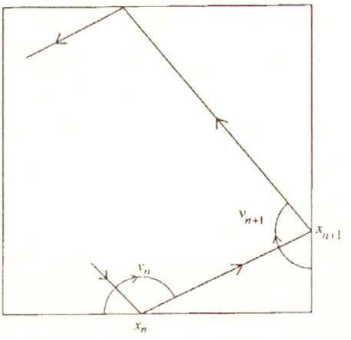

FIG. 2. The co-ordinate system used to describe the motion of a particle in a square.

- the position x_n at the square's boundary at the moment of the n-th reflection (measured counterclockwise from the fixed vertex of the square);
- the angle ν_n measured from the tangent to the boundary to the velocity vector of the point after reflection (clockwise).

To complete the definition of the system we assume some reflection law T : $(0,\pi) \to (0,\pi)$, $T(\nu_{\text{inc}}) = \nu_{\text{ref}}$ (Fig. 3). For example, in this formalism, the conservative reflection law is given by the map

$$\nu_{\text{ref}} = T(\nu_{\text{inc}}) = \pi - \nu_{\text{inc}}.$$

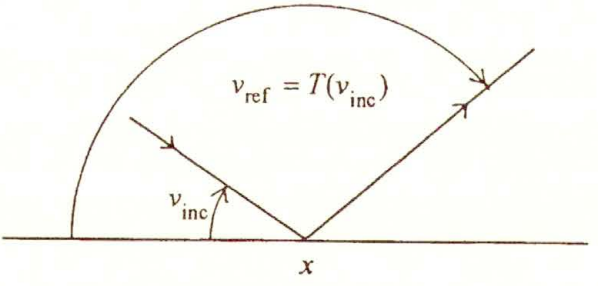

FIG. 3. The reflection law in local co-ordinates.

Thus, the motion is described by the two-dimensional map

$$F_T : [0,L) \times (0,\pi) \to [0,L) \times (0,\pi),$$
$$F_T(x_n,\nu_n) = (x_{n+1},\nu_{n+1}), \tag{2.1}$$

where the subscript in F_T denotes the dependence of the function on the reflection law T, and L is the length of the boundary of the square.

We consider the following two reflection laws:

$$T_1 : (0,\pi) \to (0,\pi),$$
$$\nu_{\text{ref}} = T_1(\nu_{\text{inc}}) = \frac{4}{\pi}\nu_{\text{inc}}(\pi - \nu_{\text{inc}}), \tag{2.2}$$

and

$$T_2 : (0,\pi) \to (0,\pi),$$
$$\nu_{\text{ref}} = T_2(\nu_{\text{inc}}) = \begin{cases} 2\nu_{\text{inc}} & \text{for} \quad \nu_{\text{inc}} \in (0,\pi/2), \\ 2(\pi - \nu_{\text{inc}}) & \text{for} \quad \nu_{\text{inc}} \in [\pi/2,\pi). \end{cases} \tag{2.3}$$

T_1 is a unimodal map which is ergodic and chaotic [12]. T_2 is the so-called tent map, also ergodic and chaotic [13].

These maps are topologically conjugate [14]; the equivalence is given by the homeomorphism

$$g(\nu) = 2 \arcsin \sqrt{\frac{\nu}{\pi}}, \tag{2.4}$$

i.e. the following diagram is commutative:

$$\begin{array}{ccc} (0,\pi) & \xrightarrow{T_1} & (0,\pi) \\ \downarrow g & & \downarrow g \\ (0,\pi) & \xrightarrow{T_2} & (0,\pi) \end{array} \tag{2.5}$$

This diagram yields the following implications:

I. If $\nu_k \to \tilde{\nu}$ (so $T_1(\nu_k) \to T_1(\tilde{\nu})$) then the g-corresponding sequences satisfy: $g(\nu_k) \to g(\tilde{\nu})$ and $T_2(g(\nu_k)) \to g(T_1(\tilde{\nu}))$.

II. If the orbit $\{T_1^n(\nu_0), n = 0,1,2,...\}$ has some properties like periodicity, asymptotic periodicity or density, then the g-corresponding $\{T_2^n(g(\nu_0)), n = 0,1,2,...\}$ orbit has the same properties.

3. Results

Consider the motion of the particle in a square. In the models presented, the velocity of the particle inside the square is constant and the reflection law at the boundary is given by either T_1 or T_2. It was proved in [5] that if the reflection law is defined by T_1 then the motion F_{T_1} of the particle is asymptotically periodic, i.e. for almost all initial points (x_0,ν_0), after sufficiently many reflections, the

particle moves closer and closer to the edges of the square. More precisely, the angle ν_n tends to π and so the motion of the particle converges to the periodic changes of the positions x_n from vertex to vertex.

Now assume that the reflection law is defined by T_2. We show that the motion F_{T_2} differs qualitatively from F_{T_1}. To study the behaviour of the system we observe the second co-ordinate ν of motion of the particle. First notice that due to the geometry of the square (see Fig. 4), the velocity ν_n changes in the following way:

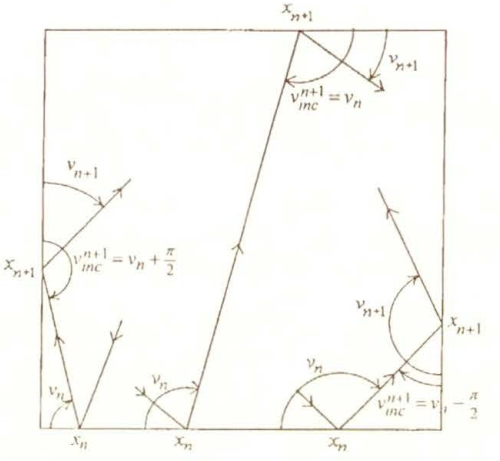

FIG. 4. Types of reflections in a square.

a) $\nu_{n+1} = T_2(\nu_n) = \begin{cases} 2\nu_n & \text{for} \quad \nu_n \in (\pi/4, \pi/2) \\ 2(\pi - \nu_n) & \text{for} \quad \nu_n \in [\pi/2, 3\pi/4) \end{cases}$ if the particle moves from one side to the opposite one. Notice that this is possible only when $\pi/4 < \nu_n < 3\pi/4$, which restricts the domain of the velocity in (2.3).

b) $\nu_{n+1} = 2\left(\frac{\pi}{2} - \nu_n\right)$ if the particle goes from one side to the clockwise adjacent side; this is possible only when $0 < \nu_n < \pi/2$.

c) $\nu_{n+1} = 2\left(\nu_n - \frac{\pi}{2}\right)$ if the particle goes from one side to the counterclockwise adjacent side; this is possible only when $\pi/2 < \nu_n < \pi$.

From the above we see that our two-dimensional system F_{T_2} is not a simple extension of the one-dimensional law T_2: due to the geometry of the square, the second co-ordinate is modified in comparison to the simple reflection law. Moreover, as we shall see below, the function describing the evolution of the second co-ordinate is multi-valued over the interval $(\pi/4,\ 3\pi/4)$ – see Fig. 5 (the choice of the value from two possibilities depends of the first co-ordinate, i.e. the position of the particle).

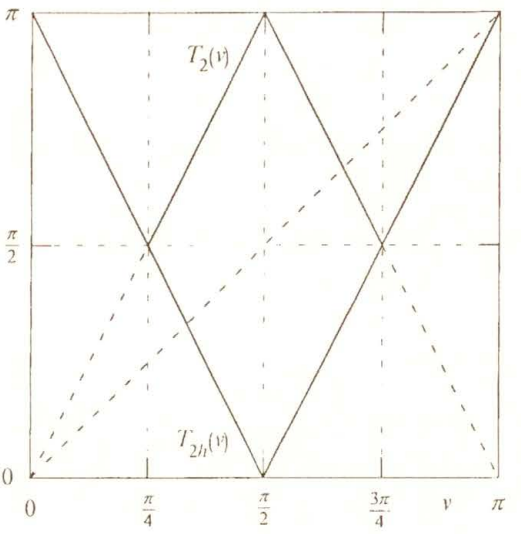

FIG. 5. The plot of the multi-valued map governed by the reflection law T_2.

Let us introduce a new function, based on the properties b) and c) of the reflection law:

$$T_{2h}(\nu) = \begin{cases} 2(\pi/2 - \nu) & \text{for} \quad 0 < \nu < \pi/2, \\ 2(\nu - \pi/2) & \text{for} \quad \pi/2 \leq \nu < \pi. \end{cases} \tag{3.1}$$

This function will be used for the study of the evolution of the second co-ordinate of F_{T_2}.

Observe that

$$T_{2h} = T_2 \circ h, \tag{3.2}$$

where h is a universal function, inherently connected with the shape of the square:

$$h(\nu) = \begin{cases} \nu + \pi/2 & \text{for} \quad 0 < \nu < \pi/2, \\ \nu - \pi/2 & \text{for} \quad \pi/2 \leq \nu < \pi. \end{cases} \tag{3.3}$$

One can see that after n reflections, the velocity of the particle, in the system of co-ordinates, is of the following form:

$$\nu_n = T_{\alpha_n} \circ T_{\alpha_{n-1}} \circ \ldots \circ T_{\alpha_1}(\nu_0), \tag{3.4}$$

where the subscripts are $\alpha_i = 2$ or $2h$ for $i = 1, 2, \ldots, n$. The sequence $(\alpha_i)_{i=1}^n$ is determined by the initial point (x_0, ν_0).

Notice that the reflection law T_2 has the following property:

$$T_2(\nu) = T_2(\pi - \nu). \tag{3.5}$$

Moreover, the function T_{2h} satisfies the condition:

$$T_{2h}(\nu) = \pi - T_2(\nu). \tag{3.6}$$

Both the above properties are satisfied for every $\nu \in (0, \pi)$.

From (3.5) and (3.6) we have

$$T_{2h}^2(\nu_0) = T_{2h}(T_{2h}(\nu_0)) = T_{2h}(\pi - T_2(\nu_0)) = \pi - T_2(\pi - T_2(\nu_0)) = \pi - T_2^2(\nu_0), \tag{3.7}$$

and generally, by induction,

$$\nu_n = T_2^n(\nu_0) \quad \text{or} \quad \nu_n = \pi - T_2^n(\nu_0). \tag{3.8}$$

We come to the conclusion that after the n-th reflection, the second co-ordinate of $F_{T_2}^n(x_0, \nu_0)$ is either $T_2^n(\nu_0)$ or the point symmetrical to $T_2^n(\nu_0)$ with respect to $\pi/2$. Now, because T_2 is ergodic (with an invariant measure equivalent to the Lebesgue measure), [13], we conclude that for almost all initial points ν_0 the set $\{\tilde{\nu}_n = T_2^n(\nu_0), n = 0, 1, 2, ...\}$ is dense in $(0, \pi)$ [9]. Thus, for almost all initial points (x_0, ν_0), the set of velocities $\{\nu_n, n = 1, 2, ...\}$ corresponding to each of them is dense in a set of Lebesgue measure of at least $\pi/2$. We see that the motion F_{T_2} is completely different from the motion F_{T_1}, where the sequence of velocities ν_n converged to the constant value π, independently of the initial position x_0 and the starting velocity ν_0.

Observe that an analogous result can be obtained for rectangles.

To end this section, we point out an interesting property of the relation (3.2). Consider the following chaotic and mixing reflection law:

$$T_3(\nu) = 2\nu \pmod{\pi}. \tag{3.9}$$

For this law applied to the motion of the particle in the square, the formula (3.2) becomes

$$T_{3h} = T_3 \circ h = T_3. \tag{3.10}$$

This is an example of a law invariant with respect to the function h. This class of reflection laws has an unusual property that the evolution of the second co-ordinate ν of particle's motion F_{T_3} is independent of the position x (the first co-ordinate of F_{T_3}).

4. Final remarks and conclusions

The problems studied in this paper were inspired by previous investigations connected with description of a single particle motion. The particle's motion with a non-classical reflection law arises in a number of practical physical phenomena.

The models of this kind can be observed in very rarefied gases, the so-called Knudsen gases [1, 4]. The investigation of the reflection law models allows us to predict, under some additional mathematical assumptions, the qualitative properties of the one-particle distribution function of the gas (e.g. the analyticity).

Another problem, directly related to the reflection law models, is the motion of a particle in accelerators [15]. Moreover, in this case the particle's motion can be described by the so-called "standard maps" which turned out to be the Poincaré maps generated by the moving particle [11, 16–17]. These maps are topologically conjugate to some dynamical systems obtained in the study of reflection law models [5].

The transfer of properties from smaller to extended dynamical systems can also be analysed in the motion of the particle in a viscous medium under the influence of a kick force. This phenomenon was modelled and investigated in [18].

Among many applications of chaos one can find also the recent utilisation of chaotic dynamical systems to construct secure communication (see e.g. [19–20]). In [21–22] we proposed the method of extending dynamical systems to construct safe cryptosystems. The results obtained in the above give some suggestions how such extensions can be performed. In the case of the block cryptosystems, the encryption and decryption is based on multiple inverse iterations and forward iterations. The secret key is introduced into the reflection law (the velocity of the particle) and the message is considered as the position of the particle [23]. Under the appropriate way of transferring the properties of the reflection law, the initial position of the particle cannot be reconstructed from the final position without the knowledge of the initial particle velocity (our secret key).

The considerations of this paper point out the interesting problem of constructing a chaotic and ergodic reflection law which would guarantee the transfer of these properties to certain extended dynamical systems, like the motion of a particle in a wide class of typical containers or some secure cryptosystems.

Our models show that there are no simple relations between the properties of a reflection law and the properties of the motion of the particle. Even for the same class of the reflection laws (in topological sense) with very strong properties like ergodicity and chaos, the qualitative properties of the motion of the particle (in commonly used containers) can be essentially different. It is an interesting open problem to find additional assumptions on the reflection law which would ensure the transfer of the above properties. It seems that such type of reflections could be interesting from the physical point of view.

References

1. H. Babovsky, *Initial and boundary value problems in kinetic theory. I. The Knudsen gas, II. The Boltzmann equation*, Transp. Theor. Stat. Phys., **13**, Part I pp. 455–474, Part II 475–498, 1984.

2. J. SCHNUTE, M. SHINBROT, *Kinetic theory and boundary conditions for fluids*, Can.J.Math, **25**, 1183–1215, 1973.

3. M. SHINBROT, *Entropy change and no-slip condition*, Arch. Rat. Mech. Anal., **67**, 351–363, 1978.

4. J. SZCZEPAŃSKI, E. WAJNRYB, *Long-time behaviour of the one-particle distribution function for the Knudsen gas in a convex domain*, Physical Review A, **44**, 3615–3621, 1991.

5. J. SZCZEPAŃSKI, E. WAJNRYB, *Do ergodic or chaotic properties of the reflection law imply ergodicity or chaotic behaviour of a particle's motion?*, Chaos, Solitons & Fractals, **5**, 77–89, 1995.

6. S. GOLDSTEIN, C. KIPNIS, N. IANIRO, *Stationary states for a mechanical systems with stochastic boundary conditions*, J. Stat. Phys. **41**, 915, 1985.

7. K. HIKAMI, P. P. KULISH, M. WADATI, *Integrable spin systems with long range interactions*, Chaos, Solitons & Fractals, **2**, 5, 543–550, 1992.

8. H. B. -LIN, *Chaos*, World Sc. Publ. Corp., 1984.

9. W. PERRY, *Topics in ergodic theory*, Cambridge Univ. Press, Cambridge 1981.

10. Y. POMEAU, *Intermittancy: a simple mechanism of continuous transition from order to chaos*, [in: Bifurcation Phenomena in Mathematical Physics and Related Topics], p. 155, Reidel 1980.

11. J-M. STRELCYN, *The "coexistence problem" for conservative dynamical systems: A Review*, Colloqium Mathematicum, **62**, 2, 331–345, 1991.

12. P. COLLET, J.-P. ECKMANN, *Iterated maps on the interval as dynamical systems*, A. JAFFE, D. RUELLE, BIRKHÄUSER, Boston 1980.

13. A. A. KOSJAKIN, E. A. SANDLER, *Ergodic properties of some class of piecewise smooth maps on the interval* [in Russian], Matematika, **3**, 32–40, 1972.

14. S. M. ULAM, J.von NEUMANN, *On combinations of stochastic and deterministic processes*, Bull. Amer. Math. Soc., **53**, 1120, 1947.

15. J. M. HOWETT, M. MONTH, S. TURNER, *Nonlinear dynamics, aspects of particle accelerators*, Proceedings, Sardinia, Lecture Notes in Physics, Springer, Berlin 1985.

16. Y. H. ICHIKAVA, T. KAMIMURA, T. HATORI, S. Y. KIM, *Stochasticity and symmetry of the standard map*, Prog. Theor. Phys., Supplement, **98**, 1–18, 1989.

17. R. S. MACKAY, *Transition to chaos for area preserving maps*, [in:] Nonlinear Dynamics Aspects of Particle Acceleretors, J. M. JOWETT, M. MONTH and S. TURNER [Eds.], Lecture Notes in Physics, 247, 390–454, Springer, 1986.

18. C. BECK, *Ergodic properties of a kicked damped particle*, Comm. Math. Phys., **130**, 51–60, 1990.

19. S. HAYES, C. GREBOGI, E. OTT, *Communicating with chaos*, Physical Review Letters, **70**, 20, 3031–3034, 1993.

20. W. MARTIENSSEN, B. HÜBINGER, R. DOERNER, *Chaotic cryptology*, Annalen der Physik, **4**, 35–42, 1995.

21. Z. KOTULSKI, J. SZCZEPAŃSKI, *Discrete chaotic cryptography*, Annalen der Physik, **6**, 5, 381–394, 1997.

22. Z. KOTULSKI, J. SZCZEPAŃSKI, *Discrete chaotic cryptography (DCC). New method for secure communication*, Proc. Non-linear Evolution Eequations and Dynamical Systems '97, http://www.roma1.infn.it/~ragnisco/proc97.htm, 1997.

23. Z. KOTULSKI, J. SZCZEPAŃSKI, K. GÓRSKI, A. PASZKIEWICZ, A. ZUGAJ, *Application of discrete chaotic dynamical systems in cryptography – DCC method* (submitted).

POLISH ACADEMY OF SCIENCES
INSTITUTE OF FUNDAMENTAL TECHNOLOGICAL RESEARCH
e-mail: zkotulsk@ippt.gov.pl
e-mail: jszczepa@ippt.gov.pl

Received March 13, 1998.

Arch. Mech., 50, 5, pp. 877–905, Warszawa 1998
FIFTY YEARS OF THE ARCHIVES OF MECHANICS

On the cyclic yield surface of some engineering materials under complex stress conditions

L. DIETRICH and Z. L. KOWALEWSKI (WARSZAWA)

THE PAPER PRESENTS a new method of mechanical parameters analysis. It deals with determination of a "cyclic yield surface" for selected engineering materials on the basis of cyclic curves experimentally obtained under a complex stress state. Location of the cyclic yield surface with respect to that of the initial yield locus may constitute the basis for evaluation of the material sensitivity to the cyclic deformation. Tests have been carried out with the use of PA6 aluminium alloy and 18G2A low-alloy steel, both in the as-received state. The experimental programme was the same for both considered materials. Firstly, an initial yield surface was determined using a number of specimens which were loaded up to the plastic range along different loading paths. Secondly, cyclic predeformations due to various loading paths in the plane stress state were induced by cyclic loading at ambient temperature under constant ($\Delta\varepsilon = \pm 0.65\%$) and gradually decreasing strain amplitude (from $\Delta\varepsilon = \pm 0.65\%$ to 0%). Finally, subsequent yield surfaces were determined using the single specimen method. It is shown that depending on the material, a cyclic loading induces softening (low-alloy steel) or hardening (aluminium alloy) effect in the strain range considered. All differences in material responses to cyclic prestraining for the tested materials are discussed in detail.

1. Introduction

SOLVING THE PROBLEMS associated with a variation of material properties due to cyclic loading inducing permanent deformation of the construction is regarded as one of the most important tasks of the plasticity theory [1–19]. A rapid progress observed nowadays in this area deals directly with the qualitative changes in the experimental technique, i.e. with development of both the computer systems enabling us to control the multiaxial testing machines working in the closed loop of feedback, and digital registration of experimental results together with their further conversion, using more powerful computers and novel software.

The steady-state cyclic deformation resistance of a material is usually described on the basis of the cyclic stress-strain curve [2]. According to the definition of the cyclic stress-strain curve, it is the locus of tips of the stable hysteresis loops from several companion tests at different, completely reversed constant strain amplitudes. Such a steady-state "stress amplitude – strain amplitude" curve is often compared with the monotonic stress-strain curve, Fig. 1. Depending on the mutual location of these curves, the cyclically induced changes in deformation resistance can be identified, i.e. softening if the cyclic curve is below the monotonic curve, and hardening if the cyclic curve lies above the monotonic curve.

Some materials are insensitive to the cyclic deformation and, as a consequence, in these cases the cyclic curve does not differ from the monotonic one.

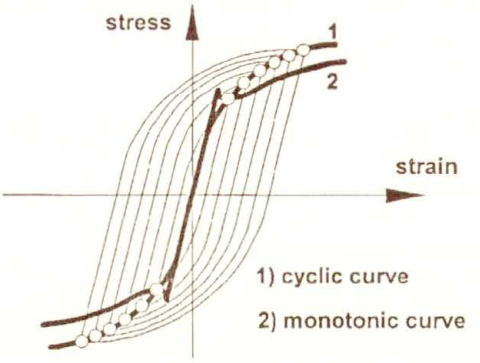

FIG. 1. Comparison of a typical cyclic and monotonic curves.

According to the definition given above, the cyclic stress-strain curve is obtained by connecting the tips of the stable hysteresis loops from several separate tests carried out at different, completely reversed strain ranges. Each test is performed at a constant strain amplitude. The loop can be achieved for some materials after several cycles. For the others, however, approximately half their fatigue life is required. Since this method requires a number of testpieces and relatively long testing time, it is rarely used in practice. To overcome these inconveniences, alternative procedures for determining the cyclic curves using only a single specimen are applied. The most known tests, described in detail by MORROW [1], are as follows:

(A) Multiple step tests,
(B) Incremental step tests,
(C) Monotonic tension after cyclic straining,
(D) Individual hysteresis loop,
(E) Decremental test.

The last method is regarded as the fastest and the most effective. It requires to load a specimen to a stable hysteresis loop under cycling loads at selected constant strain amplitudes, followed by cycling with a gradually decreasing strain amplitude up to the zero level. A number of cycles with a gradually decreasing strain amplitude should be sufficient to determine the cyclic curve with desired accuracy. Such a method was successfully used by LAMBA and SIDEBOTTOM [8] to obtain cyclic curves under nonproportional loading. The method was also applied to determine cyclic curves for different proportional cyclic loading paths in the strain space considered.

The main aims of the experimental project, the results of which are presented in the paper, were threefold. Firstly, it had to give an answer to the question: how

a plastic prestrain induced in metals during manufacturing processes of semifinished elements may change their mechanical properties. Secondly, the programme of tests had to determine up to what degree the known deformation history under cyclic loading may change the original anisotropy of the tested materials, and the third aim of the project was to determine a "cyclic yield surface" for the selected ranges of plastic deformation, on the basis of cyclic curves experimentally obtained under a complex stress state. The cyclic yield surface reflects the material ability to hardening or softening due to cyclic loading in different directions of the (σ_{xx}, τ_{xy}) stress plane. Although the cyclic yield surface does not describe the mechanical properties of a material subject to cyclic straining in an arbitrarily chosen direction, it may be treated as an envelope of the yield surfaces for a material subject to prior cyclic deformation in various directions. Its location with respect to that of the initial yield locus may constitute the basis for evaluation of the material sensitivity to the cyclic deformation.

2. Experimental details

Tests have been carried out with the use of low-alloy steel and aluminium alloy, both in the as-received state. Notations of these materials according to Polish Standards as well as their chemical composition are given in Table 1 and Table 2. According to ISO Standards 4950/2-1981, the chemical composition of the steel in question corresponds to that of the high yield strength steel with grade E355.

Table 1. Chemical composition of the 18G2A low-alloy steel manufactured according to Polish Standards.

	C	Mn	Si	P_{max}	S_{max}
	[%]	[%]	[%]	[%]	[%]
18G2A	max 0.2	1.0 – 1.5	max 0.55	0.04	0.04

Table 2. Chemical composition of the PA6 aluminium alloy manufactured according to Polish Standards.

	Cu	Mg	Mn
	[%]	[%]	[%]
PA6 aluminium alloy	3.8 – 4.8	0.4 – 1.1	0.4 – 1.0

All tests were carried out on tubular thin-walled specimens, manufactured from rods of 45 [mm] diameter. In the case of steel, the rods were manufactured

by rolling, whereas those for aluminium alloy – by extrusion. An engineering drawing of the specimen is shown in Fig. 2.

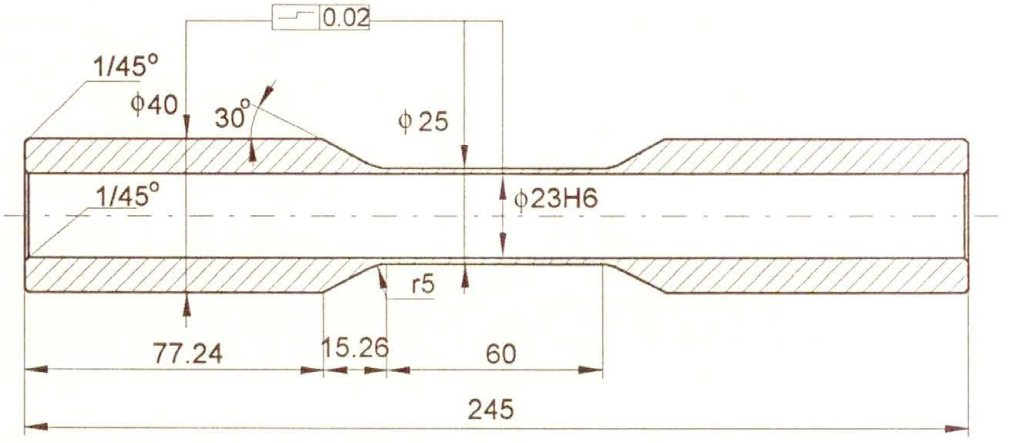

FIG. 2. Dimension of the specimen.

All experiments reported in this paper were carried out with the use of the INSTRON electrohydraulic, closed-loop, servo-controlled, biaxial testing machine enabling combined loading in tension – compression – torsion – reverse torsion.

The strains were measured by means of strain gauge rosettes bonded to the outer surface of the specimen on its gauge length. More details concerning the experimental procedure are given in [17].

3. Experimental programme

The experimental programme for both materials comprised three steps.

Firstly, an initial yield surface was determined for each material. In order to determine the initial yield surface, eight specimens were selected, each of them was loaded with different ratios of stress components in the two-dimensional stress space (σ_{xx}, τ_{xy}). In the next step of the experimental programme, prior deformation of specimens by means of proportional cyclic loading in selected directions of the (σ_{xx}, τ_{xy}) stress plane was carried out. The prestraining programme comprised two stages:

(1) cyclic loading for constant amplitude of total effective strain $\Delta\varepsilon = \pm 0.65\%$,

(2) cyclic loading with gradually decreasing total effective strain amplitude from $\Delta\varepsilon = \pm 0.65\%$ to $\Delta\varepsilon = \pm 0.0\%$.

The programme of constant strain amplitude cycles included 81 quarter-cycles. It was used to achieve the saturation cycle.

The programme of cyclic loading with decreasing strain amplitude comprised 30 full cycles. It followed just after the constant amplitude cycles were carried out, and was applied in order to determine cyclic curves.

For both materials eight different strain paths were considered, Fig. 3. These

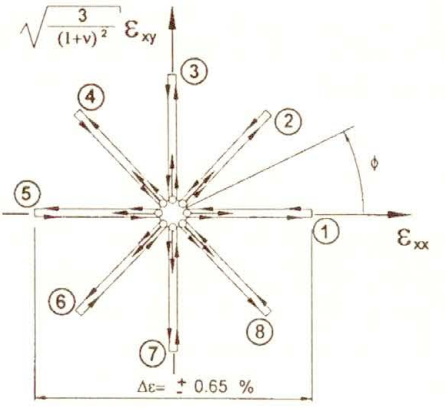

FIG. 3. Proportional cyclic loading paths for prestraining the materials.

paths were obtained by cyclic loading under strain control mode. Denotation of the vertical axis in Fig. 3 contains Poisson's ratio ν which for both materials was not equal to 0.5 in the strain range considered in the programme. The experimentally determined Poisson's ratios for the steel and aluminium alloy were equal to 0.34 and 0.30, respectively.

When the cyclic prestraining process of each specimen was completed, determination of the subsequent yield surface was performed on the INSTRON testing machine with the use of the single-specimen method, Fig. 4. In this technique a

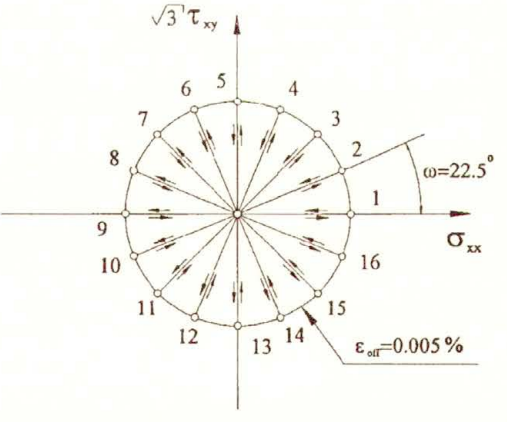

FIG. 4. Loading sequence for yield locus determination using single-specimen method.

specimen was loaded along various loading paths, each time until some measurable and limited plastic strain was observed (in our case the offset strain equal to $\varepsilon_{\text{off}} = 5 \times 10^{-5}$ was selected as the yield point). At each yield point the specimen was unloaded and again loaded in another direction until the entire yield locus was obtained. These directions varied from each other by a chosen angular increment assumed to be 22.5°. The experimental procedure comprised 16 points determined from the selected proportional loading paths. In Fig. 4 the increasing numbers at the yield points indicate the loading sequence.

4. Yield condition

SZCZEPIŃSKI [21] has proposed, on the basis of the Mises anisotropic yield condition [20], more general form of the yield condition for materials displaying the Bauschinger effect and rotation of the yield locus axes with respect to the coordinate system. That yield condition has been adopted in numerical calculations presented in the paper.

Generally, the Mises anisotropic yield condition in the form derived by Szczepiński can be expressed by the following relationship [21]:

$$
\begin{aligned}
(4.1) \qquad f(\sigma_{ij}) = {} & k_{12}(\sigma_{xx} - \sigma_{yy})^2 + k_{23}(\sigma_{yy} - \sigma_{zz})^2 + k_{31}(\sigma_{zz} - \sigma_{xx})^2 \\
& + 2\tau_{xy}\left[k_{16}(\sigma_{zz} - \sigma_{xx}) + k_{26}(\sigma_{zz} - \sigma_{yy})\right] \\
& + 2\tau_{yz}\left[k_{24}(\sigma_{xx} - \sigma_{yy}) + k_{34}(\sigma_{xx} - \sigma_{zz})\right] \\
& + 2\tau_{zx}\left[k_{35}(\sigma_{yy} - \sigma_{zz}) + k_{15}(\sigma_{yy} - \sigma_{xx})\right] \\
& - 2k_{45} \cdot \tau_{yz} \cdot \tau_{zx} - 2k_{56} \cdot \tau_{zx} \cdot \tau_{xy} - 2k_{64} \cdot \tau_{xy} \cdot \tau_{yz} \\
& + k_{44} \cdot \tau_{yz}^2 + k_{55} \cdot \tau_{zx}^2 + k_{66} \cdot \tau_{xy}^2 \\
& - b_{12}(\sigma_{xx} - \sigma_{yy}) - b_{23}(\sigma_{yy} - \sigma_{zz}) - b_{31}(\sigma_{zz} - \sigma_{xx}) \\
& + b_{44} \cdot \tau_{yz} + b_{55} \cdot \tau_{zx} + b_{66} \cdot \tau_{xy} = 1.
\end{aligned}
$$

In our experimental project, the tests have been performed under plane stress conditions for which only σ_{xx} and τ_{xy} were not equal to zero. When this is substituted into the relation (4.1), the yield condition simplifies as follows:

$$
\begin{aligned}
(4.2) \qquad f(\sigma_{ij}) = {} & (k_{12} + k_{31})\sigma_{xx}^2 - 2 \cdot k_{16} \cdot \tau_{xy} \cdot \sigma_{xx} + k_{66} \cdot \tau_{xy}^2 \\
& + (b_{31} - b_{12})\sigma_{xx} + b_{66} \cdot \tau_{xy} = 1,
\end{aligned}
$$

where coefficients k_{ij}, b_{ij} are functions of the yield limits determined from experiments at tension, compression, torsion, and reverse torsion tests.

Expression (4.2) represents the equation of a curve of second order, usually written in the form:

$$A\sigma_{xx}^2 + 2B\sigma_{xx}\tau_{xy} + C\tau_{xy}^2 + 2D\sigma_{xx} + 2F\tau_{xy} = 1, \tag{4.3}$$

where coefficients A and D denote functions of the yield limits at tension and compression. The coefficients C and F are related to the shear yield limits obtained from the tests under torsion and reverse torsion.

The B coefficient, which is proportional to the rotation of a yield surface with respect to (σ_{xx}, τ_{xy}) co-ordinate system, has no such simple physical interpretation as the coefficients described above, and it cannot be deduced from uniaxial tests. In order to find its value it is necessary to carry out at least one test in a complex stress state.

The yield condition in form (4.3) is determined by five material parameters which can be identified with such ellipse parameters as lengths of its axes, co-ordinates of ellipse centre, and rotation angle with respect to the co-ordinate system.

5. Experimental results

5.1. Results for the materials in the as-received state

Initial yield surfaces for aluminium alloy and low-alloy steel, both in the as-received state, obtained for the offset $\varepsilon_{\text{off}} = 5 \times 10^{-5}$, are shown in Fig. 5 and

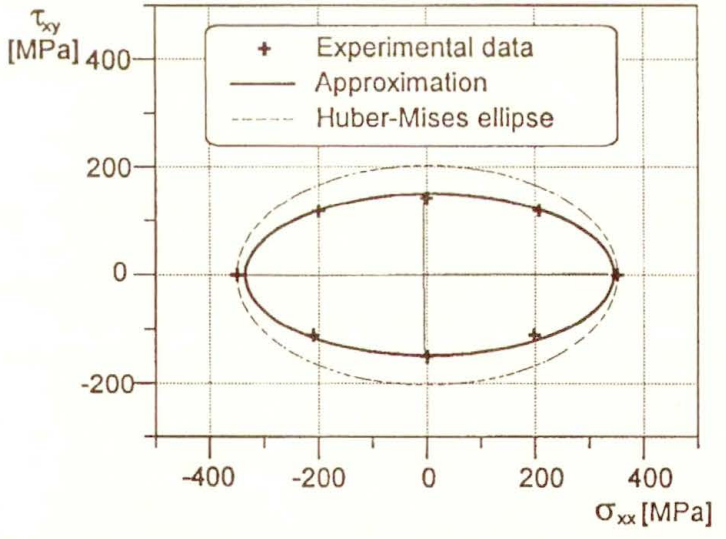

FIG. 5. Experimental points and fitted yield surface, Eq. (4.3), for the as-received aluminium alloy.

Fig. 6, respectively. Points in these figures represent experimental results while ellipses are determined by the least squares evaluation of the A, B, C, D, F coefficients in equation (4.3).

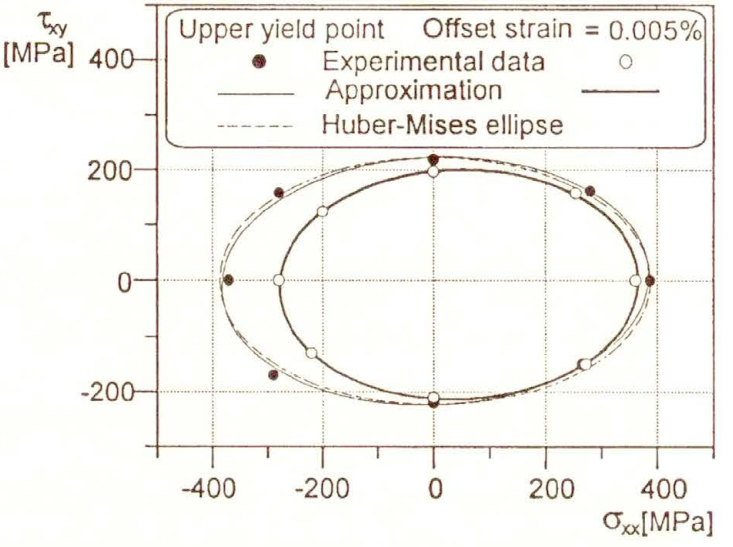

FIG. 6. Experimental points and fitted yield surfaces, Eq. (4.3), for the as-received low-alloy steel.

It is seen that the materials in the as-received state exhibit certain initial anisotropy which can be clearly identified by comparison of the experimental results with predictions obtained using the isotropic Huber-Mises yield condition. In both figures the Huber-Mises ellipses are plotted by broken lines.

In the case of aluminium alloy, an initial anisotropy is reflected by flattening of the theoretical yield surface calculated using the isotropic Huber-Mises yield condition.

Similarly to the aluminium alloy, also the low-alloy steel tested exhibits anisotropic behaviour in the as-received state. In this case, however, the effect manifests itself by the shift of the yield surface in the direction of tension.

The steel tested indicated upper and lower yield limits. The observations of the upper and lower yield points did not confirm an anisotropy of the mechanical properties of the steel observed for the assumed yield offset. In Fig. 6, besides the yield locus for the assumed offset strain, also the yield surface corresponding to the upper yield limit is presented. That surface was built on the basis of the "effective stress – effective strain" diagrams representing eight different directions in the two-dimensional stress space (σ_{xx}, τ_{xy}). As it is clearly shown, the upper yield point surface does not exhibit anisotropic effects. Hence, it can be described accurately by the isotropic Huber-Mises yield condition (ellipse plotted by

broken line in Fig. 6). However, it has to be noted that for each direction under consideration, the upper yield point corresponds to a different strain level. In other words, the ellipse reflecting the upper yield points obtained for various loading combinations does not represent any yield definition. Mutual location of the yield surfaces presented in this figure reveals a certain form of the anisotropy of the steel.

Summing up all of these remarks, it can be stated that both materials exhibit anisotropic properties in the as-received state coming from the industrial forming processes. In the case of steel however, we can observe isotropic properties in the sense of the upper yield limit, but the courses of the stress-strain characteristics up to the upper yield point for various loading paths tested in the programme are not coincident, identifying in this manner anisotropic character of the material in the strain range under consideration.

5.2. Results for the materials prestrained due to cyclic loading

The second step of the experimental procedure comprised the cyclic deformation carried out under constant strain amplitude with the objective to attain a saturated cyclic state, and cyclic deformation with gradually decreasing strain amplitude in order to obtain cyclic curves. An example of this process in case of torsion - reverse torsion cycles of aluminium alloy is presented in the Fig. 7a. The stress response onto the deformation programme given in Fig. 7a is shown in Fig. 7b.

In Fig. 7c the results for the cyclic loading with constant strain amplitude are illustrated in the form of the stress-strain diagram. As it is clearly seen, the saturation cycle was not achieved for the assumed programme of constant cyclic loading. The same effect was also observed for the remaining tests carried out for other directions of cyclic loadings.

Just after the constant strain amplitude cycles were carried out, the programme of cyclic loading with decreasing strain amplitude followed. An example of a typically observed stress response due to this part of programme is shown in Fig. 7d. The results in the form of a stress-strain diagram for the cyclic loading with decreasing strain amplitude illustrate the method for determination of the cyclic curve as a set of tips of the loops for cycles with decreasing strain amplitude. The results shown in this figure are plotted in the stress - total strain diagram. Using the DADiSP software, they can be automatically converted to a diagram of stress against plastic strain. Such transformation is presented in Fig. 7e.

In order to show how the initial anisotropy influences the response of the material to cyclic loading, the results for another loading path (tension - compression cycles) are presented in Figs. 8a, b, c, d. The sequence of figures is similar to that in the Figs. 7b, c, d, e, i.e. in Fig. 8a a stress response to the programme shown in Fig. 7a is presented, the stress response for constant strain amplitude cycling is

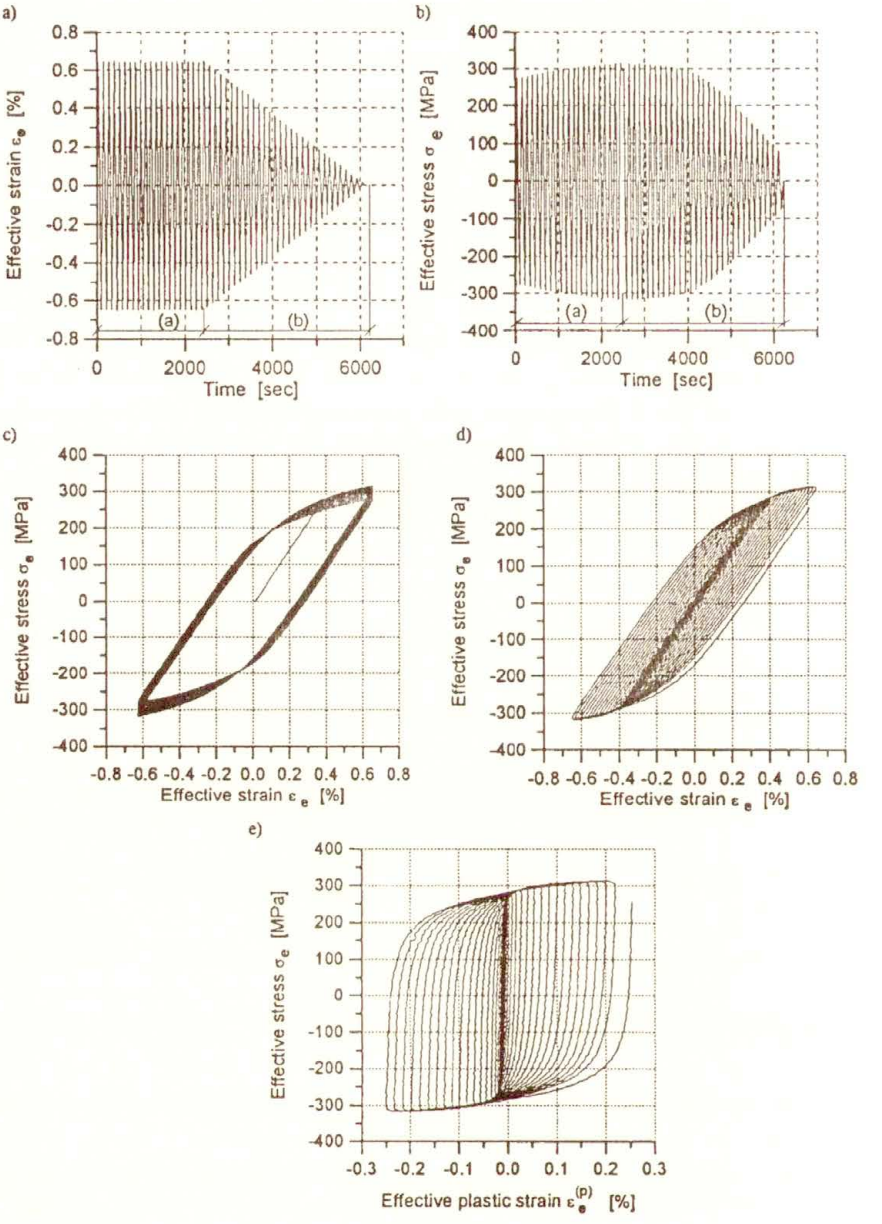

FIG. 7. a) Programme of cyclic loading for aluminium alloy (cycling in torsion-reverse torsion). b) Stress response to the strain-controlled cyclic loading shown in Fig. 7a. c) Stress response to the strain-controlled cyclic loading with constant strain amplitude. d) Stress response to the strain-controlled cyclic loading with decreasing strain amplitude. e) Stress - plastic strain diagram of the stress response to the programme of cyclic loading with decreasing strain amplitude.

shown in Fig. 8b. Figure 8c presents the stress response to the cyclic programme with gradually decreasing strain amplitude, and Fig. 8d shows the same results after subtraction of the elastic strain. It has to be noted that the width of the loops obtained during tension-compression cycles are significantly smaller than the loops achieved during cycling in torsion-reverse torsion (compare Figs. 7e and 8d).

The results for the steel in the case of cycling in tension-compression are demonstrated in Figs. 9 a, b, c, d, e. Again the stress response to the deformation programme given in Fig. 9a is shown in Fig. 9b. In the next figure (Fig. 9c), the

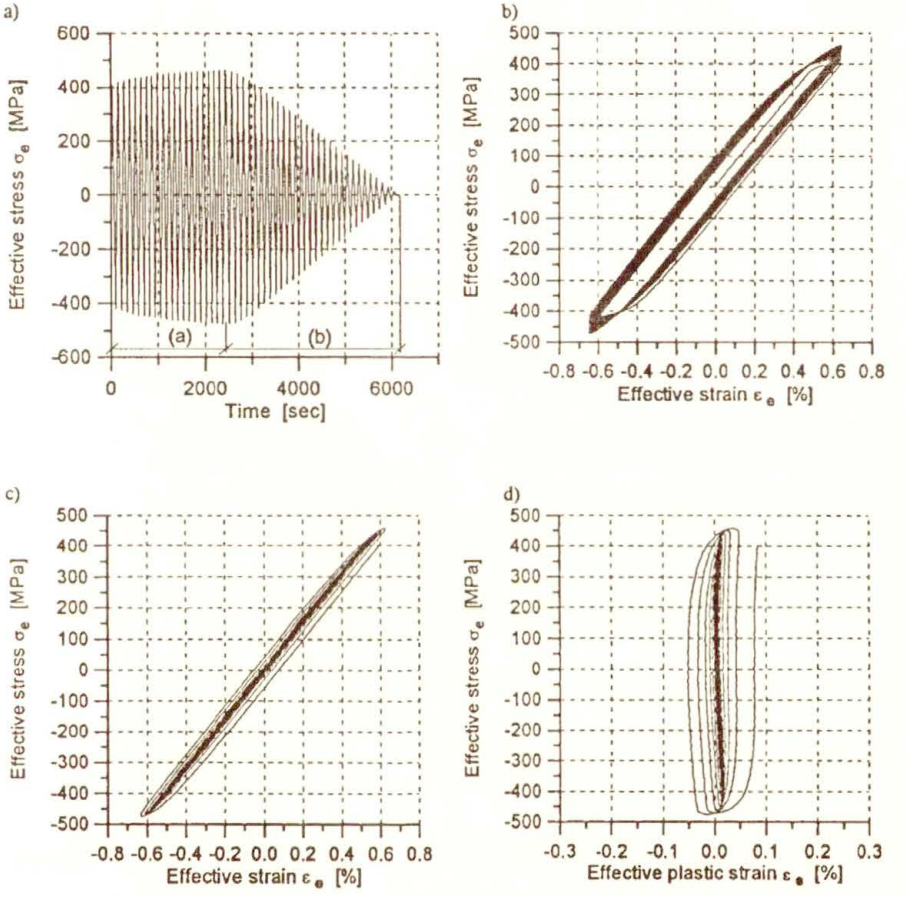

FIG. 8. Stress responses to cyclic loading of aluminium alloy (cycling in tension-compression). a) Stress response to the strain-controlled cyclic loading shown in Fig. 7a. b) Stress response to the strain-controlled cyclic loading with constant strain amplitude. c) Stress response to the strain-controlled cyclic loading with decreasing strain amplitude. d) Stress - plastic strain diagram of the stress response to the programme of cyclic loading with decreasing strain amplitude.

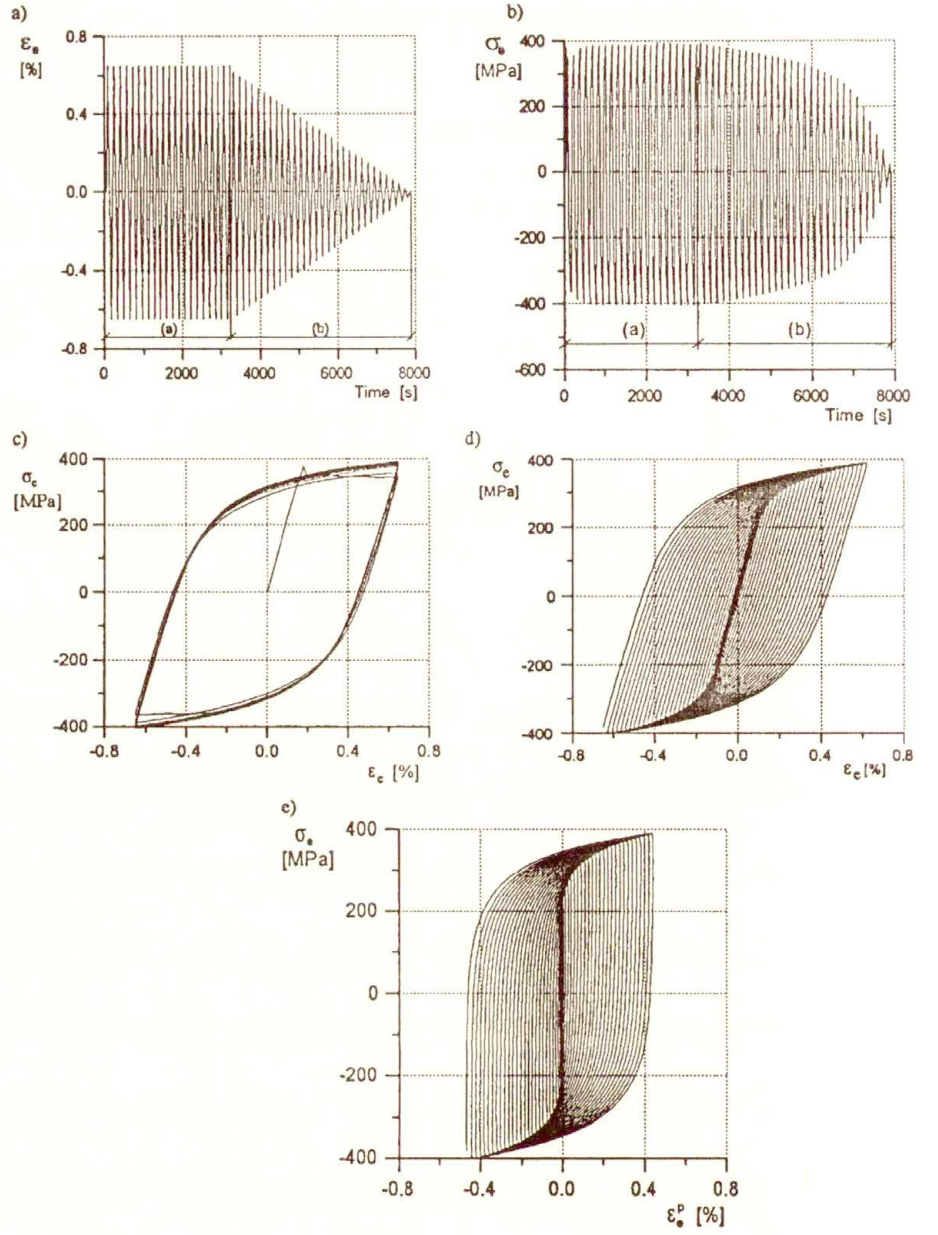

FIG. 9. a) Programme of cyclic loading for low-alloy steel (cycling in tension-compression). b) Stress response to the strain-controlled cyclic loading shown in Fig. 9a. c) Stress response to the strain-controlled cyclic loading with constant strain amplitude. d) Stress response to the strain-controlled cyclic loading with decreasing strain amplitude. e) Stress - plastic strain diagram of the stress response to the programme of cyclic loading with decreasing strain amplitude.

results for the cyclic loading with constant total strain amplitude are illustrated in the form of the stress-strain diagram. As it is clearly seen, the saturation cycle was achieved for the assumed programme of constant strain amplitude cycling relatively quickly, since it required only five full cycles. The same effect was also achieved for the remaining tests carried out for other directions of cyclic loadings. An example of a typically observed stress response due to the programme of cyclic loading with decreasing strain amplitude is shown in the next two diagrams. In Fig. 9d, the stress versus total strain is presented, whereas in Fig. 9e a diagram of stress versus plastic strain is shown.

In the case of the steel, independently of the cyclic loading paths considered, no essential differences in the width of the loops were observed, what distinguishes the results from those obtained for aluminium alloy.

The cyclic curves for aluminium alloy determined for all directions of cyclic deformation are compared in Fig. 10. All these curves exhibit different courses

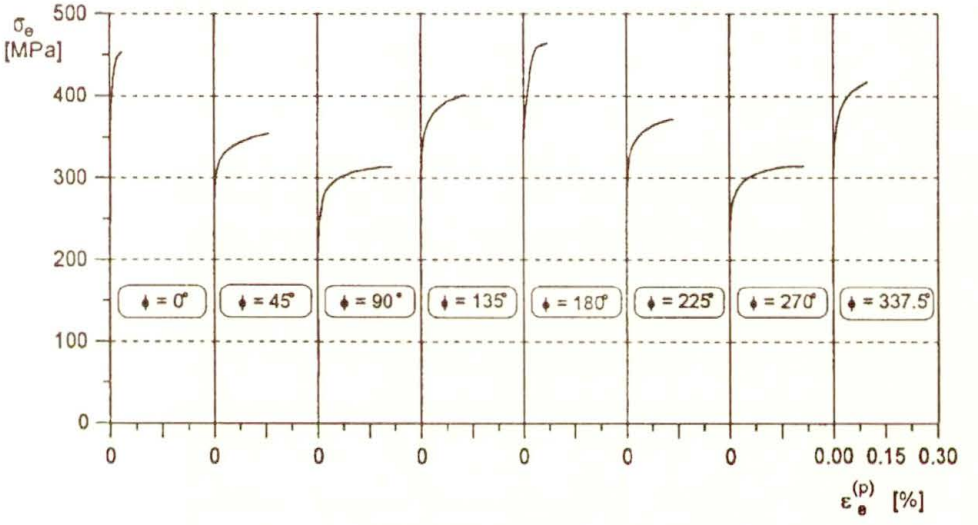

FIG. 10. Stress-strain curves of aluminium alloy for various directions of proportional cyclic loading.

and shapes. On the basis of cyclic curves, the cyclic yield locus has been determined, Fig. 11. Such a surface represents the ability of the material to variation of mechanical parameters due to cyclic deformation for different orientations in the plane stress state. It has been determined for the same yield offset as that used to obtain the initial yield surface ($\varepsilon_{\text{off}} = 5 \times 10^{-5}$) in order to enable their comparison. Comparative studies of the shapes and dimensions of the initial and cyclic yield surfaces, Fig. 11, show that the history of cyclic deformation in the plastic range induces hardening of the material. It is interesting to note that the greatest hardening was achieved in the directions of tension and compression

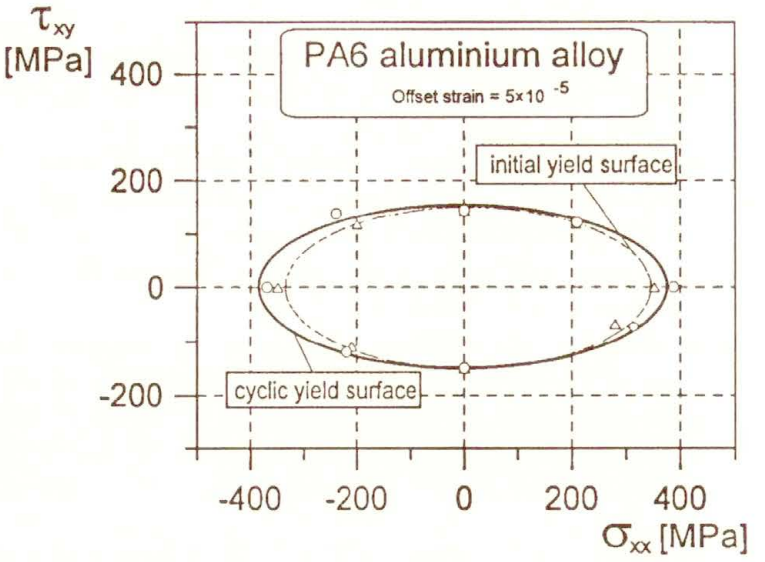

FIG. 11. Comparison of the cyclic yield surface with the initial yield locus for aluminium alloy.

while the smallest hardening was observed in the direction coincident with that of the initial anisotropy resulting from the forming processes (this direction corresponds to torsion-reverse torsion). It is clear that the initial anisotropy was not forgotten due to the cyclic process.

The cyclic curves for the steel determined for all directions of cyclic deformation are compared in Fig. 12. Contrary to the results for aluminium alloy, all

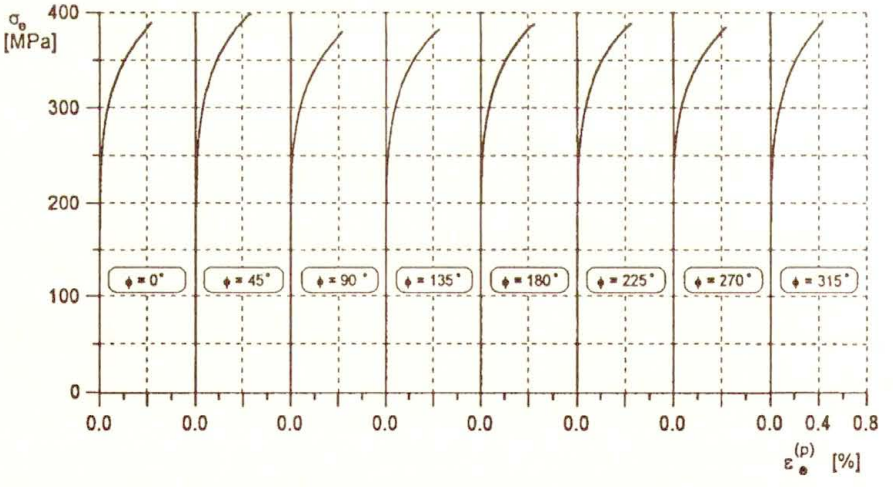

FIG. 12. Stress-strain curves of low-alloy steel for various directions of proportional cyclic loading.

these curves show a similar course and shape, especially at low level of the plastic strain (up to 0.01%). Here again, on the basis of cyclic curves, the cyclic yield locus has been determined, Fig. 13. Since the cyclic yield surface has been obtained for the same yield offset as that used to obtain the initial yield surface, it is easy to compare them and formulate the concluding remarks. Analysis of the shapes and dimensions of the initial and cyclic yield surfaces proves that the history of cyclic deformation in the plastic range for all directions induced softening of the material. It is interesting to note that, independently of the anisotropy observed in the as-received material, the centre of the cyclic yield locus is located in the origin of the co-ordinate system. Hence, it can be concluded that in steel, an initial anisotropy was forgotten due to the cyclic process, and the material exhibits a memory for the prestress induced during cyclic deformation.

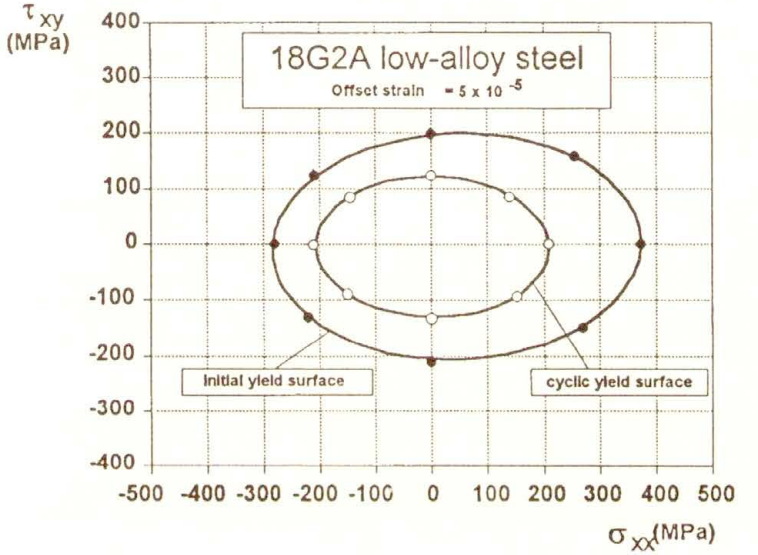

FIG. 13. Comparison of the cyclic yield surface with the initial yield locus for low-alloy steel.

After cyclic predeformation, yield surfaces for selected offset strain were determined by the technique of sequential probes of the single specimen. All yield surfaces determined for aluminium alloy after cyclic loading along selected proportional paths are shown in Fig. 14 for the offset strain equal to 5×10^{-5}. They are compared with the initial yield surface, plotted in the middle of Fig. 14, for the same offset strain. Numbers from 1 to 8 denote the data obtained for the material after different proportional cyclic loading paths, the orientation of which was described by $\phi = 0°$; 45°; 90°; 135°; 180°; 225°; 270°; 315°, respectively (cf. with Fig. 3). Points in Fig. 14 denote experimental results, while ellipses represent the best fit obtained by using equation (4.3). Yield surfaces, of the same offset,

for the aluminium alloy prestrained due to cyclic loading have significantly greater dimensions in comparison to those for the initial yield surface. This means that the aluminium alloy tested after cold work exhibits hardening effect in the strain range considered. Since the evolution and mutual location of the yield loci are not clearly reflected in Fig. 14, they are compared together in Fig. 15a, b. In

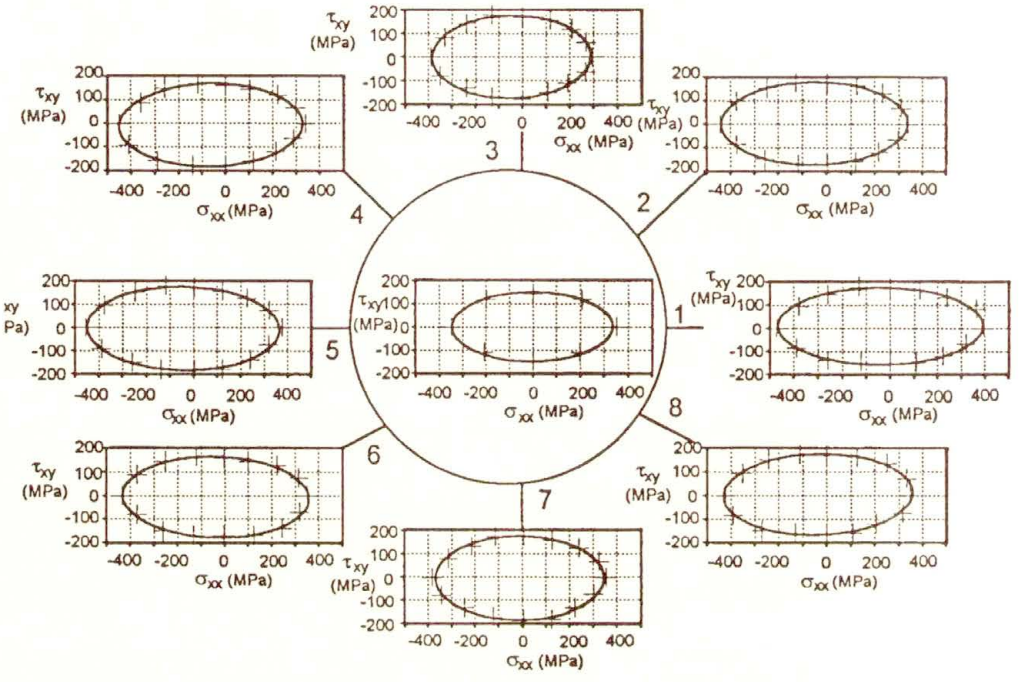

FIG. 14. Experimental points and fitted yield surfaces for aluminium alloy prestrained due to cyclic loading along various proportional paths, offset strain 5×10^{-5}.

order to keep clear view, the data points in Fig. 15a, b are omitted. Numbers in both figures denote orientations of the proportional cyclic loading paths. Shown in Fig. 15a are yield surfaces for the material prestrained due to cyclic loading in directions described by $\phi = 0°$; $\phi = 90°$; $\phi = 180°$; $\phi = 270°$, whereas in Fig. 15b are shown subsequent yield surfaces for the remaining cyclic loading paths considered in the experimental programme. The shape analysis of these yield surfaces leads to the conclusion that the dimensions of yield locus are dependent on the direction of cyclic preloading. The greatest hardening effect was achieved in the tension and compression directions. It is shown that the sense of the loading direction in the first cycle for the chosen direction changes solely the location of the yield locus centre without any other visible differences, especially in the shape and dimensions of the surface. It was confirmed for all the directions examined.

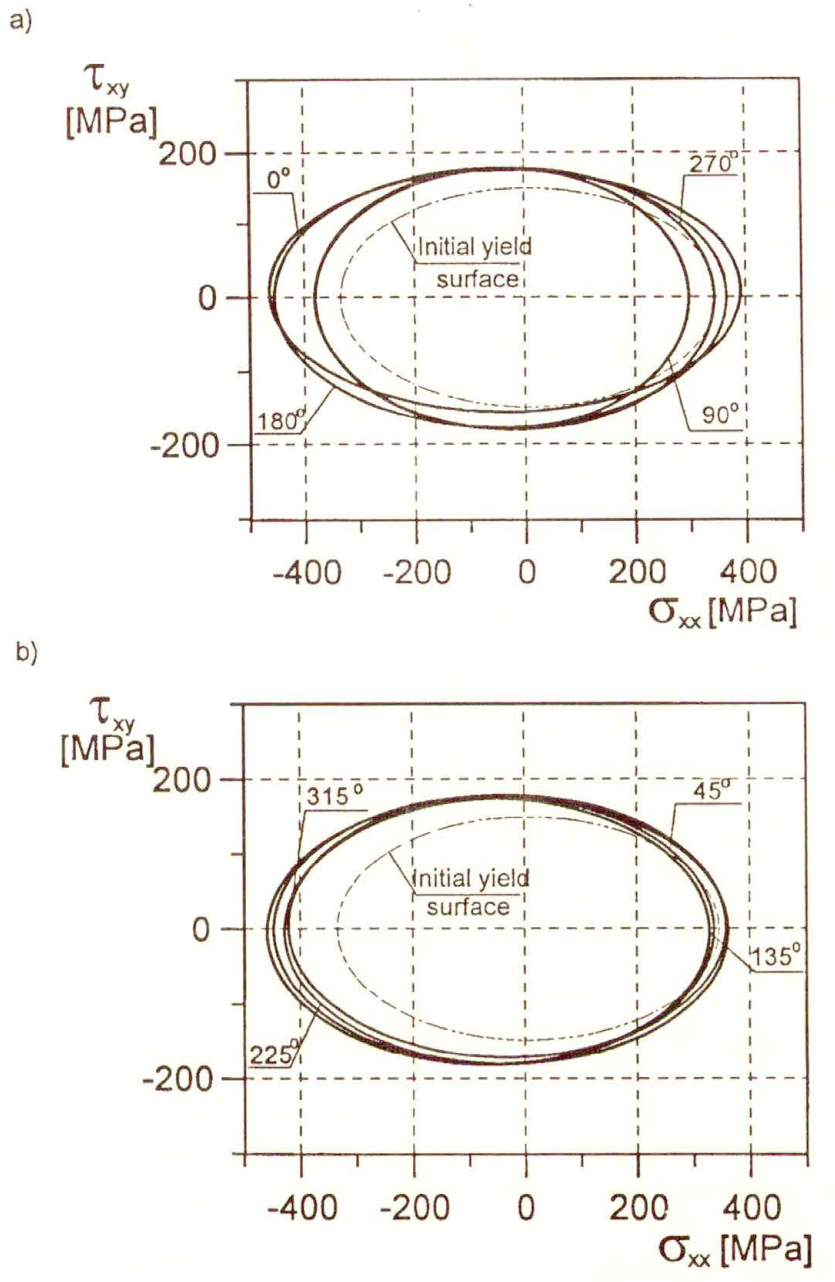

FIG. 15. Comparison of the initial yield surface with subsequent yield loci (aluminium alloy) a) after prestraining due to cyclic loading along the following proportional strain paths: 0°, 90°, 180°, 270°, offset strain 5×10^{-5}; b) after prestraining due to cyclic loading along the following proportional strain paths: 45°, 135°, 225°, 315°, offset strain 5×10^{-5}.

In the next two figures are shown the results for steel. In Fig. 16 are presented experimental points together with ellipses reflecting the shapes and dimensions of the subsequent yield surfaces which have been determined using the yield

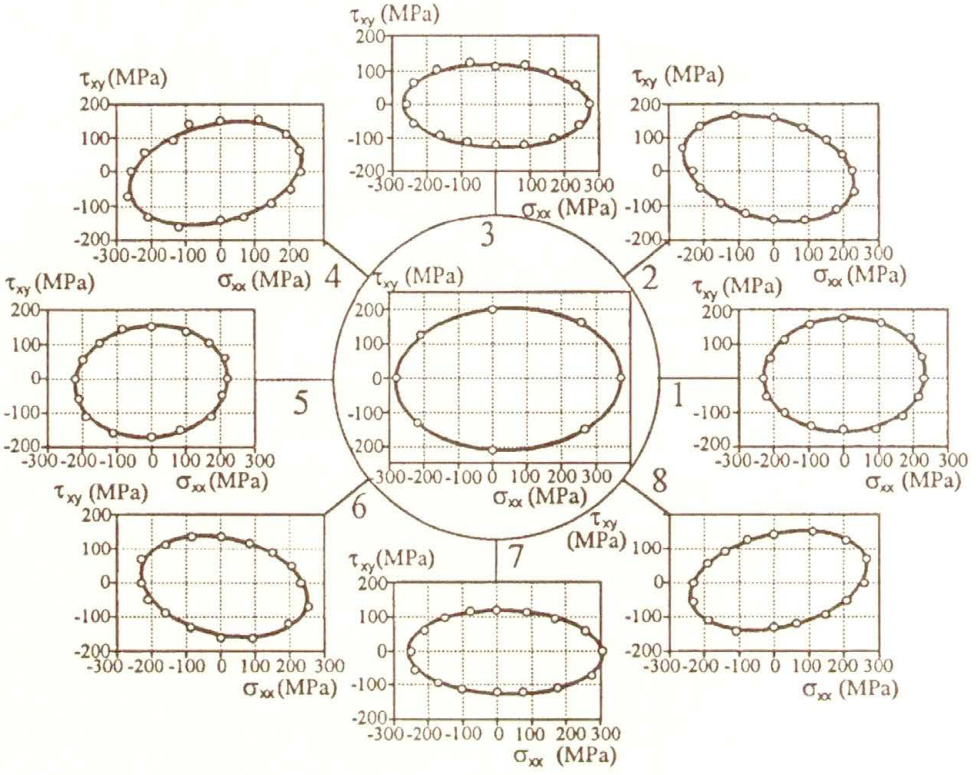

FIG. 16. Experimental points and fitted yield surfaces for the steel prestrained due to cyclic loading along various proportional paths, offset strain 5×10^{-5}.

condition in the form of equation (4.3). As it is clearly seen, a good agreement is achieved between the experimental data and the results following from the approximation. Similarly to the data analysis of aluminium alloy, in order to enable accurate assessment of the steel yield loci variations, in Fig. 17 a, b are shown subsequent yield surfaces at one co-ordinate system without experimental points. They are compared with the initial yield surface (bold line) for the same offset strain ($\varepsilon_{\text{off}} = 5 \times 10^{-5}$). Again numbers in both figures denote orientation of the proportional cyclic loading paths. Yield surfaces, of the same offset strain, for the steel prestrained due to cyclic loading have significantly smaller dimensions in comparison to those for the initial yield surface, so they are located within it. This means that the low-alloy steel tested after cyclic cold work exhibits softening effect in the strain range considered. The shape analysis of these yield surfaces

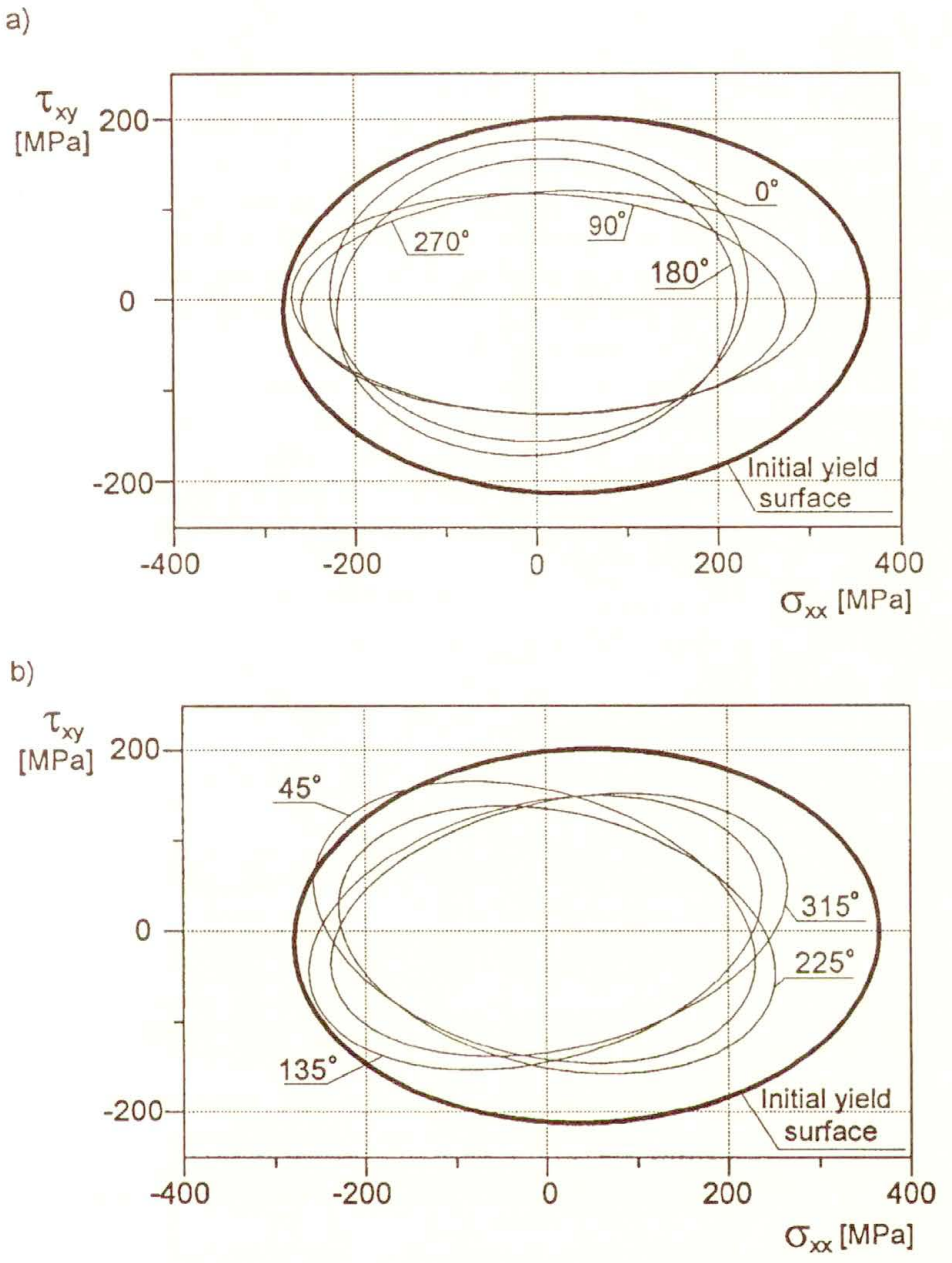

FIG. 17. Comparison of the initial yield surface with subsequent yield loci (low-alloy steel) a) after prestraining due to cyclic loading along the following proportional strain paths: 0°, 90°, 180°, 270°, offset strain 5×10^{-5}; b) after prestraining due to cyclic loading along following proportional strain paths: 45°, 135°, 225°, 315°, offset strain 5×10^{-5}.

leads to the conclusion that the dimensions of yield locus are dependent on the direction of cyclic preloading. The greatest softening effect was always achieved in the direction which was coincident with that used in the preliminary cyclic deformation. The effect of the cyclic loading sense in the first cycle is clearly illustrated in Fig. 17a for example for $\phi = 90°$ and $\phi = 270°$. It is shown that the sense of the loading direction in the first cycle for the chosen direction changes solely the location of the yield locus centre without any other visible differences. It was observed for all the directions examined.

More accurate analysis concerning the degree of the prestraining effect can be attained on the basis of graphical illustrations of the variation of yield surface dimensions as a function of the predeformation direction. The variation of the major and minor semi-axes of the subsequent yield surfaces for the steel due to cyclic prestraining is shown in Fig. 18 as a function of cyclic loading direction.

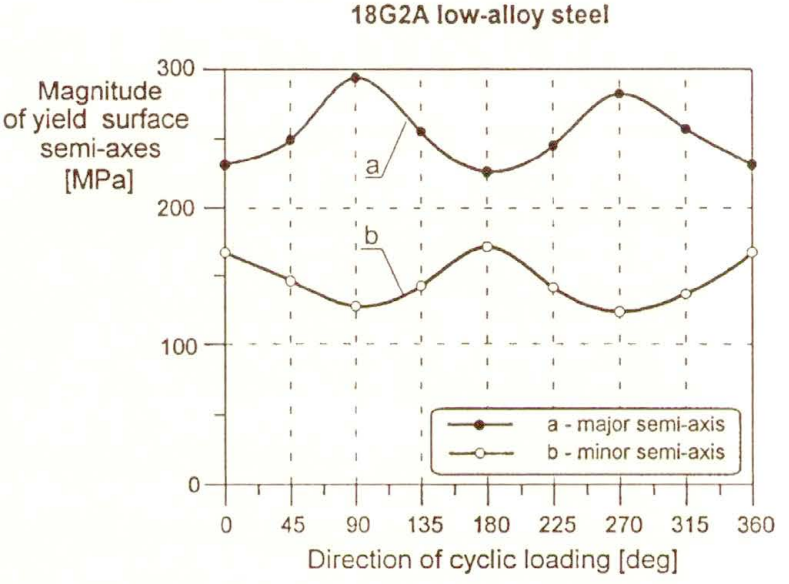

FIG. 18. Variations of the major and minor semi-axes of subsequent yield surfaces for the steel.

The same diagram for the aluminium alloy is presented in Fig. 19. From these diagrams it can be observed how the cyclic deformation changes basic dimensions of the yield surface.

The major semi-axis of the initial yield surface for steel was equal to 326 MPa, while the minor one was equal to 204 MPa. The same dimensions for the aluminium alloy were 341 MPa and 150 MPa, respectively.

The effect of softening is clearly demonstrated for the steel in Fig. 18. The maximum softening observed for this material was achieved for those directions

which were coincident with the cyclic ones. Moreover, a confirmation of the conclusion that for the selected proportional loading path, the degree of softening was not sensitive to the sense of loading, can be easily found. For example, the degree of softening for the "positive torsion-negative torsion" direction was almost the same, independently of the sense of cyclic process initiation, i.e. the positive torsion (90°) or the negative torsion (270°). The smallest softening effect was observed for the direction perpendicular to that at the cyclic loading used.

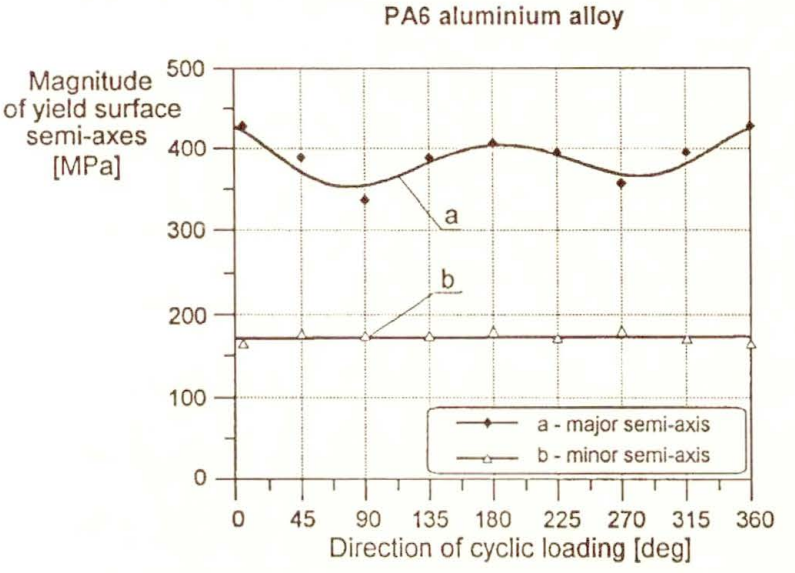

FIG. 19. Variations of the major and minor semi-axes of subsequent yield surfaces for the aluminium alloy.

Completely opposite effects were observed for the aluminium alloy, Fig. 19. The material generally exhibits a hardening effect. Although for the directions coincident with cyclic loading the maximum hardening was observed, the degree of this effect was not the same for all the directions considered. It is interesting to note that for the aluminium alloy there were no clear differences in the magnitude of minor axes of the subsequent yield surfaces. The reason of such behaviour results from the manufacturing processes used to produce rods of aluminium alloy. These processes induced anisotropy which could not be changed by the cyclic loading applied in the experimental programme.

In Fig. 19 it is also easy to find a confirmation of the conclusion that for the selected proportional cyclic loading path the degree of hardening was almost not sensitive to the sense of loading. For example, the degree of hardening for the tension-compression direction was almost the same (the difference was less than 5%), independently of the sense of the cyclic process initiation, i.e. the tension (0°) or the compression (180°).

It is interesting to study how cyclic deformation influences the rotation of yield surfaces. In the case of steel tested, the rotation depends on the cyclic loading path. Experimental data illustrating the rotation of the initial yield locus due to cyclic loading path orientation are shown in Fig. 20 in form of circles for the steel, and crosses for the aluminium alloy. Lines in this figure correspond to the approximations carried out using the least squares method. A significant rotation of the yield surface is observed for the steel. It depends on the orientation of the cyclic loading path. However, as it is shown in Fig. 20, the angle of rotation of the yield surface almost does not depend on the sense of loading. It means that there are no significant differences in rotation for cyclic loading determined by those ϕ which describe the same direction, that is 0° and 180°, 45° and 225°, 90° and 270°, 135° and 315°.

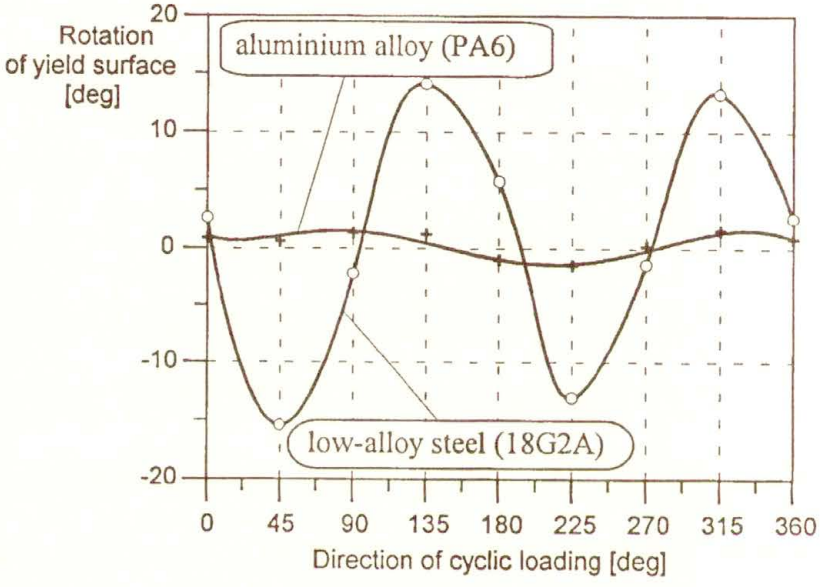

FIG. 20. Comparison of the yield surfaces rotation due to cyclic prestraining.

In the case of aluminium alloy the results show an opposite effect, that is there was not observed any significant rotation of the subsequent yield surfaces due to the same programme of cyclic loading as that applied during the steel tests.

In order to complete the analysis of both materials, in Figs. 21 and 22 are presented the variations of yield limits due to cyclic prestraining for the low-alloy steel and aluminium alloy, respectively. Initial values of the yield limits obtained for the same offset strain equal to 5×10^{-5} are shown in Table 3 for the low-alloy steel and in Table 4 for the aluminium alloy.

Table 3. Yield limits for the as-received low-alloy steel (offset strain 5×10^{-5}).

Tension yield limit	Compression yield limit	Torsion yield limit	Reverse torsion yield limit
372 MPa	280 MPa	198 MPa	210 MPa

Table 4. Yield limits for the as-received aluminium alloy (offset strain 5×10^{-5}).

Tension yield limit	Compression yield limit	Torsion yield limit	Reverse torsion yield limit
341 MPa	341 MPa	150 MPa	150 MPa

All yield limits considered for the steel decreased after cyclic prestraining. Maximum decreasing of the corresponding yield limits was obtained for the directions coincident with cyclic loading. As shown in Fig. 21, the tension and

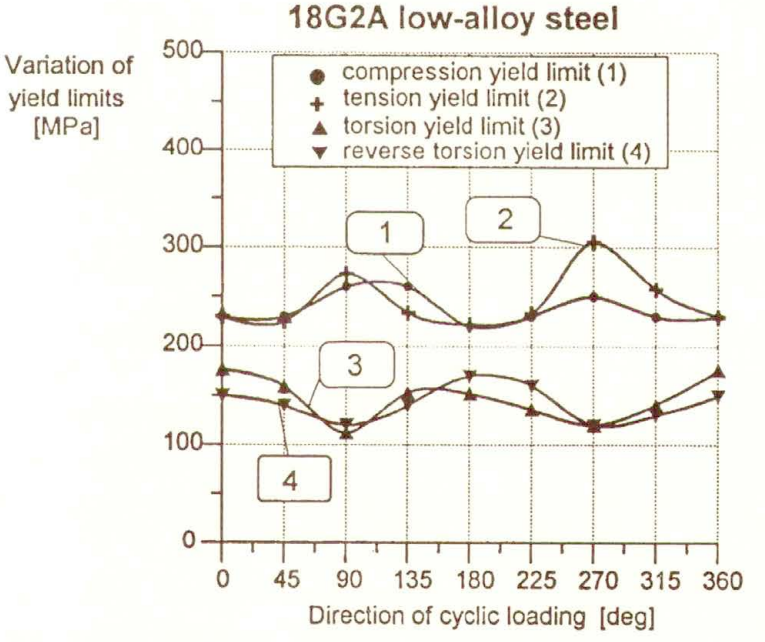

FIG. 21. Variations of yield limits due to cyclic prestraining of the steel.

compression yield limits do not differ considerably after prestraining. Since these parameters before cyclic loading differ by more than 20%, it can be concluded

that the process of cyclic prestraining caused forgetting of the initial anisotropy resulting from the manufacturing processes of rods used as the blanks for specimens.

In the case of the aluminium alloy, almost all yield limits increased (except the tension yield limits for the directions of cyclic loading described by the value of ϕ equal to 45°, 90° and 135°) after cyclic loading in comparison to those determined for the material in the as-received state. Contrary to the steel, the torsion and reverse torsion yield limits for the aluminium alloy after prestraining do not depend on the cyclic loading direction. For all directions the same values of these limits were obtained and they can be approximated with a good accuracy by straight lines, Fig. 22. Such a result suggests that the range of strain realised during cyclic loading was not sufficient to change the initial anisotropy of the aluminium alloy, and the material still exhibits a memory for the maximum prestress induced during the manufacturing processes.

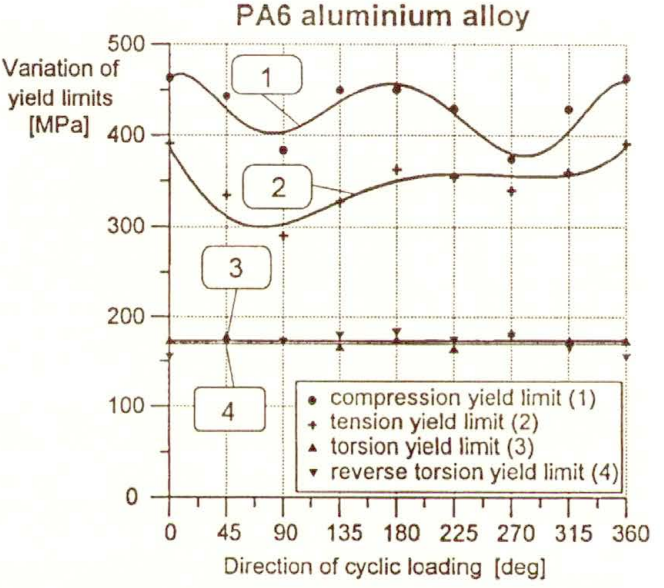

FIG. 22. Variations of yield limits due to cyclic prestraining of the aluminium alloy.

6. Applicability assessment of the cyclic yield surface concept

Having cyclic curves and the results from monotonic loading tests used to obtain subsequent yield surfaces for the materials tested after prestraining, the directions of maximum softening/or hardening due to cyclic loading can be identified in the strain range considered. It can be done using two methods. Using the first method, the cyclic yield surface shown earlier, can be constructed on the basis of cyclic curves.

In the second method, a surface being an envelope of all yield loci determined for the cyclically prestrained material can be constructed. Such a surface can be obtained on the basis of stress-strain diagrams coming from the first probes of the single-specimen method used to determine the subsequent yield surfaces. To construct this surface, the results obtained from eight first probes were used. Since each time the first probe was taken to be coincident with the direction of the first cyclic loading, the experimental programme for both materials enables us to determine eight points creating the envelope mentioned above. Assuming the yield offset to be $\varepsilon_{\text{off}} = 5 \times 10^{-5}$, the surfaces being envelopes of all subsequent yield loci presented in Fig. 14 for the aluminium alloy and in Fig. 16 for the steel, can be constructed. In the case of steel, the surface obtained in this way represents the maximum softening of the material. In Fig. 23 it is compared with the cyclic

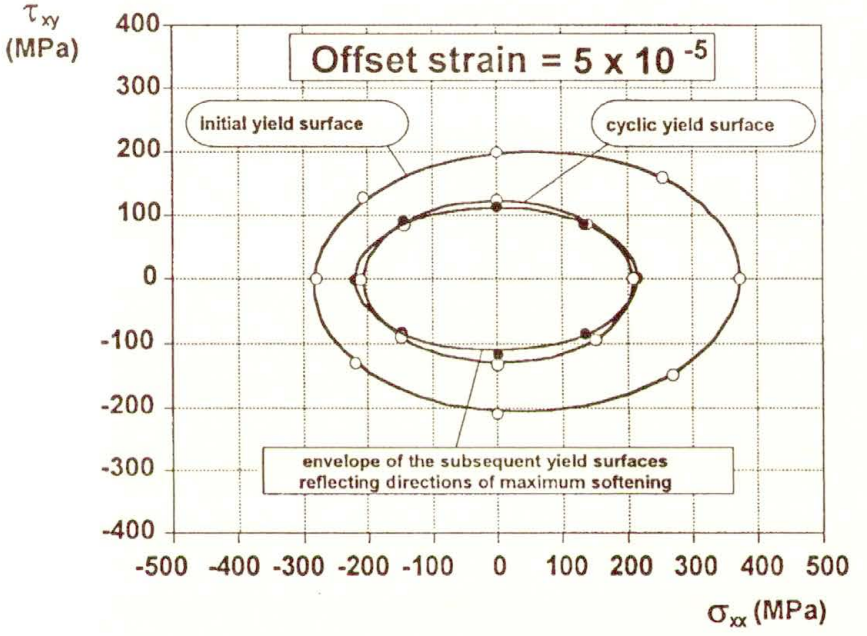

FIG. 23. Comparison of the envelope of subsequent yield surfaces, reflecting directions of maximum material softening due to cyclic loading, with the cyclic yield surface, offset strain 5×10^{-5} (results for the steel).

yield surface determined on the basis of cyclic curves, Fig. 12, and with the initial yield locus. As it is clearly shown, a close agreement was achieved in locations and sizes between the cyclic yield surface and the envelope. Thus, it confirms the equivalence and applicability of both methods of mechanical properties analysis for the steel subject to prior cyclic deformation in the plane stress state.

In the case of aluminium alloy, the surface being an envelope of all subsequent yield loci is shown in Fig. 24.

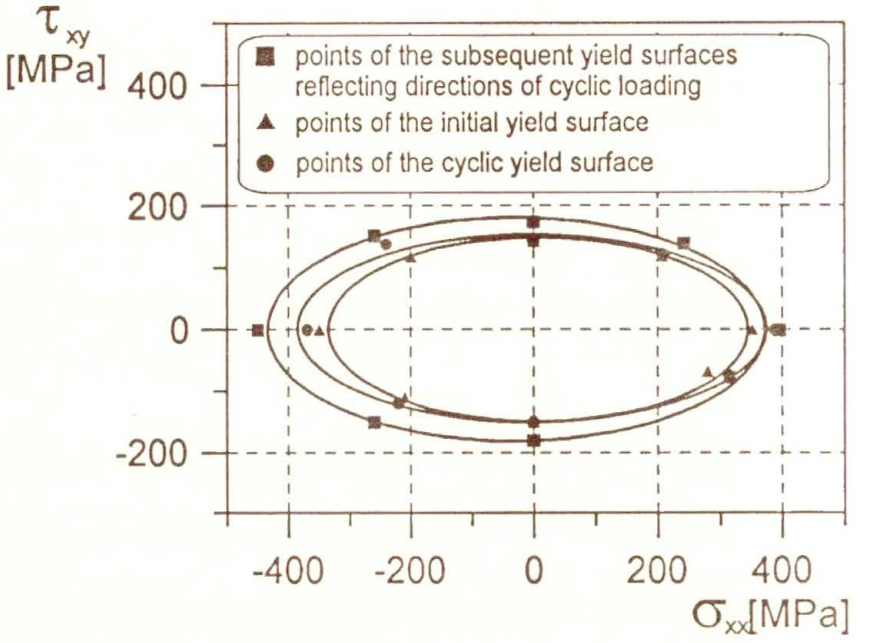

FIG. 24. Comparison of the envelope of subsequent yield surfaces, reflecting directions of maximum material hardening due to cyclic loading, with the cyclic yield surface, offset strain 5×10^{-5} (results for the aluminium alloy).

It is compared with the cyclic yield locus as well as with the initial yield surface. Contrary to the steel specimens, significant differences can be observed between the cyclic yield surface and the envelope. In view of this, the question arises why for one material a close agreement can be achieved between the cyclic yield surface and the envelope, but for the others considerable discrepancies are observed? In order to explain this problem, we must return to the results concerning cyclic loading. It has been shown for the aluminium alloy that the saturation cycle was not achieved during cyclic loading with the constant strain amplitude. The results for steel indicate that in order to obtain the saturation cycle, only a few full cycles with constant strain amplitude were necessary. It seems that the lack of stable behaviour of the aluminium alloy during cyclic loading applied is the main reason for the differences between the cyclic yield surface and the envelope. Therefore, it can be stated that the applicability of the cyclic yield surface concept to the mechanical properties analysis is limited to those cases in which the material tested reaches the stable hysteresis loop during proportional cyclic loading.

7. Final remarks

Determination of the true constitutive equations for cyclic plasticity provides many difficulties since, up to now, the majority of experimental investigations have been carried out at uniaxial stress states. Therefore, the available experimental data for multiaxial stress conditions are limited and, as a consequence, they do not fully reflect all aspects of the material behaviour under cyclic loadings. Since the paper presents the results of tests carried out under complex stress state, it completes somehow the lack of data in this area and my be useful in modelling the material behaviour. The data obtained allow us to formulate a few important concluding remarks.

It was observed that the shape and location of the initial yield surfaces determined for both the aluminium alloy and steel, for clearly defined yield offset, identify the anisotropy of the materials coming from the manufacturing processes.

A cyclic loading programme induces softening of the steel in the considered strain range accompanied by a remarkable reduction of the yield loci dimensions. In the case of aluminium alloy, the same programme induces the hardening effect reflected by the increase of yield loci dimensions.

The amount of softening in the case of steel, and hardening in the case of aluminium alloy depends on the direction with respect to cyclic prestraining. The greatest effects were always observed in the same direction as that used during predeformation process whereas the smallest ones were observed in the direction perpendicular to that in the cyclic loading applied.

If the number of cycles is sufficient to achieve the state of saturation, the concept of the cyclic yield surface reflects well the ability of a material to change mechanical properties due to cyclic deformation in different orientations of the plane stress state.

The analysis of the dimensions of the cyclic yield surface for the 18G2A steel proves that the material exhibits the same softening level for all directions examined, and moreover, it forgets the initial anisotropy induced during strain history coming from the manufacturing processes. The same analysis for the aluminium alloy proves that the material exhibits various amounts of hardening, depending on the initial anisotropy.

Acknowledgement

The authors gratefully acknowledge the support of the State Committee for Scientific Research under Grant 3 0154 91 01.

References

1. J. D. MORROW, *Cyclic plastic strain energy and fatigue of metals, internal friction, damping and cyclic plasticity*, ASTM STP 378, American Society for Testing and Materials, 45–87, 1965.
2. P. W. LANDGRAF, J. D. MORROW, T. ENDO, *Determination of the cyclic stress-strain curve*, J. Materials, **4**, 176–188, 1969.
3. E. KREMPL, *Cyclic plasticity: Some properties of the hysteresis curve of structural metals at room temperature*, ASME Journal of Basic Engineering, **93**, 317–323, 1971.
4. R. MARJANOVIC, W. SZCZEPIŃSKI, *Yield surfaces of the M-63 brass prestrained by cyclic biaxial loading*, Arch. Mech., **26**, 311–320, 1974.
5. J. LIPKIN, J. C. SWEARENGEN, *On the subsequent yielding of an aluminium alloy following cyclic prestraining*, Metallurgical Transactions A, **6A**, 167–177, 1975.
6. J. MIASTKOWSKI, *Yield surface of material subjected to combined cyclic loading*, Arch. Mech., **30**, 203–215, 1978.
7. H. S. LAMBA, O. M. SIDEBOTTOM, *Proportional biaxial cyclic hardening of annealed oxygen-free high-conductivity copper*, Journal of Testing and Evaluation, **6**, 260–267, 1978.
8. H. S. LAMBA, O. M. SIDEBOTTOM, *Cyclic plasticity for nonproportional paths*, ASME J. Engng. Materials and Technology, **100**, 96–111, 1978.
9. E. TANAKA, S. MURAKAMI, M. OOKA, *Effects of plastic strain amplitudes on non-proportional cyclic plasticity*, Acta Mechanica, **57**, 167–182, 1985.
10. E. TANAKA, S. MURAKAMI, M. OOKA, *Effects of strain path shapes on non-proportional cyclic plasticity*, J. Mech. Phys. Solids, **33**, 559–575, 1985.
11. D. L. MCDOWELL, *A two-surface model for transient nonproportional cyclic plasticity*, ASME J. App. Mech., **52**, 298–308, 1985.
12. CHR. BOLLER, T. SEEGER, *Materials data for cyclic loading. Part A: Unalloyed steels* (Materials Science Monographs, 42A), Amsterdam – Oxford – New York – Tokyo, Elsevier 1987.
13. W. TRĄMPCZYŃSKI, *The experimental verification of the evolution of kinematic and isotropic hardening in cyclic plasticity*, J. Mech. Phys. Solids, **36**, 417–441, 1988.
14. A. BENALLAL, P. LEGALLO, D. MARQUIS, *An experimental investigation of cyclic hardening of 316 stainless steel and 2024 aluminium alloy under multiaxial loadings*, Nucl. Eng. Des., **114**, 345–353, 1989.
15. E. KREMPL, H. LU, *The path and amplitude dependence of cyclic hardening of type 304 stainless steel at room temperature*, [in:] Biaxial and Multiaxial Fatigue, M. W. BROWN, K. J. MILLER [Eds.], 89–106, Mechanical Engineering Publications, London 1989.
16. H. ISHIKAWA, K. SASAKI, *Stress-strain relations of SUS304 stainless steel after cyclic preloading*, ASME J. Engng. Materials and Technology, **111**, 417–423, 1989.
17. Z. L. KOWALEWSKI, M. ŚLIWOWSKI, *Effect of cyclic loading on the yield surface evolution of 18G2A low-alloy steel*, Int. J. Mech. Sci., **39**, 1, 51–68, 1997.
18. Z. L. KOWALEWSKI, *Assessment of cyclic properties of 18G2A low-alloy steel at biaxial stress state*, Acta Mechanica, **120**, 1–4, 71–90, 1997.
19. Z. L. KOWALEWSKI, *Effect of cyclic prestraining on plastic behavior of 18G2A low-alloy steel at complex stress state*, Proc. of Plasticity: The Sixth Int. Symp. on Plasticity and Its Current Applications, A. S. KHAN [Ed.], Juneau, Alaska, USA, July 14–18, 359–360, 1997.

20. R. V. MISES, *Mechanik der plastischen Formänderung von Kristallen*, Zeitschr. Angew. Math. Mech., **8**, 161–185, 1928.

21. W. SZCZEPIŃSKI, *On deformation-induced plastic anisotropy of sheet metals*, Arch. Mech., **45**, 3–38, 1993.

POLISH ACADEMY OF SCIENCS
INSTITUTE OF FUNDAMENTAL TECHNOLOGICAL RESEARCH
e-mail: ldietric@ippt.gov.pl
e-mail: zkowale@ippt.gov.pl

Received March 26, 1998.

Arch. Mech., 50, 5, pp. 907–916, Warszawa
FIFTY YEARS OF THE ARCHIVES OF MECHANICS

Boundary conditions for a capillary fluid in contact with a wall

H. GOUIN (MARSEILLE) and W. KOSIŃSKI (WARSZAWA)

CONTACT OF A FLUID with a solid or an elastic wall is investigated. The wall exerts "molecular forces" on the fluid which is locally strongly non-homogeneous. The problem is approached with a fluid energy of the second gradient form and a wall surface energy depending on the value of the fluid density in the contact. From the virtual work principle and taking into account the fluid density, its derivative normal to the wall and the curvature of the surface, limit conditions are obtained.

1. Introduction

THE PHENOMENON OF SURFACE wetting is a subject of many experiments [1]. Such experiments have been used to determine many important properties of the wetting behaviour for liquid on low energy surface [2]. In fact the wetting transition of fluids in contact with solid surfaces is an important field of research both for mechanics and physical chemistry. In the recent paper [3], the first author using statistical methods has proposed an explicit form for the energy of interaction between solid surfaces and liquids. This energy yields a bridge connecting statistical mechanics and continuum mechanics. To obtain the boundary conditions between fluid and solid, it is also necessary to know the behaviour of the fluid as well as the solid.

We propose a mechanical model similar to that used in the mean-field theory of capillarity that leads to the second gradient theory of continuous media in fluid mechanics [4]. The theory is conceptually more straightforward than the Laplace one to build a model of capillarity [5, 6]. That theory takes into account systems in which fluid interfaces are present [7]. The internal capillarity is one of the simplest cases since we are able to calculate the surface tension in the case of thin interfaces as well as in thick ones [8]. It is possible to obtain the nucleation of drops and bubbles [9].

It seems that the approximation of the mean-field theory is too simple to be quantitatively accurate. However, it does provide a qualitative understanding. Moreover, the point of view, that the fluid in interfacial region may be treated as a bulk phase with a local free energy density and an additional contribution arising from the nonuniformity which may be approximated by a gradient expansion truncated at the second order terms, is most likely to be successful and perhaps even quantitatively accurate near the critical point [10].

In this paper we connect both the interaction of a solid surface and a fluid phase by means of the virtual work principle. The distribution of fluid energy in the volume and the surface density energy on the solid surface yield the boundary conditions. The conditions are different from those obtained for a classical fluid within the theory of gas dynamics. We obtain an embedding effect for the density of the fluid; moreover, the conditions take into account the curvature of the surface. The result is extended to the case of an elastic wall. A discussion is obtained depending on the value of the density of the fluid at the surface.

Let us use asterisk $*$ to denote *conjugate* (or *transpose*) mappings or covectors (line vectors). For any vectors $\mathbf{a}, \mathbf{b}$ we shall use the notation $\mathbf{a}^*\mathbf{b}$ for their *scalar product* (the line vector is multiplied by the column vector), $\mathbf{a} \cdot \mathbf{b}$ and $\mathbf{a}\mathbf{b}^*$ for their *tensor product* (the column vector is multiplied by the line vector) $\mathbf{a} \otimes \mathbf{b}$. The product of a mapping A by a vector $\mathbf{a}$ is denoted by $A\,\mathbf{a}$. Notation $\mathbf{b}^*A$ means covector $\mathbf{c}^*$ defined by the rule $\mathbf{c}^* = (A^*\mathbf{b})^*$. The divergence of a linear transformation A is the covector $\mathrm{div}A$ such that, for any constant vector $\mathbf{a}$,

$$\mathrm{div}(A)\,\mathbf{a} = \mathrm{div}\,(A\,\mathbf{a}).$$

If $f(\mathbf{x})$ is a scalar function of the vector $\mathbf{x}$ associated with the Euler variables in the physical space, $\partial f/\partial \mathbf{x}$ is the linear form associated with the gradient of f and consequently, $\left(\dfrac{\partial f}{\partial \mathbf{x}}\right)^* = \mathrm{grad}\, f$.

2. Continuous mechanical model of capillary layers

We consider a fluid in contact with a solid. The fluid occupies the domain D and its boundary Σ which is common with the solid wall. Physical experiments prove that the fluid is nonhomogeneous in the neighbourhood of Σ [10]. It is also possible to consider the fluid as a continuous medium by taking into account a "capillary layer" existing in the vicinity of Σ and a form of its stress tensor [11]. One way to present the behaviour of such a fluid is to consider the specific internal energy ε as a function of the density ρ as well as grad ρ. Such an expression is known in continuum mechanics as *internal capillary energy*, see [4, 5]. It is related to molecular models of strongly nonhomogeneous fluids in the frame of the mean field theory and is equivalent to the van der Waals model of capillarity (see the review by ROWLINSON and WIDOM [10]). The energy ε is also a function of the specific entropy. In the case of isothermal media at a given temperature, the specific internal energy is replaced by the specific free energy. In the mechanical case, the entropy or the temperature are not concerned by the virtual variations of the medium. Consequently, for an isotropic fluid, it is assumed that

$$\varepsilon = f(\rho, \beta),$$

where $\beta = \operatorname{grad}\rho \cdot \operatorname{grad}\rho$. The fluid is subjected to external forces represented by a force potential Ω per unit mass as a function of Eulerian variables $\mathbf{x}$.

We denote by $\Sigma \ni \mathbf{x} \longrightarrow B(\mathbf{x}) \in R$ the surface density of energy of the solid wall. The total energy E of the fluid in D and its boundary Σ is the sum of the three terms expressing: internal energy E_f, potential energy E_p and surface energy E_S: $E = E_f + E_p + E_S$, with

$$E_f = \int_D \rho\varepsilon(\rho,\beta)\, dv\,, \qquad E_p = \int_D \rho\, \Omega(\mathbf{x})\, dv, \qquad E_S = \int_\Sigma B\, ds.$$

Let us denote by δ a variation of the position of the fluid as in [12]. The variation is associated with the *virtual displacement*

$$D \ni x \to \delta\mathbf{x} = \boldsymbol{\zeta}(\mathbf{x}).$$

We have the following results presented in the Appendix,

$$\delta E_f = \int_D (-\operatorname{div}\sigma)\cdot\boldsymbol{\zeta}\, dv + \int_\Sigma \left\{ -A\frac{d\zeta_n}{dn} + \left(\frac{2A}{R_m}\mathbf{n} + \operatorname{grad}_{tg} A + \sigma\,\mathbf{n}\right)\cdot\boldsymbol{\zeta}\right\} ds \tag{2.1}$$

with

$$\sigma = -P\mathbf{I} - C\,\operatorname{grad}\rho\otimes\operatorname{grad}\rho = -P\mathbf{I} - C\left(\frac{\partial\rho}{\partial\mathbf{x}}\right)^* \frac{\partial\rho}{\partial\mathbf{x}},$$

where $C = 2\rho\varepsilon'_\beta$ and $P = \rho^2\varepsilon'_\rho - \rho\operatorname{div}(C\operatorname{grad}\rho)$, ε'_ρ denotes the partial derivative of ε with respect to ρ, $\zeta_n = \mathbf{n}^*\boldsymbol{\zeta}$ where $\mathbf{n}$ is the external unit normal to Σ and $A = C\rho\,\dfrac{d\rho}{dn}$ where $\dfrac{d\rho}{dn} = \dfrac{\partial\rho}{\partial\mathbf{x}}\,\mathbf{n}$.

The scalar R_m is the mean curvature of Σ and grad_{tg} is the tangential part of grad relatively to Σ.

Moreover,

$$\delta E_p = \int_D \rho\,\frac{\partial\Omega}{\partial\mathbf{x}}\,\boldsymbol{\zeta}\, dv = \int_D \rho\operatorname{grad}\Omega\cdot\boldsymbol{\zeta}\, dv, \tag{2.2}$$

and using the results presented in the Appendix,

$$\delta E_S = \int_\Sigma \left(\delta B - \left(\frac{2B}{R_m}\mathbf{n} + \operatorname{grad}_{tg} B\right)\cdot\boldsymbol{\zeta}\right) ds. \tag{2.3}$$

One assumes that the volumetric mass in the fluid has a limit, interfacial value ρ_s at the wall Σ (which is not the surface density of the wall but the mass

density per unit volume as in the shock wave analysis). One assumes also that B is a function of ρ_s only. These hypotheses are confirmed by results presented in [3]. Then,

$$\delta B = B'(\rho_s)\delta\rho_s = -\rho_s B'(\rho_s)\ \mathrm{div}\ \boldsymbol{\zeta}\,.$$

Let us denote $G = -\rho_s B'_{\rho_s}$. Consequently,

$$\int_\Sigma \delta B\ ds = \int_\Sigma G\ \mathrm{div}\ \boldsymbol{\zeta}\ ds = \int_\Sigma \left(G\ \frac{d\zeta_n}{dn} - \frac{2G}{R_m}\mathbf{n}\cdot\boldsymbol{\zeta} - \mathrm{grad}_{tg} G\ \cdot\boldsymbol{\zeta}\right) ds$$

(see Appendix).

Now, $H = B(\rho_s) - \rho_s B'_{\rho_s}(\rho_s)$ is the Legendre transformation of B with respect to ρ_s. Then,

$$\delta E_S = \int_\Sigma \left(G\ \frac{d\zeta_n}{dn} - \left(2H\ \frac{\mathbf{n}}{R_m} + \mathrm{grad}_{tg} H\right)\cdot\boldsymbol{\zeta}\right) ds. \tag{2.4}$$

The d'Alembert-Lagrange *principle of virtual works* is expressed in the form [12]:

$$\forall D \ni \mathbf{x} \to \boldsymbol{\zeta}(\mathbf{x}), \qquad \delta E = 0. \tag{2.5}$$

Consequently, from the fundamental lemma of variation calculus, we obtain the balance equation in the fluid D and the boundary conditions on the solid wall Σ.

Equilibrium equations

From any arbitrary variation $D \ni \mathbf{x} \to \boldsymbol{\zeta}(\mathbf{x})$ such that $\boldsymbol{\zeta} = \mathbf{0}$ on Σ, we take first

$$\int_D \left(\rho\ \frac{\partial \Omega}{\partial \mathbf{x}} - \mathrm{div}\ \sigma\right)\cdot\boldsymbol{\zeta}\ dv = 0.$$

Consequently,

$$\mathrm{div}\ \sigma - \rho\frac{\partial \Omega}{\partial \mathbf{x}} = 0. \tag{2.6}$$

This equation is the well known equilibrium equations [5, 7, 9]

Boundary conditions

a) Case of a rigid (undeformed) wall.

We consider a rigid wall. Consequently, the virtual displacements satisfy on Σ the condition $\mathbf{n}^*\,\boldsymbol{\zeta} = 0$. Then,

$$\int_\Sigma \left\{ (G - A)\ \frac{d\boldsymbol{\zeta}_n}{dn} + \left(\frac{2(A-H)}{R_m}\mathbf{n} + \mathrm{grad}_{tg}(A-H) + \sigma\mathbf{n}\right)\cdot\boldsymbol{\zeta}\right\} ds = 0$$

at the rigid wall.

Hence, we deduce the boundary conditions at the rigid wall:

$$\text{for } \mathbf{x} \in \Sigma: \qquad G - A = 0 \tag{2.7}$$

and moreover, there exists a Lagrange multiplier $\Sigma \ni \mathbf{x} \to \lambda(\mathbf{x}) \in R$ such that

$$\frac{2(A-H)}{R_m}\mathbf{n} + \operatorname{grad}_{tg}(A-H) + \sigma\mathbf{n} = \lambda\,\mathbf{n}. \tag{2.8}$$

b) Case of an elastic (non-rigid) solid wall.

In such a case the equilibrium equation (2.6) is unchanged. On Σ, moreover, the condition (2.7) is also unchanged. The only different condition comes from the fact that we do not have anymore the slipping condition for the virtual displacement ($\mathbf{n}^*\boldsymbol{\zeta} = 0$).

Due to the possible deformation of the wall, the virtual work of mechanical stresses on Σ is,

$$\delta E_e = \int_{\Sigma} \mathbf{t}^*\boldsymbol{\zeta}\, ds$$

with $\mathbf{t} = \mathbf{T}\,\mathbf{n}$ representing the stress (loading) vector, where $\mathbf{T}$ is the value of the Cauchy stress tensor of the elastic wall on the boundary Σ. Relation (2.8) is replaced by:

$$2\,\frac{(A-H)}{R_m}\mathbf{n} + \operatorname{grad}_{tg}(A-H) + \sigma\mathbf{n} = -\mathbf{t}. \tag{2.9}$$

3. Analysis of the boundary conditions

Relation (2.7) yields:

$$C\,\frac{d\rho}{dn} + B'_{\rho_s} = 0 \tag{3.1}$$

and we obtain

$$H - A = B.$$

Consequently, from the definition of σ,

$$\sigma\ \mathbf{n} = P\mathbf{n} - C\frac{d\rho}{dn}\operatorname{grad}\rho.$$

Then the tangential part of equation (2.8) is always verified and equation (2.8) yields the value of the Lagrange multiplier λ.

For an elastic (non-rigid) solid wall we obtain

$$t^*_{tg} = 0 \qquad \text{and} \qquad t_n = \frac{2B}{R_m} + P - B'_{\rho_s}\frac{d\rho}{dn}, \tag{3.2}$$

where t^*_{tg} and t_n are the tangential and the normal components of $\mathbf{t}$, respectively. Taking into account (3.1), $t_n = P + \dfrac{2B}{R_m} + \dfrac{1}{C}(B'_{\rho_s})^2$ and equations (3.2) yield the value of the stresses in the elastic (nonrigid) medium. The only new condition comes from (3.1).

We have the next consequences. In [3] it is proposed the surface energy in the form $B(\rho_s) = -\gamma_1\rho_s + \dfrac{\gamma_2}{2}\rho_s^2$, with γ_1, and γ_2 as two positive constants. We obtain the condition for the fluid density on the wall

$$C\,\frac{d\rho}{dn} = \gamma_1 - \gamma_2\rho_s, \tag{3.3}$$

and hence $\dfrac{d\rho}{dn}$ is positive (or negative) in the vicinity of the wall if $\rho_s < \rho_i$ (or $\rho_s \geq \rho_i$) with $\rho_i = \gamma_1/\gamma_2$ which is the *bifurcation fluid density* at the wall.

If $\rho_s < \rho_i$, we have a lack of fluid density at the wall. If $\rho_s \geq \rho_i$, we have an excess of fluid density at the wall.

4. Conclusion

For a conservative medium, the first gradient theory corresponds to the case of compressibility. To take into account the superficial effects acting between solids and fluids, we propose to use the model of fluids endowed with capillarity. The theory interpretes the capillarity in a continuous way and contains Laplace's theory. The model corresponds for solids to "elastic materials with couple stresses" indicated by TOUPIN in [13].

We notice that the extension to the dynamic case is straightforward: by the virtual work principle, equation (2.6) takes the form:

$$\rho\gamma - \mathrm{div}\sigma + \rho\frac{\partial\Omega}{\partial\mathbf{x}} = 0,$$

where γ denotes the acceleration of the fluid. Equations (3.1)–(3.3) and consequences in Sec. 3 are unchanged.

Appendix

First of all, we recall the following fact from the differential geometry: Let Σ be a surface in the 3-dimensional space and $\mathbf{n}$ its external normal.

For any vector field $\boldsymbol{\zeta}$,

$$\mathbf{n}^*\,\mathrm{rot}(\mathbf{n}\times\boldsymbol{\zeta}) = \mathrm{div}\,\boldsymbol{\zeta} + \frac{2}{R_m}\,\mathbf{n}^*\boldsymbol{\zeta} - \mathbf{n}^*\,\frac{\partial\boldsymbol{\zeta}}{\partial\mathbf{x}}\,\mathbf{n}.$$

Then, for any scalar field A, we obtain :

$$\text{(A.1)} \qquad A \operatorname{div} \boldsymbol{\zeta} = A \frac{d\zeta_n}{dn} - \frac{2A}{R_m}\zeta_n - (\operatorname{grad}^*_{lg} A)\, \boldsymbol{\zeta} + \mathbf{n}^* \operatorname{rot}\,(A\mathbf{n} \times \boldsymbol{\zeta})$$

$$= \operatorname{tr}\left[\left(\frac{\partial A}{\partial \mathbf{x}}(\mathbf{n}\mathbf{n}^* - 1) - \frac{2A}{R_m}\,\mathbf{n}^*\right)\boldsymbol{\zeta}\right] + A\frac{d\boldsymbol{\zeta}_n}{dn} + \mathbf{n}^* \operatorname{rot}(A\mathbf{n} \times \boldsymbol{\zeta}).$$

Let us calculate δE_f : since D is a material volume,

$$E_f = \int_D \rho\, \varepsilon\, dv \;\Rightarrow \delta E_f = \int_D \rho\, \delta\varepsilon\, dv$$

with $\delta\varepsilon = \dfrac{\partial \varepsilon}{\partial \rho}\ \delta\rho + \dfrac{\partial \varepsilon}{\partial \beta}\ \delta\beta$. From $\delta\ \dfrac{\partial \rho}{\partial \mathbf{x}} = \dfrac{\partial \delta\rho}{\partial \mathbf{x}} - \dfrac{\partial \rho}{\partial \mathbf{x}}\ \dfrac{\partial \boldsymbol{\zeta}}{\partial \mathbf{x}}$, we deduce:

$$\rho\varepsilon'_\beta\ \delta\beta = 2\rho\ \varepsilon'_\beta\ \delta\left(\frac{\partial \rho}{\partial \mathbf{x}}\right)\ \frac{\partial \rho^*}{\partial \mathbf{x}} = C\left(\left(\ \frac{\partial \delta\rho}{\partial \mathbf{x}} - \frac{\partial \rho}{\partial \mathbf{x}}\ \frac{\partial \boldsymbol{\zeta}}{\partial \mathbf{x}}\ \right)\right)\frac{\partial \rho^*}{\partial \mathbf{x}}$$

with $2\rho\varepsilon'_\beta = C$.

In the mean-field molecular theory, the quantity C is assumed to be constant [10], but it is not necessary. One can suppose that the scalar C is a general function of ρ and even β. Then

$$\rho\varepsilon'_\beta\ \delta\beta = \operatorname{div}(C \operatorname{grad}\ \rho\ \delta\rho) - \operatorname{div}(C \operatorname{grad}\ \rho)\delta\rho - \operatorname{tr}\left(C \operatorname{grad}\rho \operatorname{grad}^*\rho \frac{\partial \boldsymbol{\zeta}}{\partial \mathbf{x}}\right).$$

Due to the fact that $\delta\rho = -\rho \operatorname{div}\ \boldsymbol{\zeta}$ (see [12]),

$$\rho\delta\varepsilon = \operatorname{div}(C \operatorname{grad}\ \rho\ \delta\rho) - \left(\rho^2\varepsilon'_\rho - \rho \operatorname{div}(C \operatorname{grad}\ \rho\ )\right)\operatorname{div}\ \boldsymbol{\zeta}$$

$$-\operatorname{div}(C \operatorname{grad}\rho \operatorname{grad}^*\rho\ \ \boldsymbol{\zeta}) + \operatorname{div}(C \operatorname{grad}\ \rho \operatorname{grad}^*\rho)\ \boldsymbol{\zeta}$$

$$\rho\delta\varepsilon = \operatorname{div}\,(C \operatorname{grad}\rho\ \delta\rho - (C \operatorname{grad}\ \rho \operatorname{grad}^*\rho)\boldsymbol{\zeta} - P\boldsymbol{\zeta})$$

$$+\frac{\partial P}{\partial \mathbf{x}}\boldsymbol{\zeta} + \operatorname{div}(C \operatorname{grad}\ \rho \operatorname{grad}^*\ \rho)\ \boldsymbol{\zeta}.$$

Then

$$\delta E_f = \int_D \left(\ \frac{\partial P}{\partial \mathbf{x}} + \operatorname{div}(C \operatorname{grad}\ \rho \operatorname{grad}^*\rho)\right)\boldsymbol{\zeta}\ dv$$

$$+ \int_D \operatorname{div}\,(-C\rho \operatorname{grad}\ \rho \operatorname{div}\ \boldsymbol{\zeta} - C \operatorname{grad}\ \rho \operatorname{grad}^*\rho\ \ \boldsymbol{\zeta} - P\boldsymbol{\zeta})\, dv$$

$$= \int_D -(\operatorname{div}\sigma)\boldsymbol{\zeta}\ dv + \int_\Sigma (-A \operatorname{div}\boldsymbol{\zeta} + \mathbf{n}^*\sigma\ \boldsymbol{\zeta})ds.$$

Taking into account (A.1), we deduce immediately

$$\delta E_f = \int_D -(\mathrm{div}\sigma)\boldsymbol{\zeta}\, dv + \int_\Sigma \left(-A\frac{d\boldsymbol{\zeta}_n}{dn} + \left(\frac{2A}{R_m}\mathbf{n}^* + \mathrm{grad}^*_{lg}A + \mathbf{n}^*\sigma\right)\boldsymbol{\zeta}\right) ds$$

$$+ \int_\Sigma \mathbf{n}^*\mathrm{rot}(A\ \mathbf{n}\times\boldsymbol{\zeta})\ ds.$$

But, $\int_\Sigma \mathbf{n}^*\mathrm{rot}(A\ \mathbf{n}\times\boldsymbol{\zeta})\ ds = \int_\Gamma A\mathbf{t}\cdot(\mathbf{n}\times\boldsymbol{\zeta})d\ell = \int_\Gamma A(\mathbf{t},\mathbf{n},\boldsymbol{\zeta})\ d\ell\ ,$

where Γ is the line boundary of Σ and $\mathbf{t}$ its tangent unit vector. If $\mathbf{n}' = \mathbf{t}\times\mathbf{n}$, we obtain the relation

$$\text{(A.2)}\qquad \delta E_f = \int_D (-\mathrm{div}\sigma)\boldsymbol{\zeta}\, dv + \int_\Sigma \left(-A\frac{d\boldsymbol{\zeta}_n}{dn} + \left(\frac{2A}{R_m}\mathbf{n}^* + \mathrm{grad}^*_{lg}A\right.\right.$$

$$\left.\left. + \mathbf{n}^*\sigma\right)\boldsymbol{\zeta}\right) ds + \int_\Gamma A\mathbf{n}'^*\boldsymbol{\zeta}\sigma\, d\ell.$$

In the following, we assume that Σ has no boundary and consequently, the term associated with Γ vanishes.

Let us calculate δE_S

$$E_S = \int_\Sigma B\ ds.$$

Then

$$\text{(A.3)}\qquad \delta E_S = \int_\Sigma \left\{\delta B\ - \left(\mathbf{n}^*\ \frac{2B}{R_m} + \mathrm{grad}^* B(\mathbf{1}-\mathbf{nn}^*)\right)\boldsymbol{\zeta}\right\} ds + \int_\Gamma A\mathbf{n}'^*\boldsymbol{\zeta}\ d\ell.$$

We notice that $\mathrm{grad}^* B(\mathbf{1}-\mathbf{nn}^*)$ belongs to the tangent plane to Σ.

Let us prove Eq. (A.3). If we write $E_S = \int_\Sigma B\ \det(\mathbf{n}, d_1\mathbf{x}, d_2\mathbf{x})$ where $d_1\mathbf{x}$ and $d_2\mathbf{x}$ are the coordinate lines of Σ, we may write

$$E_S = \int_{\Sigma_0} B\ \det\ F\ \det(F^{-1}\mathbf{n}, d_1\mathbf{X}, d_2\mathbf{X}),$$

where Σ_0 is the image of Σ in a reference space in Lagrangian coordinates $\mathbf{X}$, and F is the deformation gradient tensor $\partial\mathbf{x}/\partial\mathbf{X}$.
Then,

$$\delta E_S = \int_{\Sigma_0} \delta B\ \det\ F \det(F^{-1}\mathbf{n}, d_1\mathbf{X}, d_2\mathbf{X}) + \int_{\Sigma_0} B\ \delta\Big(\det\ F \det(F^{-1}\mathbf{n}, d_1\mathbf{X}, d_2\mathbf{X})\Big).$$

Moreover,

$$\int_{\Sigma_0} B\delta\Big(\det\ F\ \det\ (F^{-1}\mathbf{n}, d_1\mathbf{X}, d_2\mathbf{X})\Big) = \int_{\Sigma} B\ \mathrm{div}\boldsymbol{\zeta}\ \ \det\ (\mathbf{n}, d_1\mathbf{x}, d_2\mathbf{x})$$

$$+B\ \det\ \left(\frac{\partial \mathbf{n}}{\partial \mathbf{x}}\boldsymbol{\zeta}, d_1\mathbf{x}, d_2\mathbf{x}\right) - B\ \det\ \left(\frac{\partial \boldsymbol{\zeta}}{\partial \mathbf{x}}\mathbf{n}, d_1\mathbf{x}, d_2\mathbf{x}\right)$$

$$= \int_{\Sigma} \left(\mathrm{div}(B\boldsymbol{\zeta}) - \mathrm{grad}^* B\ \boldsymbol{\zeta} - B\mathbf{n}^*\ \frac{\partial \boldsymbol{\zeta}}{\partial \mathbf{x}}\ \mathbf{n}\right) ds.$$

From (A.1) we obtain

$$\mathrm{div}(B\boldsymbol{\zeta}) - B\ (\mathrm{div}\ \mathbf{n})\ \ \mathbf{n}^*\boldsymbol{\zeta} - \mathbf{n}^*\ \frac{\partial B\boldsymbol{\zeta}}{\partial \mathbf{x}}\ \ \mathbf{n} = \mathbf{n}^*\mathrm{rot}\ (B\mathbf{n}\times\boldsymbol{\zeta}).$$

Then,

$$\int_{\Sigma_0} B\delta\left(\det\ F\ \det\ (F^{-1}\mathbf{n}, d_1\mathbf{X}, d_2\mathbf{X})\right) = \int_{\Sigma_0} (B\ (\mathrm{div}\ \mathbf{n})\mathbf{n}^*$$

$$+\ \mathrm{grad}^* B(\mathbf{n}\mathbf{n}^* - \mathbf{1}))\,\boldsymbol{\zeta}\ ds + \int_{\Sigma} \mathbf{n}^*\mathrm{rot}\ (B\mathbf{n}\times\boldsymbol{\zeta})ds$$

and we obtain (A.3) with $\mathrm{div}\ \mathbf{n} = -\ \dfrac{2}{R_m}$.

We assume that Σ has no boundary and consequently, the term associated with Γ is null.

Acknowledgment

The authors are grateful to the Polonium Program of Co-operation No. 7075 between the Polish Committee for Scientific Research (KBN) and French Foreign Office for the financial support of this research.

References

1. A. E. Van Giessen, D. J. Bukman, B. Widom, *Contact angles of liquid drops on low-energy solid surfaces*, J. Colloid Interface Sci., **192**, 257–265, 1997.
2. J. W. Cahn, *Critical point wetting*, J. Chem. Phys., **66**, 3667–3672, 1977.
3. H. Gouin, *Energy of interaction between solid surfaces and liquids*, J. Phys. Chem., **102**, 1212–1218 , 1998.
4. P. Germain, *La méthode des puissances virtuelles en mécanique des milieux continus*, J. de Mécanique, **12**, 235–274, 1973.
5. P. Casal, *La théorie du second gradient et la capillarité*, Comptes Rendus Acad. Sc. Paris, **274**, 1571–1574, 1972.

6. P. CASAL, H. GOUIN, *Sur les interfaces liquide-vapeur non-isothermes*, J. de Mécanique Théorique et Appliquée, **7**, 689–718, 1988.

7. H. GOUIN, *Utilization of the second gradient theory in continuum mechanics to study the motion and thermodynamics of liquid-vapor interfaces*, Physicochemical Hydrodynamics – Interfacial Phenomena, B, **174**, 667–682, 1987.

8. F. DELL'ISOLA, W. KOSIŃSKI, *Deduction of thermodynamic balance law for bidimensional nonmaterial directed continua modelling interface layers*, Arch. Mech., **45**, 3, 333–359, 1993.

9. F. DELL'ISOLA, H. GOUIN, G. ROTOLI, *Nucleation of spherical shell-like interfaces by second gradient theory: numerical simulations*, Eur. J. Mech. B/Fluids, **15**, 545–568, 1996.

10. J. S. ROWLINSON, B. WIDOM, *Molecular theory of capillarity*, Clarendon Press, Oxford 1984.

11. P. SEPPECHER, *Equilibrium of a Cahn-Hilliard fluid on a wall: influence of the wetting properties of the film upon the stability of a thin film*, Eur. J. Mech. B/Fluids, **12**, 69–84, 1993.

12. J. SERRIN, *Mathematical principles of classical fluid mechanics*, [in:] Encyclopedia of Physics, S. FLÜGGE [Ed.], vol. VIII/1, Springer-Verlag, Berlin 1959.

13. R.A. TOUPIN, *Elastic materials with couple stresses*, Arch. Rat. Mech. Anal., **11**, 385–398, 1962.

L.M.M.T., FACULTÉ DES SCIENCES
UNIVERSITÉ D'AIX-MARSEILLE, CASE 322
Avenue Escadrille Normandie-Niemen
13397 Marseille Cedex 20, FRANCE
e-mail: henri.gouin@meca.u-3mrs.fr

and

INSTITUTE OF FUNDAMENTAL TECHNOLOGICAL RESEARCH
POLISH ACADEMY OF SCIENCES
e-mail: wkos@ippt.gov.pl

Received April 16, 1998.

Arch. Mech., 50, 5, pp. 917–926, Warszawa
FIFTY YEARS OF THE ARCHIVES OF MECHANICS

On waves due to a line source in front of a vertical wall with a gap

SUDESHNA BANERJEA AND C. C. KAR (CALCUTTA)

IN THE PRESENT PAPER waves due to presence of a line source in front of a vertical wall with a gap are studied. A simple expression for amplitude of radiated waves at infinity is obtained by application of Green's integral theorem.

1. Introduction

WATER WAVE PROPAGATION in presence of a vertical barrier form an important class of problems within the framework of linearised theory. Among the various types of problems in this class, the study of wave motion due to presence of line source in front of an obstacle has been made by various researchers.

EVANS [2], while studying the wave motion produced by small oscillations of a partially immersed vertical plate, obtained as a special case the amplitude of radiated waves due to presence of a line source in front of a vertical plate partially immersed in deep water by simple application of Green's integral theorem. Later BASU and MANDAL [3] and MANDAL [4] used the same technique to find the amplitude of radiated waves when the vertical barrier is completely submerged and extends infinitely downwards, or is submerged up to a finite depth below the mean free surface.

In the present paper, the wave motion due to a line source present in front of a vertical wall with a gap in deep water is studied. These problems have relevance in manoeuvring of a ship near a wall (cf. [7]). In general, a study of wave motion in presence of a vertical wall with a gap has practical application in construction of breakwaters. Here the amplitude of radiated waves at infinity is obtained by applying Green's integral theorem in the fluid region to two suitably chosen functions. One of the functions represents the velocity potential which is the solution of the corresponding problem of scattering of a normally incident wave train by a vertical wall with a gap. This solution is given in [6]. However, we have obtained it here by a different method using an integral equation formulation based on Havelock's expansion of the water wave potential. The other function is chosen in appropriate form, the unknown velocity potential describing the motion in the given problem. From the results thus obtained, it is observed that, when the source is situated within the gap in the wall, then the wall has no effect on the source.

2. Statement and formulation of the problem

We consider a vertical wall extending from above the mean free surface and having a gap given by $x = 0$ and $y \in L \equiv (0, a) \cup (b, \infty)$ in deep water occupying the region $y \geq 0$ with $y = 0$ as the mean free surface (cf. Fig. 1). The motion is generated in water due to a harmonically oscillating line source of unit strength and circular frequency σ, acting at the point (ξ, η), $(\xi > 0, \eta > 0)$ in front of the wall.

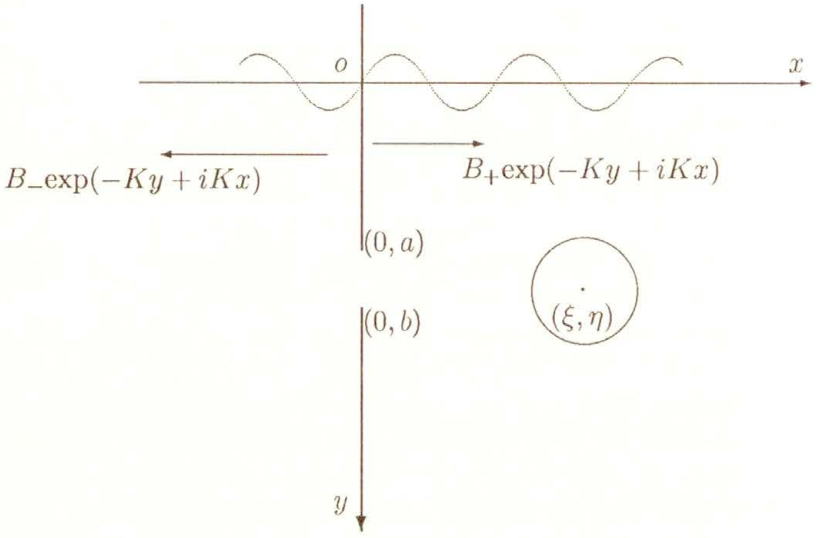

FIG. 1.

Assuming the linearised theory, the motion is described by the velocity potential $\mathrm{Re}\{\Phi(x, y) \exp(-i\sigma t)\}$ where Φ satisfies the following boundary value problem:

(2.1) $$\nabla^2 \Phi = 0 \text{ in the fluid region except at } (\xi, \eta),$$

(2.2) $$K\Phi + \Phi_y = 0 \text{ on } y = 0,$$

where $K = \sigma^2/g$, g being acceleration of gravity,

(2.3) $$\Phi_x = 0, \qquad x = 0, \qquad y \in L,$$

(2.4) $$\Phi \sim \ln \rho \text{ as } \rho \to 0 \qquad \text{where} \qquad \rho = \{(x - \xi)^2 + (y - \eta)^2\}^{1/2},$$

(2.5) $$r^{1/2} \nabla \Phi \text{ is bounded as } r \to 0, \qquad r = \{(x)^2 + (y - c)^2\}^{1/2},$$

$$c = a \text{ or } b$$

(2.6) $$\nabla \Phi \to 0 \text{ as } y \to \infty,$$

$$\Phi \sim \begin{cases} B_+ \exp(-Ky + iKx) & \text{as } x \to \infty, \\ B_- \exp(-Ky - iKx) & \text{as } x \to -\infty, \end{cases} \tag{2.7}$$

where $B_\pm$ (unknown) are (complex) amplitudes of radiated waves at infinity on either side of the wall. Let $G(x, y; \xi, \eta)$ denote the potential due to a line source of unit strength at $(\xi, \eta), (\eta > 0)$ in the absence of the barrier which is given by (cf. [1]),

$$G(x, y\,; \xi, \eta) = -2 \int_0^\infty \frac{M(k, \eta) M(k, y)}{k(K^2 + k^2)} \exp(-k \mid x - \xi \mid) dk \tag{2.8}$$

$$-2\pi i \exp(-K(y + \eta) + iK \mid x - \xi \mid),$$

where $M(k, \eta) = k \cos k\eta - K \sin k\eta$.

We express the potential function Φ as

$$\Phi = G + \phi, \tag{2.9}$$

where ϕ is the correction of G due to the presence of the barrier. Then ϕ satisfies the equations:

$$\nabla^2 \phi = 0, \qquad y > 0, \tag{2.10}$$

$$K\phi + \phi_y = 0 \qquad \text{on} \qquad y = 0, \tag{2.11}$$

$$\phi_x(0, y) = f(y) = -G_x(0, y; \xi, \eta), \qquad x = 0, \quad y \in L \equiv (0, a) \cup (b, \infty), \tag{2.12}$$

$$r^{1/2} \nabla \phi \text{ is bounded as } r \to 0, \tag{2.13}$$

$$\nabla \phi \to 0, \qquad \text{as} \quad y \to \infty, \tag{2.14}$$

$$\phi \sim \begin{cases} B & \exp(-Ky + iKx), \quad x \to \infty \\ -B & \exp(-Ky - iKx), \quad x \to -\infty \end{cases} \tag{2.15}$$

where B (unknown) is the complex amplitude of scattered field. It may be noted here that because of (2.12), ϕ is odd in x.

3. Method of solution

Let $\psi(x, y)$ denote the potential describing the motion due to normal incidence of a progressive wave $\exp(-Ky + iKx)$ from negative infinity upon the vertical

wall $x = 0$, $y \in L \equiv (0, a) \cup (b, \infty)$ present in deep water. The explicit form for $\psi(x, y)$ can be obtained as (see Appendix and also [6]):

$$\psi(x,y) = \begin{cases} \exp(-Ky + iKx) + R\ \exp(-Ky - iKx) \\ \quad + \int_0^\infty D(k) M(k,y) \exp(kx) dk, \quad x < 0 \\ T \exp(-Ky + iKx) \\ \quad + \int_0^\infty C(k)\ M(k,y)\ \exp(-kx) dk, \quad x > 0, \end{cases} \tag{3.1}$$

where $M(k, y)$ is given by (2.8)

$$R = A_1 I = \frac{Ii}{J + iI},$$

$$T = 1 - R = -iJA_1 = \frac{J}{(J + Ii)},$$

$$A_1 = \frac{i}{(J + Ii)},$$

$$J = \frac{\exp(-Ka)}{K} + \delta\alpha_2(K) - \frac{2\alpha_2(K, F_1)}{\pi}, \tag{3.2}$$

$$I = \delta\{\alpha_1(K) - \alpha_3(K)\} - \frac{2}{\pi}\{\alpha_1(K, F_1) - \alpha_3(K, F_1)\},$$

$$\delta = \frac{\{K^{-1}\ \exp(Ka) + \frac{2}{\pi}\alpha_2(-K, F_1)\}}{\alpha_2(-K)},$$

$$\alpha_i(K) \equiv \alpha_i(K, 1), \qquad \alpha_i(K, F_1) = \int_{t_i} \frac{uF_1(a, b, u)}{R_0(u)} \exp(-Ku) du,$$

where $R_0(u) = \mid u^2 - a^2 \mid^{1/2} \ \mid u^2 - b^2 \mid^{1/2}$

$$t_i = \begin{cases} (-a, a), & i = 1, \\ (a, b), & i = 2, \\ (b, \infty), & i = 3, \end{cases}$$

$$F_1(a, b, u) = \int_0^a \frac{R_0(v)}{v^2 - u^2} dv.$$

Therefore,

$$-C(k) = D(k) = \frac{2}{\pi}\frac{A_1}{k(k^2+K^2)}\left[-\sin ka + k\int_a^b \frac{uS(u)}{R_0(u)}\cos kudu\right]$$

$$s(u) = \left[\delta - \frac{2}{\pi}F_1(a,b,u)\right].$$

Applying Green's integral theorem to the harmonic functions ϕ, ψ within the region bounded by the lines

$$y = 0, \quad 0 < x \leq X; \quad x = 0^+, \quad 0 \leq y < a; \quad x = 0^-, \quad 0 \leq y < a;$$

$$y = 0, \quad -X \leq x < 0; \quad x = -X, \quad 0 \leq y \leq Y; \quad y = Y, \quad -X \leq x < 0;$$

$$x = 0^-, \quad b < y < \infty; \quad x = 0^+, \quad b < y < \infty; \quad y = Y, \quad 0 \leq x \leq X;$$

$$x = X, \quad 0 \leq y \leq Y;$$

for $X,\ Y \to \infty$ we obtain

$$iB = \int_0^a g(y)f(y)dy + \int_b^\infty g(y)f(y)dy \tag{3.3}$$

where

$$g(y) = \psi(0^+, \psi(0^+, y), y) - \psi(0^-, y).$$

Using the expression for $g(y)$ from (B.9), the following simplifications can be made.

$$\int_0^a f(y)g(y)dy = -\int_0^a \frac{2y\ \exp(Ky)}{R_0(y)}s(y)h_1(y)dy,$$

$$\int_b^\infty f(y)g(y)dy = \int_b^\infty \frac{2ys(y)h_2(y)}{R_0(y)}\exp(Ky)dy, \tag{3.4}$$

where

$$h_1(y) = A_1\int_0^y f(t)\exp(-Kt)dt,$$

$$h_2(y) = A_1\int_\infty^y f(t)\exp(-Kt)dt,$$

$s(y)$ is given by (3.2) and $f(y)$ can be obtained from (2.12) and (2.8) as

$$f(y) = -G_x(0, y;\ \xi, \eta) = 2 \int_0^\infty \frac{M(k,y)M(k,\eta)}{k^2 + K^2}\ \exp(-k\xi)dk$$

$$+2\pi K\ \exp(-(y+\eta) + iK\xi).$$

Thus, using (3.4) and (B.9) in (3.3), we get B in the form

$$B\ = -2\pi i \left[R\ \exp(-K\eta + iK\xi) - \int_0^\infty C(k)M(k,\eta)\exp(-k\xi)dk \right] \tag{3.5}$$

where R and $C(k)$ are given by Eqs. (3.2).

Now $B_\pm$ can be obtained by assuming $\mid x \mid \to \infty$ in (2.9) after using (2.7), (2.8), (2.15).

Thus as $x \to \infty$, we have

$$B_+ = -2\pi i\ \exp(-K\eta - iK\xi) + B = -2\pi i\psi(-\xi, \eta). \tag{3.6}$$

Also as $x \to -\infty$,

$$B_- = -B - 2\pi i\ \exp(-K\eta + iK\xi) = \ -2\pi i\psi(\xi, \eta). \tag{3.7}$$

It is obvious that

$$B_+ + B_- = -4\pi i\ \exp(-K\eta)\ \cos K\xi. \tag{3.8}$$

This shows that if $K\xi$ is an odd multiple of $\pi/2$ and $K\eta$ is arbitrary, then the wave amplitudes at either infinity are the same, the surface elevation being exactly 180° out of phase with each other. Similar conclusion were also drawn by EVANS [2] and BASU and MANDAL [3].

Again,

$$\psi(0,\eta) = T\ \exp(-K\eta) + \int_0^\infty C(k)M(k,\eta)dk.$$

Using $(B.4)_1$ we have for $\eta \in (a, b)$

$$\psi(o,\eta) = (T + R)\ \exp(-K\eta)$$

and immediately it follows from (B.3) that

$$\psi(0,\eta) = \exp(-K\eta). \tag{3.9}$$

Therefore,

$$B_+(0,\eta) = B_-(0,\eta) = -2\pi i \exp(-K\eta). \tag{3.10}$$

This shows that the wall has no effect on the source if the source is situated within the gap in the wall.

4. Appendix

Let us consider a wall $x = 0, y \in L,\ L \equiv (0,a) \cup (b,\infty)$ immersed in deep water with $y = 0$ as a mean free surface. A train of surface waves $\exp(-Ky + iKx)$ of frequency σ is incident on the wall from negative infinity, then it is partially reflected and partially transmitted. If $Re\{\psi(x,y)\ \exp(-i\sigma t)\}$ denotes the velocity potential, then ψ satisfies the following boundary value problem:

(i) $\nabla^2\psi = 0, \qquad y \geq 0,$

(ii) $K\psi + \psi_y = 0 \quad$ on $\quad y = 0,$

(iii) $\psi_x = 0, \qquad y \in L \equiv (0,a) \cup (b,\infty),$

(iv) $r^{1/2}\nabla\psi$ is bounded as $r \to 0,$

r being the distance from the sharp edges of the plate,

(v) $\nabla\psi \to 0$ as $y \to \infty,$

(vi) $$\psi = \begin{cases} \exp(-Ky + iKx) + R\exp(-Ky - iKx), & \text{as } x \to -\infty, \\ T\ \exp(-Ky + iKx), & x \to \infty, \end{cases}$$

where R and T are reflection and transmision co-efficients, respectively, to be determined. Using Havelock's expansion of water wave potential, $\psi(x,y)$ can be expressed by

$$\psi(x,y) = \begin{cases} \exp(-Ky + iKx) + R\exp(-Ky - iKx) \\ \qquad + \int_0^\infty D(k)M(k,y)\ \exp(kx)dk, \quad x < 0 \\ T\exp(-Ky + iKx) \\ \qquad + \int_0^\infty C(k)M(k,y)\exp(-kx)dk, \quad x > 0 \end{cases} \tag{B.1}$$

where $M(k,y)$ is given by (2.8), and $C(k)$ and $D(k)$ are unknown.

Let

$$\psi(0,y) = \begin{cases} 0, & y \in L \\ F(y), & y \in (0,\infty) - L, \end{cases} \tag{B.2}$$

where by (iv)

$$F(y) = \begin{cases} O(\mid y-a \mid^{-1/2}) & y \to a, \\ O(\mid y-b \mid^{-1/2}) & \text{as} \quad y \to b. \end{cases}$$

Then by Havelock's inversion theorem,

$$\text{(B.3)} \qquad \begin{aligned} T &= 1 - R = -2i \int_a^b F(y) \exp(-Ky) dy, \\ -C(k) &= D(k) = \frac{2}{\pi} \frac{1}{k(K^2+k^2)} \int_a^b F(y) M(k,y) dy, \end{aligned}$$

Now an integral equation for $F(y)$ can be obtained from the fact that $\psi(x,y)$ is continuous across the gap in the wall. Thus,

$$\psi(+0,y) = \psi(-0,y), \qquad y \in (a,b).$$

Using (B.1) and noting (B.3) we have,

$$\text{(B.4)}_1 \qquad R \exp(-Ky) = \int_0^\infty M(k,y) C(k)\, dk, \qquad y \in (a,b).$$

Substituting $C(k)$ from (B.3) we get

$$\text{(B.4)}_2 \qquad -\frac{\pi}{2} R \exp(-Ky) = \int_0^\infty \frac{M(k,y)}{k(k^2+K^2)} \int_a^b F(t) M(k,t) dt\, dk, \quad y \in (a,b).$$

Applying the operator $(\frac{d}{dy} + K)$ to (B.3) we have the following integral equation:

$$\text{(B.5)} \qquad \int_a^b F(t) \left[K \ln \left| \frac{y-t}{y+t} \right| + \frac{1}{y-t} + \frac{1}{y+t} \right] dt = 0, \qquad y \in (a,b).$$

The solution of integral equation (B.5) is given by (cf. [5])

$$\text{(B.6)} \qquad F(x) = \frac{d}{dx} \exp(-Kx) \int_b^x \exp(Ku) \lambda(u) du$$

where

$$\lambda(u) = \frac{u A_1}{R_0(u)} \left[\delta - \frac{2}{\pi} F_1(a,b,u) \right],$$

$R_0(u)$, $F_1(a,b,u)$, δ and A_1 are given in (3.2). One relation connecting A_1 and R can be obtained by substituting $F(x)$ in $(B.4)_2$. After some simplification we obtain

$$R = \delta A_1 [\alpha_1(K) - \alpha_3(K)] - \frac{2A_1}{\pi}[[\alpha_1(K,F_1) - \alpha_3(K,F_1)], \tag{B.7}$$

where $\alpha_i(K)$ and $\alpha_i(K,F_1)$ are given by (3.2).

Also substituting $F(t)$ in the first equation of (B.3), we get another relation connecting R, A_1 which is given by

$$1 - R = \left[-\delta\ \alpha_2(K) + \frac{2}{\pi}\ \alpha_2(K,F_1) - \frac{1}{K}\exp(-Ka)\right](i.A_1). \tag{B.8}$$

Thus from (B.7) and (B.8), R and A_1 can be obtained. Again, $C(k)$ is obtained by substituting $F(t)$ in the second equation of (B.3). After simplifications, $C(k)$ can be obtained as given in (3.2).

Let $g(y) = \psi(+0,y) - \psi(-0,y)$. Using (B.1) we get

$$g(y) = -2R\exp(-Ky) + 2\int_0^\infty C(k)M(k,y)dk.$$

Therefore,

$$Kg + g_y(y) = -2\int_0^\infty C(k)(K^2+k^2)\sin ky\ dk.$$

Substituting $C(k)$ from (B.3) and making simplification we have,

$$Kg(y) + g_y(y) = \begin{cases} 0, & a < y < b, \\ \dfrac{2y\ A_1\ S(y)}{R_0(y)}, & 0 < y < a, \\ -\dfrac{2y\ A_1\ S(y)}{R_0(y)}, & b < y < \infty, \end{cases}$$

which gives after integration

$$g(y) = \begin{cases} 0, & a < y < b, \\ \exp(-Ky)\displaystyle\int_a^y \frac{2t\ S(t)\ \exp(Kt)}{R_0(t)}dt, & 0 < y < a, \\ -\exp(-Ky)\displaystyle\int_b^y \frac{2t\ S(t)\ \exp(Kt)}{R_0(t)}dt, & b < y < \infty, \end{cases} \tag{B.9}$$

where the constant of integration can be chosen to be zero, and $s(y)$, A_1 is given by (3.4).

Acknowledgement

Authors thank the referee for his suggestion to improve this paper. This work is partially supported by UGC-DSA programme at the Department of Mathematics, Jadavpur University.

References

1. R. C. THORNE, *Multipole expansion in the theory of surface waves,* Proc. Camb. Soc., 49, 701–716, 1953.
2. D. V. EVANS, *A note on the waves produced by the small oscillations of a partially immersed vertical plate,* J. Inst. Maths. Appl., **17**, 135–140, 1976.
3. U. BASU and B. N. MANDAL, *A plane vertical submerged barrier in surface water waves,* Internat. J. Math. & Math. Sci., **4**, 815–820, 1987.
4. B. N. MANDAL, *On waves due to small oscillations of a vertical plate submerged in deep water,* J. Aust. Math. Soc. Ser.B, **32**, 296–303, 1991.
5. S. BANERJEA and B. N. MANDAL, *On a singular integral equation with logarithmic and Cauchy kernel,* Int. J. Math. Edu. Technol., **26**, 267–313, 1995.
6. D. PORTER, *The transmission of surface waves through a gap in a vertical barrier,* Proc. Camb. Phil.Soc., **71**, 411–421, 1972.
7. D. V. EVANS and D. PORTER, *Hydrodynamic characteristics of a thin rolling plate in finite depth of water,* Appl. Ocean Res., **18**, 215–218, 1996..

DEPARTMENT OF MATHEMATICS
JADAVPUR UNIVERSITY
Calcutta 700032 India

Received September 10, 1997; new version June 22, 1998

INSTITUTE OF FUNDAMENTAL TECHNOLOGICAL RESEARCH
is publishing the following periodicals:

ARCHIVES OF MECHANICS – bimontly (in English)
ARCHIVES OF ACOUSTICS – quarterly (in English)
ARCHIVES OF CIVIL ENGINEERING – quarterly (in English)
ENGINEERING TRANSACTION – quarterly (in English)
COMPUTER ASSISTED MECHANICS AND ENGINEERING SCIENCES – quarterly (in English)
JOURNAL OF TECHNICAL PHYSICS – quarterly (in English)

Subscription orders for the journals edited by IFTR may be sent directly to the

Editorial Office
Institute of Fundamental Technological Research,
Świętokrzyska 21, p. 508,
00-049 WARSZAWA, Poland.

DIRECTIONS FOR THE AUTHORS

The journal *ARCHIVES OF MECHANICS (ARCHIWUM MECHANIKI STOSOWANEJ)* deals with the printing of original papers which should not appear in other periodicals.

As a rule, the volume of a paper should not exceed 40 000 typographic signs, that is about 20 type-written pages, format: 210×297 mm, leaded. The papers should be submitted in two copies. They must be set in accordance with the norms established by the Editorial Office. Special importance is attached to the following directions:

1. The title of the paper should be as short as possible.

2. The text should be preceded by a brief introduction; it is also desirable that a list of notations used in the paper should be given.

3. The formula number consists of two figures: the first represents the section number and the other the formula number in that section. Thus the division into subsections does not influence the numbering of formulae. Only such formulae should be numbered to which the author refers throughout the paper, and also the resulting formulae. The formula number should be written on the left-hand side of the formula; round brackets are necessary to avoid any misunderstanding. For instance, if the author refers to the third formula of the set (2.1), a subscript should be added to denote the formula, viz. $(2.1)_3$.

4. All the notations should be written very distinctly. Special care must be taken to write small and capital letters as precisely as possible. Semi-bold type should be underlined in black pencil. Explanations should be given on the margin of the manuscript in case of special type face.

5. It has been established to denote vectors by semi-bold type. Trigonometric functions are denoted by sin, cos, tg and ctg, inverse functions – by arc sin, arc cos, arc tg and arc ctg; hyperbolic functions are denoted by sh, ch, th and cth, inverse functions – by Arsh, Arch, Arth and Arcth.

6. Figures in square brackets denote reference titles. Items appearing in the reference list should include the initials of the first name of the author and his surname, also the full title of the paper (in the language of the original paper); moreover;

a) In the case of books, the publisher's name, the place and year of publication should be given, e.g.,

5. S. Ziemba, *Vibration analysis*, PWN, Warszawa 1970;

b) In the case of a periodical, the full title of the periodical, consecutive volume number, current issue number, pp. from ... to ..., year of publication should be mentioned; the annual volume number must be marked in black pencil so as to distinguish it from the current issue number, e.g.,

6. M. Sokołowski, *A thermoelastic problem for a strip with discontinuous boundary conditions*, Arch. Mech., **13**, 3, 337–354, 1961.

7. The authors should enclose a summary of the paper. The volume of the summary is to be about 100 words.

8. The authors are kindly requested to enclose the figures prepared on diskettes (format PCX, BitMap or PostScript).

Upon receipt of the paper, the Editorial Office forwards it to the reviewer. His opinion is the basis for the Editorial Committee to determine whether the paper can be accepted for publication or not.

The printing of the paper completed, the author receives 25 copies of reprints free of charge. The authors wishing to get more copies should advise the Editorial Office accordingly, not later than the date of obtaining the galley proofs.

The papers submitted for publication in the journal should be written in English. No royalty is paid to the authors.

Please send us, in addition to the typescript, the same text prepared on a diskette (flopy disk) 3 1/2″ or 5 1/4″ as an ASCII file, in Dos or Unix format.

EDITORIAL COMMITTEE
ARCHIVES OF MECHANICS
(ARCHIWUM MECHANIKI STOSOWANEJ)